VYSOKÉ UČENÍ TECHNICKÉ V BRNĚ
BRNO UNIVERSITY OF TECHNOLOGY

FAKULTA ELEKTROTECHNIKY A KOMUNIKAČNÍCH TECHNOLOGIÍ
ÚSTAV FYZIKY

FACULTY OF ELECTRICAL ENGINEERING AND COMMUNICATION
DEPARTMENT OF PHYSICS

DIELEKTRICKÉ VLASTNOSTI TENKÝCH VRSTEV OXIDŮ TANTALU A NIOBU

DIELECTRIC PROPERTIES OF THIN TANTALUM AND NIOBIUM OXIDE LAYERS

DOKTORSKÁ PRÁCE
DOCTORAL THESIS

AUTOR PRÁCE
AUTHOR
INES FAISEL ABUETWIRAT, BSc, MSc

VEDOUCÍ PRÁCE
SUPERVISOR
doc. Ing. KAREL LIEDERMANN, CSc.

BRNO 2014

Abstract

Dielectric relaxation spectroscopy is one of the useful methods in studying the molecular dynamics of materials. Owing to recent developments in instrumentation and advances in measurement technique, it is possible to obtain the dispersion of dielectric permittivity in a wide frequency range and for very different materials.

The purpose of my work was to investigate dielectric relaxation spectra and conductivity of oxides of titanium, niobium, tantalum, lanthanum and hafnium for field emission cathodes. The objective of the research was to analyze the frequency and temperature behaviour of these oxides, as well as their conductivity over a wide frequency and temperature range, and to attempt to determine the origin of the relaxation. As the original range of oxides has been very broad, focus was paid to tantalum (Ta) and niobium (Nb) oxides only, also with regard to their application in electrolytic capacitors.

Electrical, thermal and mechanical (processing) properties of Ta and Nb oxides have already been well established. Little is known, however, about detailed mechanisms of their dielectric relaxation.

The results acquired for Ta_2O_5 show a relaxation peak in the temperature and frequency range available, 187 K – 385 K, 1 Hz – 10 MHz. The loss peak frequency follows the Arrhenius law dependence with the activation energy of 0.048 eV. In conductivity spectra, Ta_2O_5 film exhibits a steady – state value at low frequencies and a monotonous increase at high frequencies depends on temperature. The observed conductivity followed a slightly superlinear power law. The results acquired for Nb_2O_5 show a relaxation peak in a similar temperature and frequency range, 218 K – 373 K, 1 Hz – 1 MHz. The loss peak frequency follows the Arrhenius law dependence with the activation energy of 0.055 eV. Niobium oxide capacitor shows conductivity mechanism similar to tantalum capacitor.

Abstract

Dielektrická relaxační spektroskopie je jednou z užitečných metod pro studium molekulární dynamiky materiálů. Díky nedávnému pokroku v přístrojové a měřicí technice je dnes možné získat dielektrické spektrum v širokém frekvenčním intervalu a pro velice rozdílné materiály.

Cílem mé práce bylo studium dielektrických relaxačních spekter a vodivosti oxidů titanu, niobu, tantalu, lanthanu a hafnia pro katody pracující na principu studené emise. Cílem výzkumu bylo analyzovat frekvenční a teplotní chování těchto oxidů, včetně jejich vodivosti, v širokém frekvenčním a teplotním rozsahu, a pokusit se stanovit

původ relaxačního mechanismu. Vzhledem k tomu, že původně zadaný rozsah oxidů byl dosti široký, soustředila se pozornost pouze na oxidy tantalu a niobu, rovněž s ohledem na jejich aplikace v elektrolytických kondenzátorech.

Elektrické, tepelné a mechanické (při zpracování) vlastnosti oxidů tantalu a niobu jsou dnes již dobře prozkoumány. K dispozici je však jen málo poznatků o jejich dielektrických relaxačních mechanismech.

Výsledky získané pro Ta_2O_5 ukazují existence relaxačního maxima, nacházejícího se v experimentálně dostupném teplotním a frekvenčním intervalu 187 K – 385 K a 1 Hz až 10 MHz. Frekvence ztrátového maxima se řídí Arrheniovým zákonem s aktivační energií 0.048 eV. Ve vodivostních spektrech vykazují tenké vrstvy Ta_2O_5 na nízkých frekvencích ustálenou hodnotu a při vysokých frekvencích monotónní nárůst, který závisí na teplotě. Pozorovanou vodivost lze popsat mocninnou funkcí s exponentem nepatrně větším než jedna (tzv. superlineární závislost.

Výsledky získané pro Nb_2O_5 v podobné teplotní a frekvenční oblasti, 218 K – 373 K, 1 Hz – 1 MHz rovněž ukazují jedno relaxační maximum. Frekvence ztrátového maxima se opět řídí Arrheniovým zákonem s poněkud vyšší aktivační energií 0.055 eV. Niobové kondenzátory vykazují vodivostní mechanismus shodný s kondenzátory tantalovými.

Keywords

Dielectric spectroscopy, dielectric relaxation, dielectric spectra, electrical conductivity, tantalum oxide, niobium oxide.

Klíčová slova

Dielektrická spektroskopie, dielektrická relaxace, dielektrická spektra, elektrická vodivost, oxid tantalu, oxid niobu.

Abuetwirat, I. F. *Dielectric properties of thin tantalum and niobium oxide layer*. Brno: Vysoké učení technické v Brně, Fakulta elektrotechniky a komunikačních technologií, 2014, 104 s., Research Advisor: Karel Liedermann, PhD, MEng, Assoc. Prof.

Obligatory statutory declaration

I declare that I have written my doctoral thesis “Dielectric relaxation properties of thin tantalum and niobium oxide layer” independently, under the guidance of the doctoral thesis supervisor and using the technical literature and other sources of information which are all quoted in the thesis and detailed in the list of literature at the end of the thesis.

As the author of the doctoral thesis, I furthermore declare that, as regards the creation of this doctoral thesis, I have not infringed any copyright. In particular, I have not unlawfully encroached on anyone’s personal and/or ownership rights and I am fully aware of the consequences in the case of breaking Regulation §11 and the following of the Copyright Act No. 121/2000 Coll., and of the rights related to intellectual property right and changes in some Acts (Intellectual Property Act) and formulated in later regulations, inclusive of the possible consequences resulting from the provisions of Criminal Act No. 40/2009 Coll., Section 2, Head VI, Part 4.

Brno, November 2014 Ines Faisel Abuetwirat

Acknowledgments

I would like to thank my advisor, Doc. Ing. Karel Liedermann, CSc. for his help and guidance in completing my research and thesis.

I would also like to express my special thanks to Prof. Peter Lunkenheimer of the University of Augsburg, Germany for dielectric relaxation measurements.

I would like to thank all my colleagues at Department of Physics for the friendly environment, and for their help, when I needed it most. In particular, I would like to express my deepest thanks to Dr. Tomas Palai-Dany and Dr. Vladimír Holcman.

I would like to thank my family for their love, support and encouragement. Finally, I would like to thank my beloved husband, Usama Alshbeni, for everything.

Brno, November 2014 Inas Faisel Abuetwirat

Contents

1 Background 16

2 Material under study 18

2.1 Tantalum (Ta) 18

2.2 Niobium (Nb) 19

3 Theoretical Foundations 21

3.1 Dielectric relaxation spectroscopy – state of the art 21

3.1.1 Polarization 21

3.1.2 Polarization mechanism 23

3.1.3 Classification of dielectric materials 27

3.1.4 Variation of the dielectric constant in alternating fields 27

3.1.5 Impedance dielectric spectroscopy 28

3.1.6 Dielectric spectroscopy 30

3.1.7 Single relaxation time model: the Debye equation 31

3.1.8 The analysis of dielectric data in terms of relaxation time (frequency) 33

3.1.9 The relation between dielectric relaxation and chemical structure 35

3.1.10 Temperature dependence 36

3.1.11 Time domain dielectric spectroscopy charging /discharging currents and Hamon approximation 38

3.2 Conduction mechanisms 41

3.2.1 Bulk-limited conduction 41

3.2.2 Electrode limited process 43

3.3 Electrolytic capacitor 46

3.3.1 Parallel Plate Capacitor 46

3.3.2 Basic features of electrolytic capacitors 46

3.3.3 Construction of tantalum oxide capacitor 47

3.3.4 Stability of tantalum oxide capacitor 50

3.3.5 Electrical performance 51

3.3.6 Niobium oxide electrolytic capacitor 55

3.3.7 Advantages of niobium oxide capacitor over tantalum capacitor. 56

3.3.8 MIS theory in electrolytic capacitors ... 57
4 Experimental methods ... 60
4.1 Overview of the methods of measurements in the DRS ... 60
4.1.1 Frequency domain measurement ... 61
4.1.2 Measurement Systems ... 61
4.1.3 Equipment for the measurement in the frequency domain ... 63
4.2 Sample preparation ... 65
4.3 Sample holder ... 66
5 Objectives of the present work ... 67
6 Measurements ... 69
6.1 HP 4284A precision LCR meter ... 70
6.2 HP E4980A precision LCR meter ... 70
6.2.1 Measurement error for HP (4284A E4980A) precision LCR meter ... 70
6.3 Novocontrol Alpha-A analyzer ... 72
6.4 Temperature dependence instruments ... 74
6.4.1 Instrumentation for frequency domain and temperature dependence at Augsburg University ... 74
6.4.2 Instrumentation for frequency domain and temperature dependence at Brno University ... 78
7 Result and Analysis ... 80
7.1 Dielectric relaxation spectrum for 1 μF / 50 V_{dc} tantalum electrolytic capacitor ... 80
7.2 Dielectric relaxation influence over several thicknesses ... 85
7.3 Relative permittivity and dissipation factor as function of temperature and frequency ... 87
7.4 Dielectric relaxation spectrum for 4.7 μF / 10 V_{dc} niobium electrolytic capacitor ... 89
7.5 Room temperature measurement on 4.7 μF / 10 V_{dc} niobium electrolytic capacitor and electrolytic tantalum oxide capacitor 1 μF/ 50 V_{dc} ... 94
8 Conclusions ... 97
9 Literature ... 100
Publications ... 102
Curriculum vitae ... 104

List of abbreviations

DRS	Dielectric relaxation spectroscopy
k	High dielectric constant
ESR	Equivalent series resistance
MIS	Metal insulator semiconductor
MOS	Metal oxide semiconductor
ICP	Inherently conductive polymer
EIS	Electrochemical impedance spectroscopy
HN	Havriliak – Negami
CC	Cole – Cole function
CD	Cole – Davidson function
T_g	Glass transition temperature
PF	Poole–Frenkel effect
SCLC	Space – charge – limited – current
FN	Flower – Nordheim
SMD	Surface mounted devise
DUT	Devise under test
HP	Hewlett-Packard

Symbols

Q	electrical charge
C	capacitance of the capacitor,
C_0	geometric capacitor
A	area of the plates
d	dielectric thickness
D	electrical displacement (≡ flux density)
ε_r	permittivity (dielectric constant)
ε'	real part of permittivity (relative permittivity)
ε''	imaginary part of permittivity (loss number)
ε_s	asymptotic value of permittivity at infinitely low frequency (f = 0, i.e. at constant field)
ε_0	vacuum (free space) permittivity,
ε_∞	asymptotic value of permittivity at infinitely high frequency
E	electric field
τ_0	relaxation time of the material (temperature dependent)
τ	inverse of the characteristic Debye relaxation frequency
σ	electrical conductivity
P	polarization vector

ω	angular frequency
μ	permanent dipole moment
t	time
T	the temperature
α	Havriliak – Negami parameter α
β	Havriliak – Negami parameter β
H	activation energy
K	Boltzmann constant
β_{PF}	Poole–Frenkel coefficient
J	current density

List of Figures

Fig. 2.1. a) Crystal structure for tantalum [3], b) Crystal structure of tantalum oxide [4], c) Crystal structure for tantalum pent-oxide [5]. 19
Fig. 2.2. The niobium - oxygen system: main oxides and some of their structural and electrical properties (conductivity was given at ~ 0 °C – 25 °C) [7]. 20
Fig. 3.1. a) CO_2 no permanent dipole moment induced, b) H_2O with induced dipole moment [8]. 22
Fig. 3.2. Molecules with polar bonds; far-left and far-right molecules have a zero molecular dipole [8]. 22
Fig. 3.3. a) Basic construction of capacitor, b), electric charge accumulated by capacitor [9]. 23
Fig. 3.4. Time development of the polarization vector for relaxation polarization type [10]. 25
Fig. 3.5. Principal behavior of the complex dielectric function in the frequency domain [12]. 28
Fig. 3.6. Impedance spectra of a resistor and a capacitor in parallel [13]. 29
Fig. 3.7. Time development of the polarization after the application of a constant field [14]. 32
Fig. 3.8. Complex permittivity predicted by Debye equation [10]. 33
Fig. 3.9. The Havriliak – Negami function in log/log view [10]. 34
Fig. 3.10. Graphical representation of the Debye's formula [14]. 34
Fig. 3.11. The Cole – Cole plot for HN function [14]. 35
Fig. 3.12. The imaginary part of complex permittivity as a function of temperature at fixed frequency [11]. 35
Fig. 3.13. Temperature dependence of the relaxation times [14]. 37
Fig. 3.14. a) ε' and ε'' as a function of ω for fixed temperatures, b) ε' and ε'' as a function of temperature for fixed frequencies [11]. 38
Fig. 3.15. Poole–Frenkel effect at a donor center [1]. 42
Fig. 3.16. Energy band diagram between a metal surface and a vacuum incorporating Schottky Effect with and without electrical field [1]. 44
Fig. 3.17. Energy band diagrams (a) no field (b) high field [1]. 45
Fig. 3.18. Electrolytic capacitor [1]. 47
Fig. 3.19. Tantalum pellet after pressing and sintered [1]. 48
Fig. 3.20. Anode and cathode plate structures in tantalum pellet [1]. 49
Fig. 3.21. Final assembly of tantalum and niobium oxide capacitor [3]. 49
Fig. 3.22. Cross section showing self-healing system [16]. 50
Fig. 3.23. The fault site in dielectric after self-healing process [16]. 50
Fig. 3.24. Theoretical ignition of failure [1]. 51
Fig. 3.25. The loss tangent is defined by the angle between the capacitor's impedance vector and the negative reactive axis. 52
Fig. 3.26. a) Equivalent circuit representations of an electrolytic capacitor, b) normalized equivalent diagram of capacitor [17]. 53
Fig. 3.27. Modulus of the impedance Z as a function of the frequency [18]. 54
Fig. 3.28. Distributed capacitive elements within the tantalum pellet structure [19]. ... 54

Fig. 3.29. Main steps of the fabrication process of niobium solid electrolyte capacitors. Anode material: sintered niobium powder. Dielectric material: anodically grown niobium pent-oxide. Cathode material: manganese dioxide [7]. ... 56
Fig. 3.30. MIS structure model for niobium and tantalum capacitors before thermodynamic equilibrium [3]. ... 57
Fig. 3.31. Ideal MIS structure before thermodynamic equilibrium, a) for tantalum capacitor [21], b) for niobium oxide capacitor [22] ... 58
Fig. 3.32. MIS structure models of niobium oxide capacitor, in equilibrium state [2]. . 58
Fig. 3.33. MIS structure model for niobium oxide capacitors after application of negative (a) and positive voltage (b) thermodynamic equilibrium [3]. ... 59
Fig. 4.1. Auto-balancing bridge method [23]. ... 61
Fig. 4.2. Measurements system for dielectric relaxation spectroscopy [14]. ... 62
Fig. 4.3. Parallel plate method [24]. ... 63
Fig. 4.4. Effect of guard electrode [24]. ... 64
Fig. 4.5. Measurement of capacitance by using guarded electrode system [25]. ... 64
Fig. 4.6. Electrode dimension [27]. ... 66
Fig. 6.1. Test fixture residuals [23]. ... 71
Fig. 6.2. Test fixture is in open connection [23]. ... 71
Fig. 6.3. Test fixture is in short connection [23]. ... 72
Fig. 6.4. Alpha-A mainframe system - setup [32] ... 73
Fig. 6.5. Simplified measuring circuit illustrating the operation of Alpha-A system [33]. ... 73
Fig. 6.6. The main parts of the Quatro Cryosystem [35]. ... 75
Fig. 6.7. Principle structure of the Novocontrol Cryo system and the QUATRO controller [36]. ... 76
Fig. 6.8. The setpoint temperature and the sample temperature in dependence of time for NOVOCONTROL Quatro Cryosystem 4.0 [36]. ... 77
Fig. 6.9. The experimental setup [37]. ... 77
Fig. 6.10. Description of individual cryostat sections from the Janis Company [10]. ... 78
Fig. 7.1. Relative permittivity versus frequency of 1 μF / 50 Vdc tantalum capacitor at different temperatures: from 187 K to 418 K. ... 81
Fig. 7.2. Relaxation peak versus frequency of 1 μF / 50 Vdc tantalum capacitor at different temperatures: from 187 K to 418 K. ... 82
Fig. 7.3. Arrhenius plot of the frequency value of relaxation peak. ... 82
Fig. 7.4. Non-linear least square fit of relaxation peak of complex permittivity versus frequency, a single HN equation at 187 K. ... 83
Fig. 7.5. Temperature dependence of the shape parameter α_{HN} of 1 μF / 50 V_{dc} at different temperatures: from 187 K to 418 K. ... 83
Fig. 7.6. Temperature dependence of shape parameter β_{HN} of 1 μF / 50 V_{dc} at different temperatures: from 187 K to 418 K. ... 84
Fig. 7.7. Temperature dependence of dielectric strength of 1 μF / 50 V_{dc} at different temperatures: from 187 K to 418 K. ... 84
Fig. 7.8. Dielectric relaxation peak versus frequency results for two different thicknesses of Ta_2O_5 (298 nm, 95 nm) and different electrode area at 284 K. ... 85

Fig. 7.9. Capacitance *vs.* temperature curves and dissipation factor for (1 μF / 50 V_{dc}, and 33 μF / 16 V_{dc}) tantalum capacitors ... 86
Fig. 7.10. The capacitance – temperature curves for (1 μF / 50 V_{dc}) tantalum capacitor. ... 87
Fig. 7.11. Effect of temperature for Ta_2O_5 1 μF / 50 V_{dc} on (a) relative permittivity, (b) dissipation factor. ... 88
Fig. 7.12. The real part of the ac conductivity as a function of frequency at different temperatures for 1 μF / 50 V_{dc} tantalum capacitor. ... 89
Fig. 7.13. Real part of complex permittivity as a function of frequency in the temperature range 218 – 373 K. ... 90
Fig. 7.14. Imaginary part of complex permittivity as a function of frequency at different temperature range. ... 91
Fig. 7.15. Non-linear least square fit of imaginary part of complex permittivity versus frequency, a single HN equation at 373 K. ... 91
Fig. 7.16. The Arrhenius plot – log fmax *vs.* 1/T for niobium oxide. ... 92
Fig. 7.17. Temperature dependence of dielectric strength for niobium thin oxide film. ... 92
Fig. 7.18. Temperature dependence of shape parameter β_{HN} of niobium thin oxide film ... 93
Fig. 7.19. Temperature dependence of the shape parameter α_{HN} of niobium thin oxide film. ... 93
Fig. 7.20. a) Real part, and b) imaginary part of complex permittivity for niobium oxide capacitor 4.7 μF/ 10 V_{dc} and tantalum capacitor 1 μF/ 25 V_{dc}. ... 95
Fig. 7.21. Loss factor of the 4.7 μF/ 10 V_{dc} niobium and 1 μF/ 25 V_{dc} tantalum oxide capacitor. ... 95
Fig. 7.22. Conductivity *vs.* frequency for niobium 4.7 μF/ 10 V_{dc} and 1 μF/ 25 V_{dc} tantalum capacitor. ... 96

Introduction

Over the course of time, the focus of dielectric science and technology has broadened from traditional dielectric and insulation materials toward a wider palette of applications, including, among else, nanocomposites, high-permittivity ceramics, or material for dielectric films used in semiconductor devices and capacitors, particularly oxides and nitrides. More recently, materials of unique dielectric responses have been studied and utilized in novel ways. The study of dielectrics is fundamental in nature and offers a unified understanding of many other disciplines in materials science.

Dielectric relaxation spectroscopy (DRS) is a subject of science on the borders between physics, chemistry, electrical engineering and materials science. It involves an investigation of dielectric relaxation processes in an extremely wide range of characteristic times (10^{-12} – 10^{+6} s). Dielectric spectroscopy studies the response of a material to an applied electric field. The term “dielectric relaxation” denotes the momentary delay (or lag) in the dielectric response of a material; i.e., it refers to the relaxation response of a dielectric medium to an external electric field.

The 4d transition metals tantalum, hafnium, niobium and titanium in combination with oxygen, as thin oxide film with high dielectric constant (ε), are a key material system for a wide range of applications in microelectronic devices due to their ability to serve in high-capacity storage capacitors without the concomitant leakage effects.

Solid tantalum capacitor is a type of electrolytic capacitor; it consists of a pellet of tantalum metal as anode, a dielectric layer of tantalum pent-oxide created on the tantalum surface by anodizing, surrounded by conductive material as a cathode. The tantalum capacitor distinguishes itself from other capacitors; its compact construction and large capacitance makes it volumetrically efficient. This volumetric efficiency is one of the main reasons they are an ideal choice in many applications such as portable electronics equipment. Also, tantalum capacitors have lower equivalent series resistance (ESR), lower leakage, and higher operating temperature than other electrolytic capacitors. High reliability and high frequency applications necessitate constant improvements in all materials associated with tantalum capacitors [1].

The purpose of the work described in this thesis was to study dielectric properties, and the conductivity mechanism in thin insulating amorphous film by using metal – insulator – semiconductor (MIS) capacitor by applying varying voltage between the substrate (the semiconductor in the case of MIS) and the metal. Thin amorphous insulating film are used in many different types of discrete electronic circuit devises, such as electrolytic capacitor, the MOS field transistor, thin film transistor, and thin film capacitor. For a particular application various factors enter into the choice of amorphous insulating thin film; for capacitor applications, a thin film, besides providing adequate insulation, should have sufficiently low dielectric losses and residual voltage effects. Residual voltage may be due to the polarization processes with long decay times, or to electronic space charge effects [2].

The films used in this study were anodic tantalum pent-oxide and niobium pent-oxide. Device application of these films includes the electrolytic capacitor.

The permittivity (ε') and the loss number (ε'') were measured as a function of frequency and temperature using a conventional ac bridge.

Chapter 3 is review of the dielectric processes, and basic conduction mechanisms in thin amorphous film, including the Poole–Frenkel Effect, Space-Charge-Limited Current, Fowler–Nordheim Tunneling, and the Schottky Effect. These mechanisms represent a list of possible sources of dc leakage current in modern tantalum capacitors [1], and an overview of basic capacitor models for parallel plate and electrolytic capacitors, the experimental methods are described in chapter 4, the objective of the present work are presented in chapter 5, the experimental procedure are described in chapter 6, and the results obtained are presented in chapter 7.

In chapter 8 the results are discussed, and the conclusions to be drawn from the work are given in chapter 9.

1 Background

An electrolytic capacitor is a capacitor that uses an electrolyte (an ionic conducting liquid) as one of its plates to achieve a larger capacitance per unit volume than other types, due to their advantage, the large capacitance of electrolytic capacitors makes them particularly suitable for passing or bypassing low-frequency signals and storing large amounts of energy. They are widely used in power energy and power electronics, and interconnecting stages of amplifiers at audio frequencies. The early use of tantalum anode instead of aluminum anode in wet electrolyte capacitors has increased the range of the operating temperatures and allowed the use of electrolytic solution of high conductivity and low freezing point. This was possible because of the high dielectric constant of tantalum oxide and the chemical stability of both tantalum and its oxide. Despite these improvements, there are still several drawbacks and durability limitation due to the limited life, and low temperature limitations, which are caused by the solidification of the electrolyte, and the large volume occupied by the electrolyte, its container, and hermetic seal. The main profit of applications of wet electrolyte solution is that the liquid electrolyte adheres to the dielectric surfaces and permits the dielectric reforming process at fault sites. All this profit has also the disadvantage like the use of solution of a base, which can lead to the formation of gases, and cannot hold the thermal cycles of surface mount kits.

The other benefits in these types of capacitors do not result only from tantalum, but from the cathode with which it was paired. The use of solid tantalum electrolytic capacitors was possible once in place of the traditional liquid electrolyte, a manganese nitrate solution was applied as the cathode plate. The oxidized pellet is impregnated with a solution of this salt and then heated to convert the salt to the solid manganese dioxide. This impregnation-heating step is repeated several times in order to coat the porous pellet with the solid semiconducting MnO_2, as semiconductor solid. The chemical deposition of MnO_2 allowed the cathode plate connection to conform to the dielectric surface, but with a completely solid structure. Tantalum capacitors now required much less volume for packaging, no longer needed a hermetic seal, had much better temperature characteristics, and a longer shelf life [1].

The developments in technology of tantalum capacitors made it possible to produce small size capacitors suitable for market needs using an epoxy resin. This improvement gave tantalum capacitors a superior performance over aluminum electrolytic capacitors. Technology continued to improve tantalum capacitors through improving the packaging and through the improving of capacitor element such as dielectric film and MnO_2 dielectric coverage.

Historically, we can see the price of raw tantalum increased drastically between 1979 and 1982 causing the price of solid tantalum capacitors, to no longer be competitive against aluminum electrolytic capacitors and other comparable capacitors. This has led

to the reduction of the amount of tantalum used per capacitor, as much as possible without reducing the rated capacitance.

To achieve such reduction in the amount of tantalum raw material used in capacitor, powder technology was utilized. These improvements in cost and size and of the solid tantalum capacitors halted their replacement by other types. Another technological advancement was the development of the molded chip-type packaging, which enabled solid tantalum capacitors to be easily applied to surface mount technologies.

One other advantage of solid tantalum capacitors is therefore high resiliency to heat, which gave them a huge advantage over other capacitors.

The need for low power, portable, digital and safe electronics devices, has placed a new set of demands on solid tantalum capacitors. This means smaller size capacitors with large storage for charge, not only that a low working voltage was necessary for power saving purposes. Also it has to operate at high frequencies and have high reliability for safety reasons.

Due to these new requirements the evaluation of the tantalum capacitor is beginning to take another turn with the use of inherently conductive polymers (ICP) for the cathode plate material. The goal of this shift is to keep the solid state benefits achieved with MnO_2 while removing its associated undesirable traits as a cathode plate contact [1].

2 Material under study

2.1 Tantalum (Ta)

Tantalum is a chemical element. Tantalum has symbol Ta and it is a rare, hard, lustrous transition metal that is highly corrosion-resistant and is a member of the refractory metals group, always with the chemically similar niobium. Tantalum has the following properties: atomic number: 73, atomic mass: 180.9479 amu, melting point: 2996.0 °C (3269.15 K, 5424.8 °F), boiling point: 3017 °C, 5462.6 °F, 3290.15 K, number of neutrons: 108, classification: transition metal, crystal structure: cubic, density at 293 K: 16 690 kg/m^{-3}, color: blue-grey. Its electronic configuration is [Xe] $4f^{14}$ $5d^3$ $6s^2$. Ta crystal lattice is a body centered cubic (bbc) characterized by an electronic structure where the outer shell (6s energy level in case of Ta) contains a pair of electrons; 5d inner shell is not completely filled. The electrical resistivity of Ta measured at 20 °C is 131 nΩ.m. Its electronegativity is 1.5 (300 K) with electron work function 4.25 eV; Ta resists corrosion. It is a superconductor below transition temperature T_c ~ 4.483 K. It is able to form oxides with the oxidation states +5 (Ta_2O_5), +4 (TaO_2), and +2 (TaO), the most stable oxidation state is +5.

Tantalum dioxide (TaO_2)

The tantalum dioxide molecules produced from laser evaporation of bulk Ta_2O_5, tantalum dioxide, we find that it formally is in the oxidation state 4. TaO_2 is a gray or blue occurring in crystalline solid.

Tantalum pent-oxide (Ta_2O_5)

Tantalum pent-oxide, also known as tantalum (V) oxide, is an inorganic compound with the formula Ta_2O_5. Ta_2O_5 is a white solid that is insoluble in all solvents but is attacked by strong bases and hydrofluoric acid, odorless powder. Ta_2O_5 is an inert material with a high refractive index and low absorption (i.e. colorless), which makes it useful for coatings. Ta_2O_5 has a density of ~ 8200 kg/m^3 and melts at about 1872 °C. It decomposes only at temperatures > 1470 °C. Both low and high temperature forms exist. The low temperature form is known as β-Ta_2O_5, and the high temperature form is known as α-Ta_2O_5. The transition point between these two forms has been reported as 1360 °C. The transition is slow but reversible. The dielectric constant of Ta_2O_5 is 26 for amorphous film, crystalline Ta_2O_5 exhibits a higher dielectric constant than amorphous Ta_2O_5 ~ 46. The tantalum pent-oxide structure changes from amorphous to crystalline at temperatures above 750 °C. It is an electrical insulator with a band gap of approximately 4.5 eV. Ta_2O_5 is used to make capacitors in automotive electronics, cell phones, and pagers, electronic circuitry; thin-film components, due to its high dielectric constant.

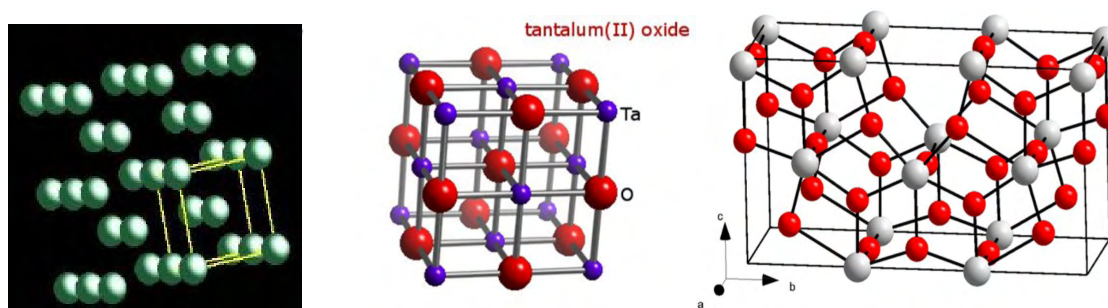

Fig. 2.1. a) Crystal structure for tantalum [3], b) Crystal structure of tantalum oxide [4], c) Crystal structure for tantalum pent-oxide [5].

2.2 Niobium (Nb)

In nature, niobium is not found free, but only in minerals. Nb has the atomic number 41 and is a soft, ductile transition metal belonging to group 5 and period 5 of the periodic table of elements. Its electronic configuration is [Kr] $4d^4$ $5s^1$. Nb crystal lattice is a body centered cubic (bbc) characterized by an electronic structure where the outer shell (5s energy level in case of Nb) contains a single electron, 4d inner shell is not completely filled. Melting point of Nb is quite high, 2477 °C, the density 8570 kg/m^3. The electrical resistivity of Nb at 20 ºC is 0.125 μΩ.m. Its electronegativity is 1.6 and work function is 3.95 – 4.87 eV. Nb is a superconductor below the transition temperature T_c ~9.3 K, Nb resists corrosion. Nb is able to form oxides with oxidation states +5 (Nb_2O_5), +4 (NbO_2) and +3 (Nb_2O_3), as well as with the rarer oxidation state +2 (NbO) [6], whose color depends on its thickness. Shades of blue, green and yellow are typical.

Niobium monoxide (NbO)

The stable niobium monoxide exhibits a defective NaCl structure with 25% ordered vacancies in the Nb- and O-sublattices. Thus, among all transition metal monoxides, the structure of NbO presents the highest number of point defects and is unique in that the Nb atoms are coordinated to only four O atoms in a square planar array. NbO has a density of ~7300 kg/m^3 and melts at about 1945 °C. Nb atoms occur in the formal oxidation state of +2 and their electronic configuration is assumed to be [Kr].$4d^3$. With respect to bulk Nb, the density of conduction electrons in NbO is already reduced, yet NbO still exhibits very high room-temperature conductivity, characteristic of metallic behavior. Its electrical resistivity amounts to about 0.21 μΩm at 25 °C. Owing to its metallic conductivity, NbO is used in Nb-based electrolytic capacitors, where it can advantageously replace Nb-metal as anode material [7].

Niobium dioxide (NbO_2)

The niobium in niobium dioxide is formally in the +4 oxidation state. The room temperature form of NbO_2 has a tetragonal lattice; electronic configuration structure is [Kr].$4d^1$. With density of 7300 kg/m^3, it melts at about 1915 °C. NbO_2 at room temperature is an N-type semiconductor; the corresponding conductivity is of the order 10^{-4} S/m with small band gap of approximately 5 eV. Above 810 °C, NbO_2 becomes a

metallic conductor. NbO_2 is insoluble in water. In industrial processes, NbO_2 is produced as an intermediate for the production of niobium metal.

Niobium pent-oxide (Nb_2O_5)

Niobium pent-oxide is a white solid occurring in both crystalline (orthogonal) and amorphous phase. The form most commonly encountered is monoclinic M-Nb_2O_5 which has a complex structure, Nb_2O_5 is the most stable niobium oxide; electronic configuration structure is [Kr].$4d^1$. Density of Nb_2O_5 depending on the crystal formation procedure is 4.6 kg/m^3; it melts at about 1512 °C, the experiment band gap width of Nb_2O_5 is generally measured in the order of 3.3 to 3.9 eV. The conductivity of Nb_2O_5 is about $10^{-16} - 10^{-6}$ S/m

Figure 2.2 shows the niobium-oxygen system.

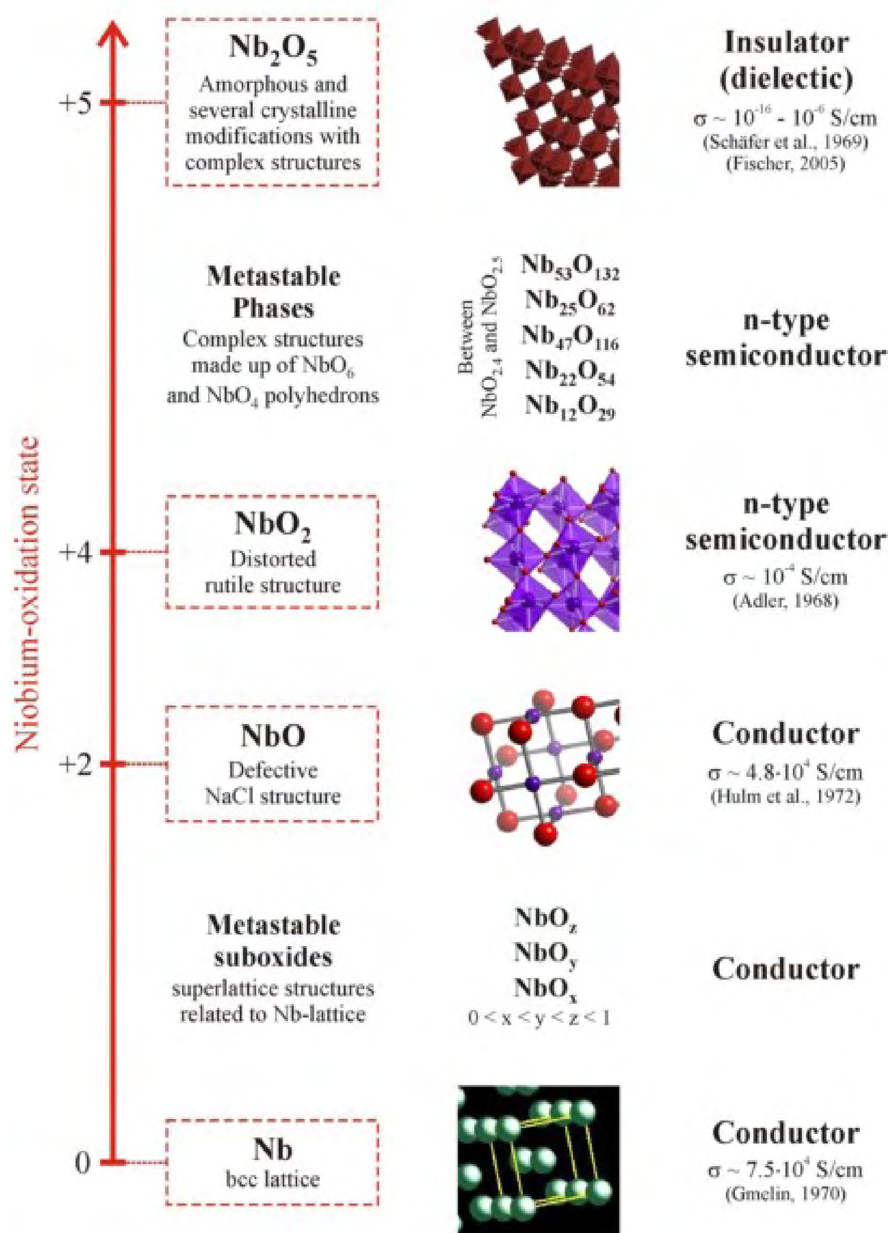

Fig. 2.2. The niobium - oxygen system: main oxides and some of their structural and electrical properties (conductivity was given at ~ 0 °C – 25 °C) [7].

3 Theoretical Foundations

3.1 Dielectric relaxation spectroscopy – state of the art

A dielectric is an electrical insulator that is polarized by the action of an applied electric field; dielectrics consist of polar molecules, or non – polar molecules, or very often both. Material consisting of polar molecules has built-in dipole moment. Under external electrical field dipoles polarize – they reorient in the electrical field and neutralize some of charge on the electrodes.

The term high-κ dielectric refers to a material with a high dielectric constant or relative permittivity (ε_r) as compared to silicon dioxide. Relative permittivity describes material properties; it is frequency dependent and it means the ratio of the amount of stored electrical charge when a voltage is applied, relative to the amount of electrical charge stored in the same capacitor in absence of the dielectric, i.e. filled with vacuum only.

Dielectric relaxation spectroscopy (DRS) is a subject of science on the borders between physics, chemistry, electrical engineering and materials science. It involves an investigation of dielectric relaxation processes in an extremely wide range of characteristic times (10^{-12}, 10^{+6}) s. Dielectric spectroscopy studies the response of a material to an applied electric field. The term "dielectric relaxation" denotes the momentary delay (or lag) in the response of a dielectric medium to an external electric field.

3.1.1 Polarization

Electric dipoles arise from opposite but equal charges separated by a distance. Molecules that possess an uneven distribution of charge (one end more positive than the other) are called polar molecules. Polar molecules are said to be permanent dipoles and have a permanent dipole moment μ.

$$\mu = q\,x \tag{3.1}$$

where q is the charge and x is the distance between the fractional charges q- and q+ in the molecule.

Water is polar and has a dipole moment of 1.85 Debye as shown below. The Debye is a unit of dipole moment and has a value of 3.336 x 10^{-30} C.m. Carbon dioxide has a net charge of zero as shown below.

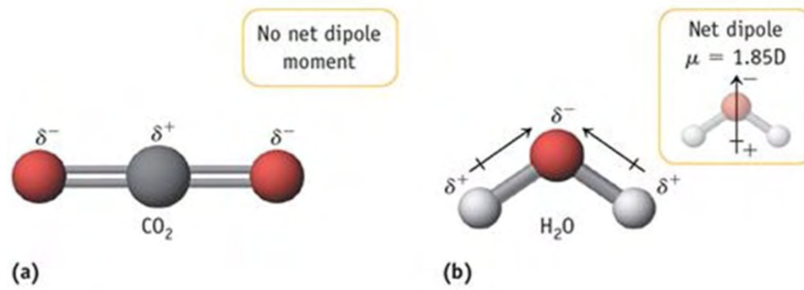

Fig. 3.1. a), CO_2 no permanent dipole moment induced,
b) H_2O with induced dipole moment [8].

The net charge within a natural atom is zero, that is the atom has no net dipole moment; however when this atom is placed in an external electric field, it will develop an induced dipole moment.

Molecules that have exactly zero dipole moment are therefore referred to as non-polar by symmetry as shown below.

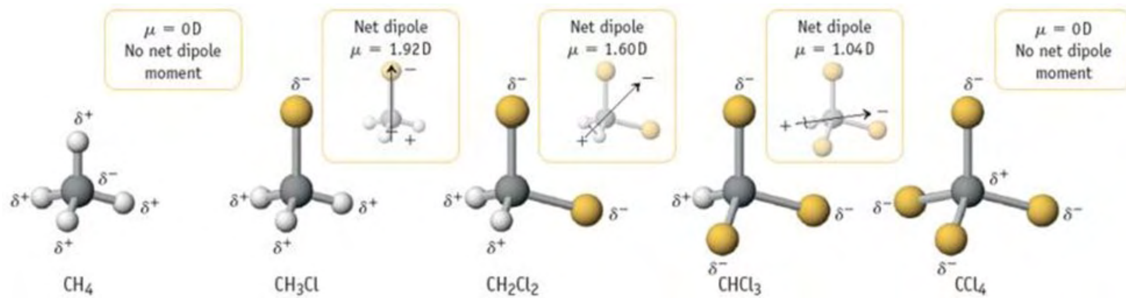

Fig. 3.2. Molecules with polar bonds; far-left and far-right molecules
have a zero molecular dipole [8].

If a material contains polar molecules, they will generally be in random orientations when no electric field is applied. An applied electric field will polarize the material by orienting the dipole moments of polar molecules. Thus the material exhibits net polarization, which leads to a dielectric constant that is determined by this orientation polarization. To relate the induced dipole moment and the field causing it we define

$$p_{induced} = \alpha . E \tag{3.2}$$

where α is a coefficient called the polarizability of the atom. It depends on the polarization mechanism, and E is the electrical field.

The polarization density P is defined as the average electric dipole moment μ per unit volume V of the dielectric material

$$\vec{P} = \frac{\sum \vec{\mu}_i}{V} = n.\alpha.\vec{E}_l \tag{3.3}$$

where n is density of dipoles.

The polarization density P defines the electric displacement field D as following

$$\vec{D} = \varepsilon_0 . \vec{E} + \vec{P} \tag{3.4}$$

If we measure the polarization of a material, we usually find a linear relationship between the polarization density and applied field P and E as follows

$$\vec{P} = \varepsilon_0 . \chi . \vec{E} \tag{3.5}$$

where ε_0 is the permittivity constant (of vacuum) (8.854×10^{-12} $F.m^{-1}$) and χ is the dielectric susceptibility.

By adding Equation (3.4) with (3.5) we obtain

$$\vec{D} = \varepsilon_0 \vec{E} + \varepsilon_0 . \chi . \vec{E} = \varepsilon_0 (1 + \chi) \vec{E} = \varepsilon_0 \varepsilon_r \vec{E} \tag{3.6}$$

where ε_r is relative permittivity of material. For many dielectrics $\chi << 1$ and ε_r is slightly above 1.

The capacitance of the capacitor increase if the gap is filled with dielectric material

$$C_d = \varepsilon_r C_0 \tag{3.7}$$

where C_0 is geometric capacitance and is equal

$$C_0 = \varepsilon_0 . \frac{A}{d} \tag{3.8}$$

where A is electrode area, and d dielectric thickness.

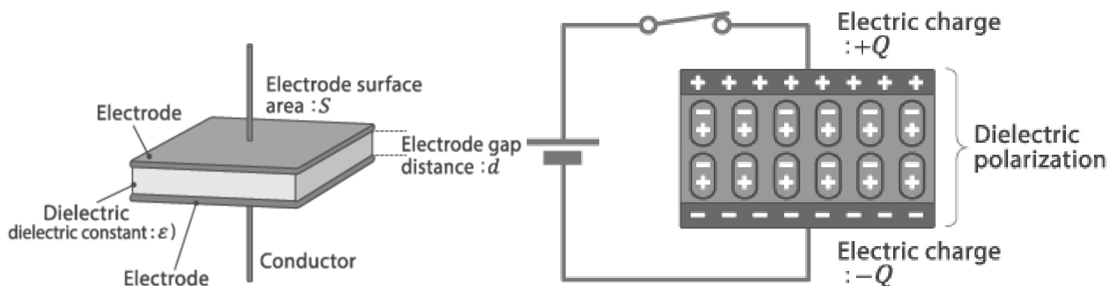

Fig. 3.3. a) Basic construction of capacitor, b) electric charge accumulated by capacitor [9].

3.1.2 Polarization mechanism

In dielectric substances several kinds of polarizations often occur along, and the weaker of them are covered with stronger mechanisms. Polarization can be – according to the time constant of polarization – divided into three basic groups:

- flexible (elastic) polarization
- relaxation polarization
- specific polarization

The above core polarization groups include several specific types of polarization:

- Flexible polarization
  - Electron
  - Ionic (flexible)
- Slow polarization
  - Dipole
  - Ionic – relaxation
- Specific polarization
  - interlayer (migration)
  - autonomic (spontaneous)
  - persistent (permanent)
  - resonance

- **Flexible (elastic) polarization**, characterized in that the coupled electrical charges (electrons, ions) are in their equilibrium positions bonded by elastic electrostatic forces. Therefore, the deflection due to an external electric field and then return to its equilibrium position after the demise of the field is going very fast compared to other types of polarization, almost immediately and without loss of energy. They do not depend on the frequency of the entire frequency range used in electronics.
  - **Electron polarization**; occurs when the electronic cloud is deformed under the force of the applied field, so that the negative and positive charges are formed. They lightly follow the frequency of photons in the visible and ultraviolet range. ($10^{-14} – 10^{-17}$ s).
  - **Ionic (atomic)** polarization is such a polarization that is caused by relative displacements between positive and negative ions in ionic crystals (for example, NaCl). Its frequency falls in the infrared ($10^{-11} – 10^{-14}$ s). Response is slower.
- **Relaxation polarization (slow),** characterized in that after applying an electric field polarization is increasing slowly, and so the polarization wane after dis-connecting field. For fixing these effects need a relatively long time. Rate of change of polarization of the electric field after connecting and disconnecting after the first approximation exponential shape and can be expressed by the equations –

- after connecting the electric field.

$$P = p_s.[1 - \exp\left(-\frac{t}{\tau}\right)] \tag{3.9}$$

- after disconnecting the electric field

$$P = p_s.\exp\left(-\frac{t}{\tau}\right) \tag{3.10}$$

This polarization is highly dependent on temperature and frequency and is accompanied by energy losses in the dielectric, which by it warms/heats. For more accurate analysis it appears that the rate of change of polarization has a complex shape. The time development of the polarization includes information about the dynamics of microscopic movements in the dielectric.

The time development of the polarization vector during connection and disconnection of the electric field is shown for a relaxing polarization in Fig. 3.4. The relaxation time is defined as the time for which, after the removal of the electric field, the level of polarization in the substance decreases to (1 / e) times the original value.

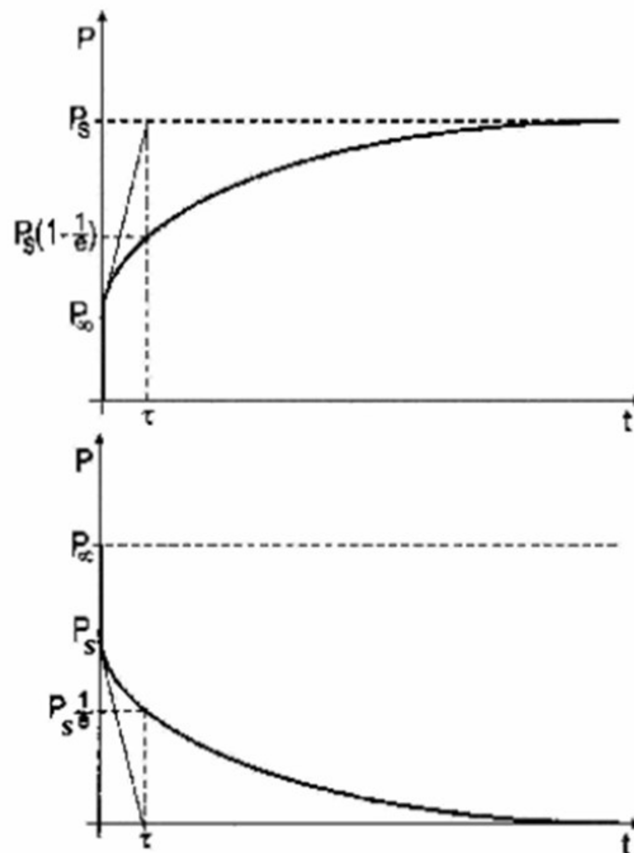

Fig. 3.4. Time development of the polarization vector for relaxation polarization type [10].

- **Dipolar (dipole, orientation) polarization**; it results from the alignment of permanent dipoles (e.g. water) in the direction of electric field. A molecule takes about 1 ps (period of motion) to rotate in a fluid; the change occurs when measurements are made at frequencies 10^{11} Hz. When the frequency of radiation exceeds the frequency of rotation of molecule orientation polarization is lost. Response will be slower.
- **Ionic relaxation polarization** occurs when positive ions are displaced in the direction of an applied field while the negative ions are displaced in the opposite direction. Again, it is accompanied by energy loss in the dielectric, and it is dependents on temperature and frequency

- **Specific polarization**, to this group polarization includes polarization, which have their own specific characteristics and are not included in the previously groups of flexible and slow polarization.
  - **Migration polarization (space charge polarization)**: occurs in inhomogeneous systems which consist of two or more materials having different conductivity (differing mobility and the concentrations of free charges) and permittivity. If such material in an electric field, then the interface of these different environments free of charge accumulate and become immobile (bound). Migration of polarization is also referred to as interlayer, respectively space charge polarization. This polarization is slowest contingent free movement of electric charges and is manifested only in the region of very low frequencies.
  - Spontaneous polarization is non-linearly dependent on the intensity of the electric field and its characteristic is the maximum, depends on the permittivity to the temperature. The spontaneous polarization is closely associated with high dielectric loss. Substances with spontaneous polarization are made of domains, the areas in which the induced electric dipoles oriented parallel and without the presence of an electric field. The direction of each electrical torque of the individual domains is different, so that the material as a whole appears to be un-polarized. The effect of external electric field causes the orientation of the electric moments of domains in the direction of the field, which outwardly appear to be very strong polarization. This phenomenon is analogous ferromagnetism and substances in which this polarization submits called ferroelectrics.
  - **Persistent (permanent) polarization** occurs in some of polar dielectrics with low electrical conductivity. Substances for which this polarization occurs are called electrets – permanently polarized body.
  - **Resonance polarization** arises as a result of its own resonance (thermal) oscillations of particles with an electrical charge to the vibrations of the external electrical field. It manifests itself in the optical spectrum of frequencies, this effect it is outside the range of frequencies used in electronics.

3.1.3 Classification of dielectric materials

Dielectric materials may be classified to two main categories: non-ferroelectric materials and ferroelectric materials. Non-ferroelectric material may be divided into three classes based on the mechanisms of the electric polarization to three classes:

Nonpolar materials

In this class of materials an electric field causes only elastic displacement of electron cloud (mainly valence electron clouds). These types of material have only electronic polarization, and only consist of a single kind of atom such as silicon (Si), diamonds (C). The appreciable absorption occurs at the resonance frequency (ω) which is in the visible or ultraviolet region. The dielectric constant should be independent of frequency for Frequencies below the resonance frequency and equal to static dielectric constant.

Polar materials

In this class of materials an electric field causes elastic displacement of electron cloud as well as elastic displacement of the relative positions of ions [11]. These types of material will possess electronic and ionic polarization. These materials are composed of molecules, and each molecule is made of more than one kind of atom without permanent dipole moment. As an example of polar material an ionic crystal may be mentioned. The appreciable absorption occurs at two resonance frequencies one corresponding to electronic polarization in the optical region and the other in the inferred region corresponding to ionic polarization.

Dipolar materials

Is a material whose molecules possess a permanent dipole moment. This class of materials will have all the tree types of polarization, electronic, ionic, and orientation polarization. Belong to this class of materials water and methyl alcohol.

3.1.4 Variation of the dielectric constant in alternating fields

If the field is switched, there is a characteristic time that the orientation polarization takes to adjust, called the relaxation time. E.g. in an ionic crystal, a typical relaxation time is ~ 10^{-11} s. Therefore, if the electric field switches direction at a frequency higher than ~ 10^{11} Hz, the dipole orientation cannot 'keep up' with the alternating field, the polarization direction is unable to remain aligned with the field, and this polarization mechanism ceases to contribute to the polarization of the dielectric.

In an alternating electric field both the ionic and the electronic polarization mechanisms can be thought of as driven damped harmonic oscillators, and the frequency dependence is governed by resonance phenomena. This leads to peaks in a plot of dielectric constant versus frequency as shown below, at the resonance frequencies of the ionic and electronic polarization modes. A dip appears at frequencies just above each resonance peak, which is a general phenomenon of all damped resonance responses, corresponding to the response of the system being out of phase with the driving force. In this case, in the areas of the dips, the polarization lags behind the field. At higher frequencies the

movement of charge cannot keep up with the alternating field, and the polarization mechanism ceases to contribute to the polarization of the dielectric.

As frequency increases, the net polarization of any material drops as each polarization mechanism ceases to contribute, and hence its dielectric constant drops.

At sufficiently high frequencies (above ~ 10^{15} Hz), none of the polarization mechanisms are able to switch rapidly enough to remain in step with the field. The material no longer possesses the ability to polarize, and the dielectric constant drops to 1 the same as that of a vacuum.

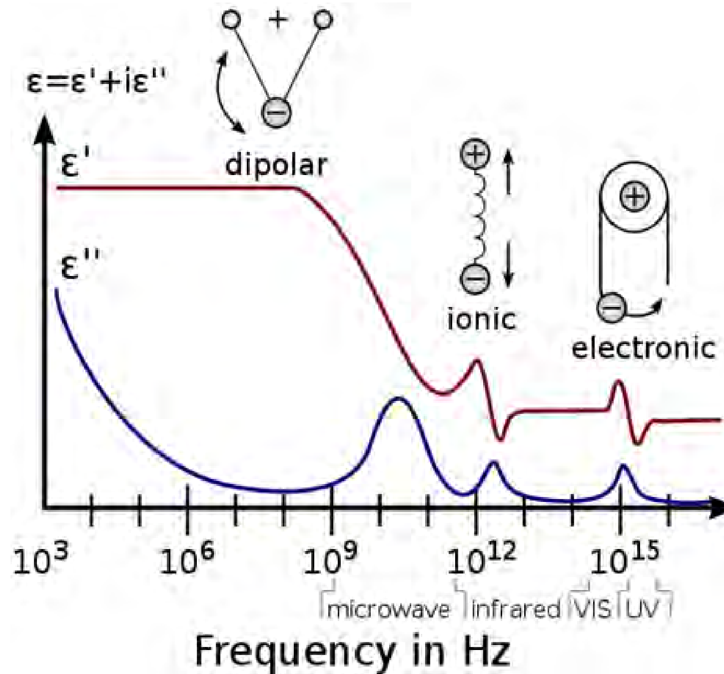

Fig. 3.5. Principal behavior of the complex dielectric function in the frequency domain [12].

3.1.5 Impedance dielectric spectroscopy

Dielectric spectroscopy (sometimes called impedance spectroscopy); it is also known as electrochemical impedance spectroscopy (EIS), is a method for electrical engineering, physics, chemistry and material science, by analyzing the impedance of a given system over a wide range of frequencies of the applied electric field. It is based on the interaction of an external field with the electric dipole moment of the sample, often expressed by permittivity. EIS often used to characterize materials in electrochemistry, semiconductors, soiled electrolytes, corrosion, solid-state devices, batteries, capacitors, fuel cell, and other electrochemical power sources. The output of the EIS is impedance spectrum which is a subject of further analyses and interpretation.

In EIS, a small sinusoidal voltage is placed on the sample at a different frequencies ranges, thus, it is alternating current. The value of the current induced by the voltage applied and the phase angle between the potential and current maxima measured by controlling computer system.

Often, data obtained by EIS is expressed graphically in a Bode plot or a Nyquist plot [13].

An example of a Bode plot is shown below for a simple electrical circuit. It consists of a resistor and a capacitor in parallel.

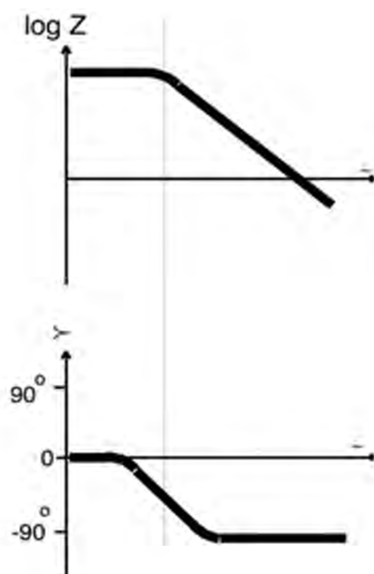

Fig. 3.6. Impedance spectra of a resistor and a capacitor in parallel [13].

Impedance is the opposition to the flow of alternating current (ac) in a complex system. A passive complex electrical system comprises both energy dissipater (resistor) and energy storage (capacitor) elements. If the system is purely resistive, then the opposition to ac or direct current (dc) is simply resistance.

For dc condition Ohms low applied

$$V = iR \tag{3.11}$$

For ac condition Ohms low applied

$$V = iZ \tag{3.12}$$

From ac conditions the impedance can be calculated by setting the input potential and measuring the induced current. When the phase angle, θ, between the voltage applied and the current induced is zero, then a pure resistance is present. When a phase angle of 90° is measured between the voltage and current at the same frequency, a pure capacitance is present. When a phase angle of 90° is measured between the voltage and current at the same frequency, a pure capacitance is present. Angles between these values can mean a combination of a capacitor and resistor is present. As impedance is a complex quantity, it is customary to plot the impedance, usually the log of the impedance magnitude, as a function of frequency and in addition the phase angle as a function of frequency. These are known as Bode plots. Almost any physico-chemical system, such as electrochemical cells, mass-beam oscillators, and even biological tissue, possesses energy storage and dissipation properties. EIS examines them. This technique has become very popular in the research and applied chemistry over the past few years and

is now being widely employed in a wide variety of scientific fields such as fuel cell testing, bimolecular interaction, and micro-structural characterization. Often, EIS reveals information about the reaction mechanism of an electrochemical process: different reaction steps will dominate at certain frequencies, and the frequency response shown by EIS can help identify the rate limiting step.

The impedance spectrum of an ideal capacitor has no real part. The imaginary part is

$$Z''_C = \frac{1}{\omega C} \tag{3.13}$$

which is in log-log plot displayed as a straight line with slope -1,

$$\log Z''_C = \log \frac{1}{\omega C} = -\log \omega - \log C \tag{3.14}$$

which intercepts the axis ω =1 for log Z''C = –log C.

The frequency dependent impedance of a resistor and a capacitor in series is:

$$Z^* = Z_R + Z_C = R + i\frac{1}{\omega C} \tag{3.15}$$

The frequency dependent impedance of a resistor and a capacitor in parallel is:

$$\frac{1}{Z} = \frac{1}{Z_R} = \frac{1}{Z_C} \Leftrightarrow Z^* = \frac{R}{1 + jR^2C^2\omega^2} - j\frac{R^2C\omega}{1 + R^2C^2\omega} \tag{3.16}$$

Until certain frequency ω=1/ τ the real part is constant, after which it drops off with slope -1. The imaginary part goes thought a maximum for ω=1/ τ. With τ = RC the eq. (3.16) for the impedance is re-cast,

$$Z^* = R\{\frac{R}{1 + (\omega\tau)^2} - j\frac{\omega\tau}{1 + (\omega\tau)^2}\} = \frac{R}{1 + i\omega\tau} \tag{3.17}$$

from which it can be seen that the characteristic angular frequency must lie at ω = 1/ τ.

The relation between the properties of a macroscopic capacitor and the properties of the dielectric between the capacitor plates is

$$C^* = \frac{\varepsilon_r^* \varepsilon_0 A}{d} \tag{3.18}$$

3.1.6 Dielectric spectroscopy

Dielectric spectroscopy is formally a branch of the impedance spectroscopy. The basic quantity used in the (DRS) is capacity, as shown in the following text, or, when converted to the dimensionless material property, permittivity ε as a function of frequency ε(ω).

Dielectric spectrum is the frequency dependence of the permittivity .the features of dielectric spectrum reveals basic physical properties of a material. Whether the material behaves as a simple resistor or capacitor, or specific molecular relaxation or ionic conductivity takes place, can be determined from the spectrum.

The dielectric in the capacitor affects the applied ac voltage, such that both amplitude and the phase are changed. The dielectric analyzer extracts the frequency dependent impedance from a comparison between the applied and the resultant voltage. For the purpose of dielectric spectroscopy, the impedance is then converted to the capacitance through the following equation

$$Z = \frac{V}{I} = \frac{1}{i\omega C} \tag{3.19}$$

And finally divided by vacuum capacitance of the cell C_0, to return the dielectric spectrum, formally written as

$$\varepsilon_r^*(\omega) = \frac{C}{C_0} = \varepsilon'(\omega) - i\varepsilon''(\omega) \tag{3.20}$$

The corresponding conductivity spectrum is calculated directly from dielectric spectrum using the relation

$$\overline{\sigma}(\omega) = \sigma(\omega) - i\sigma(\omega) = i\omega\varepsilon_0(\varepsilon_r^*(\omega) - 1) \tag{3.21}$$

3.1.7 Single relaxation time model: the Debye equation

The polarization does not establish immediately after the application of the constant electric field (dc field), but it rather takes time. A part of dipoles, in particular those, whose formation is related to the shift of the electron shell, respond to the application of the electric field much more quickly than others. Electric methods allow the observation up to frequencies of 10^{10} – 10^{11} Hz and therefore it can be said that polarization mechanism that are quicker than that cannot be monitored and we see only the result as if it happened instantaneously.

These polarizations are denoted as elastic polarizations P_∞ and the permittivity corresponding to them is denoted as optical permittivity ε_∞.

Polarizations, which need at least 10^{-11}s and more, are denoted relaxation polarizations. The permittivity corresponding to the situation, when all polarizations reach their steady state (including the slowest ones), i.e. the permittivity corresponding to the polarization P_S after an infinite time, is denoted as static ε_S.

The time development of the polarization after the application of the constant electric field (dc field) are shown below

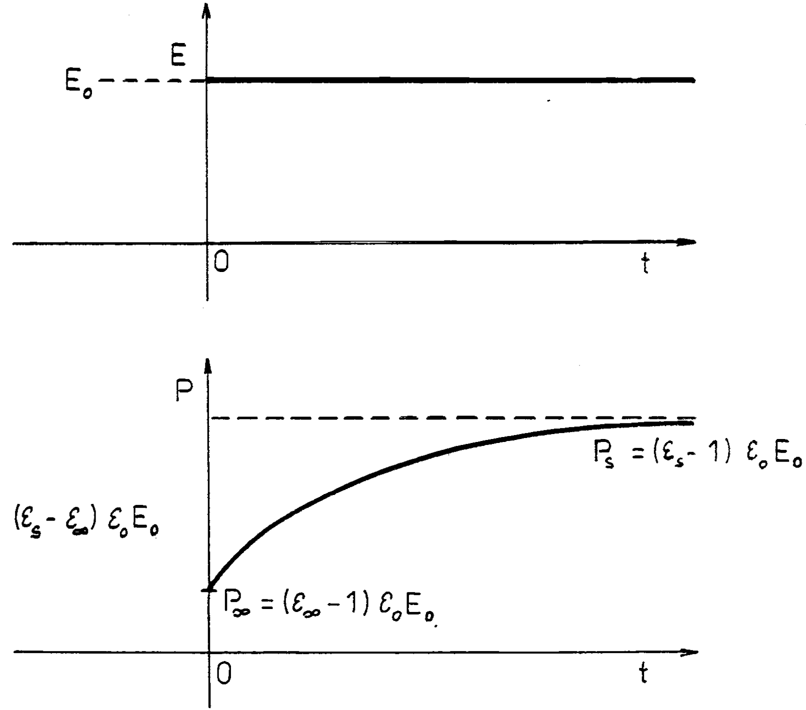

Fig. 3.7. Time development of the polarization after the application of a constant field [14].

The dipolar polarization is defined by the first order differential equation:

$$\tau \frac{dP_d(t)}{dt} + P_d(t) = (\varepsilon_S - \varepsilon_\infty)\varepsilon_0 E \tag{3.22}$$

where τ is the relaxation time characteristic of the polarization kinetics establishment.

Under dc electric field $E = E_0$ considering the boundary conditions on P_d, the solution is written:

$$P_d = (\varepsilon_S - \varepsilon_\infty)\varepsilon_0 E\left(1 - \exp(-\frac{t}{\tau})\right) \tag{3.23}$$

In this model the dielectric permittivity is given by:

$$\varepsilon(t) = \varepsilon + (\varepsilon - \varepsilon)(1 - \exp(-\frac{t}{\tau})) \tag{3.24}$$

In the presence of a dynamic electric field $E = E_0 \cos \omega t$, represented by the complex expression $E^* = E_0 \exp(i\omega t)$, the solution, in established regime, of differential equation (3.22) is:

$$\varepsilon^*(\omega) = \frac{(\varepsilon_S - \varepsilon_\infty)}{(1 + i\omega\tau)} \tag{3.25}$$

The total complex permittivity:

$$\varepsilon^*(\omega) = \varepsilon'(\omega) - i\varepsilon''(\omega) \tag{3.26}$$

is then decomposed into the real and imaginary parts as follows:

$$\varepsilon'(\omega) = \varepsilon_\infty + (\varepsilon_S - \varepsilon_\infty) \times \frac{1}{1+\omega^2\tau^2} \tag{3.27}$$

$$\varepsilon''(\omega) = (\varepsilon_S - \varepsilon_\infty) \times \frac{\omega\tau}{1+\omega^2\tau^2} \tag{3.28}$$

These expressions are designed in the literature by the Debye equations.

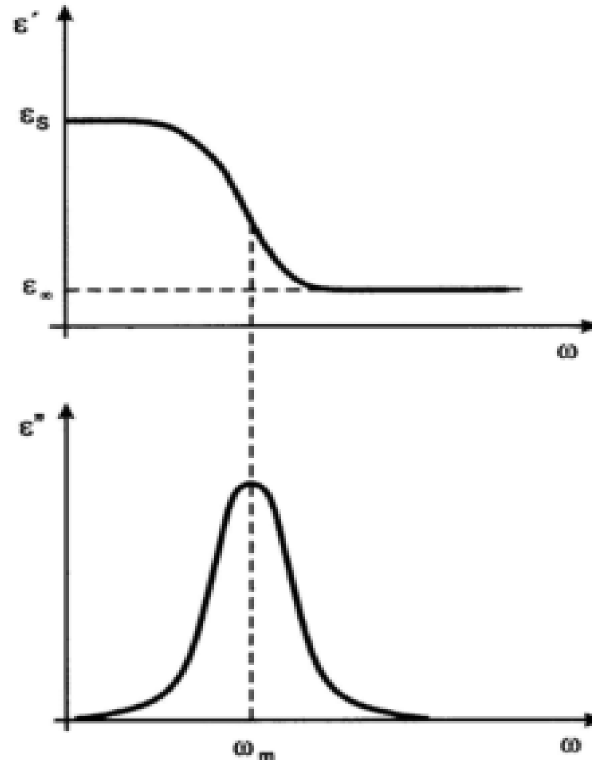

Fig. 3.8. Complex permittivity predicted by Debye equation [10].

3.1.8 The analysis of dielectric data in terms of relaxation time (frequency)

The dielectric relaxation response is generally analyzed by the Havriliak–Negami (HN) relaxation function which is a frequency-domain function. The HN function is then used to obtain the complete spectra of dynamic properties the specific relaxation time (frequency)

$$\hat{\varepsilon}(\omega) = \varepsilon_\infty + \frac{(\varepsilon_s - \varepsilon_\infty)}{[1+(j\omega\tau_0)^\alpha]^\beta} \tag{3.29}$$

where α and β represent the width and the skewness (asymmetry) of the dielectric loss number ε″(ω) when viewed in the log(ε″) – log(ω) plot.

The Havriliak–Negami function is an empirical modification of the Debye relaxation model for $\alpha = 0$ and $\beta = 1$ with a single relaxation time, e.g. (3.27) (3.28).

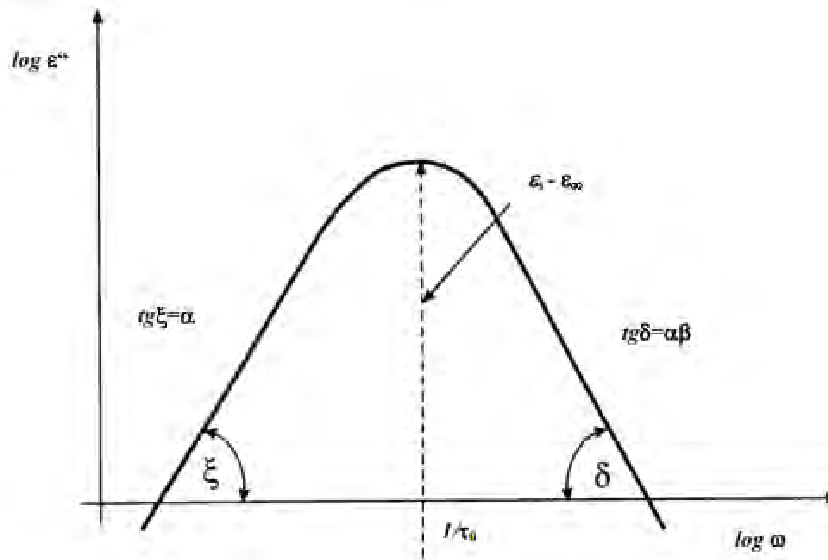

Fig. 3.9. The Havriliak–Negami function in log/log view [10].

Debye relaxation is the dielectric relaxation response of an ideal dielectric with freely rotating, non-cooperative dipoles, which assumes that dipoles do not influence each other through their interaction with the lattice in an alternating external electric field.

a) Cole-Cole (CC) function

The Cole-Cole equation is a special case of the Havriliak–Negami function when the symmetry parameter β is equal to 1 – and $0 < \alpha < 1$ that is, when the relaxation peaks are symmetric:

$$\hat{\varepsilon}(\omega) = \varepsilon_\infty + \frac{(\varepsilon_s - \varepsilon_\infty)}{1 + (j\omega\tau_0)^{1-\alpha}} \tag{3.30}$$

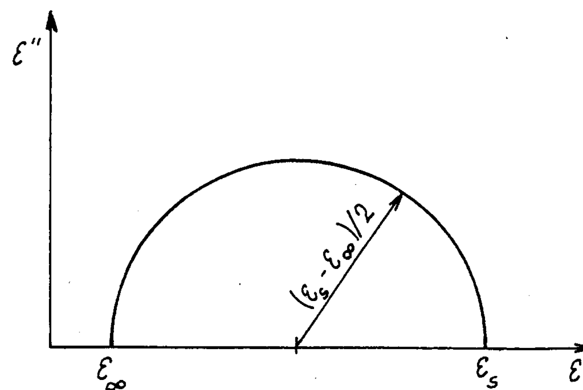

Fig. 3.10. Graphical representation of the Debye's formula [14].

b) Cole-Davidson (CD) function

The Cole-Davidson function with a distribution of relaxation times follows for $\alpha = 0$ and $0 < \beta < 1$ [9].

$$\hat{\varepsilon}(\omega) = \varepsilon_\infty + \frac{(\varepsilon_s - \varepsilon_\infty)}{1 + (j\omega\tau_0)^\beta} \tag{3.31}$$

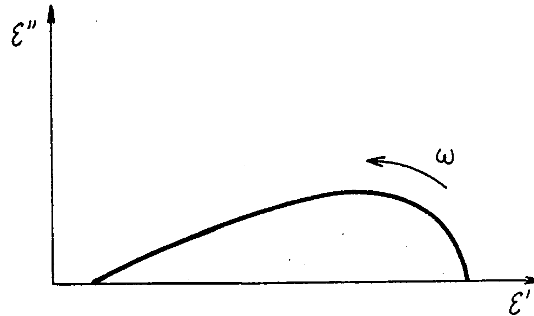

Fig. 3.11. The Cole – Cole plot for HN function [14].

3.1.9 The relation between dielectric relaxation and chemical structure

Several relaxation steps in the real part and imaginary part of the complex permittivity can be observed in single dielectric material, and these are dielectrically active if they incur significant orientation of molecular dipoles. In polymer there are mainly two types of dielectric relaxation: dipolar segmental relaxation and dipolar group relaxation.

In these two types the multiplicity of relaxation processes is seen on the curve of the temperature and frequency dependence of imaginary part of the complex permittivity. Dielectric losses caused by dipolar segmental relaxation are associated with the micro Brownian motion of segments in polymeric chains, while dielectric losses caused by dipolar group relaxation are associated with the localized movement of molecules [11].

Dielectric relaxation processes are classified by means of the thermally stimulated relaxation technique, to primary relaxation mode α, and secondary relaxation mode β, γ, δ, and so on beginning at the high temperature end, as shown in Fig. 3.12.

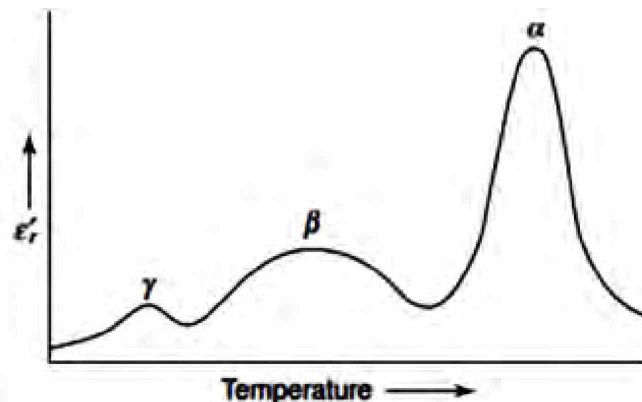

Fig. 3.12. The imaginary part of complex permittivity as a function of temperature at fixed frequency [11].

The primary relaxation mode α is the most intensive peak of imaginary part of complex permittivity observed after the vitreous transition, and near the glass transition temperature (T_g).

The dipolar segmental relaxation corresponds to the α relaxation associated with the micro Brownian motion, and the dipolar group relaxation mechanisms correspond to the β, γ, δ etc. relaxations, the imaginary part peak in the region of β relaxation is mainly due to the movement of side groups or small units of main chains or small units of main chains. The relative strength of the α and β dielectric relaxation depends on the degree of the orientation of dipolar groups through the limited mobility allowed by the β process before the more difficult, but more extensive, mobility for the α process comes into play [11]. The mechanisms of a β process may depend on the nature of the dipolar group concerned and its position on the polymer chain:

- rotation of a side group about a C–C chain.
- conformational flip of a cyclic unit involving the transition from one chain form to another, altering the orientation of a polar substituent [11].
- local motion of a segment of the main chain, since the dipolar group is directly attached to the main chain and cannot move independently.

The γ relaxation peak occurs mainly due to the movement of small kinetic units of the main or the side chains, or due to the crankshaft rotation below the glass transition temperature.

3.1.10 Temperature dependence

The temperature dependence of relaxation time exhibits a thermally activated process, mostly described by the Arrhenius equation. This can be expressed by Arrhenius equation as follows

$$\tau = \tau_{0a} \exp\left(\frac{H}{kT}\right) \tag{3.32}$$

Where τ_{0a} is pre-exponential factor, H is the activation energy, and k is Boltzmann constant.

The Arrhenius equation was described by the barrier theory or thermal activation mechanism. The relaxing entity is presented by the variation of the Gibbs free enthalpy G. The orientation of the relaxing entities corresponds to the crossing of energetic barriers separating the different minima of the G [11]. By Boltzmann equation classical description, for the transition probability p, a variation as:

$$P \propto \exp\left(-\frac{\Delta G}{kT}\right) \tag{3.33}$$

where ΔG is the height of the enthalpic barrier for two sites.

The relaxation time varies in the opposite direction to the probability, and is in the form:

$$\tau = \tau_0 \exp \frac{\Delta G}{kT} \tag{3.34}$$

We must express ΔG as a function of activation enthalpy ΔH and of the activation entropy ΔS, in order to obtain an explicit equation as a function of temperature

$$\tau = \tau_0 \exp - \frac{\Delta S}{k} \exp \frac{\Delta H}{kT} \tag{3.35}$$

So

$$\tau_{0a} = \tau_0 \exp\left(- \frac{\Delta S}{k} \right) \tag{3.36}$$

The activation entropy comes from the Boltzmann equation

$$\Delta S = k \ln \Omega \tag{3.37}$$

If Ω is the number of sites related to the relaxing entity, τ0 can by derived from Eyring's chemical activation theory:

$$\tau_0 = \frac{h}{kT} \tag{3.38}$$

where h is Planck constant

$$\tau = \tau_{0a} \exp\left(\frac{H}{kT} \right) \tag{3.39}$$

This is the Arrhenius equation.

The corresponding variation of logτ as a function of inverse temperature is shown below

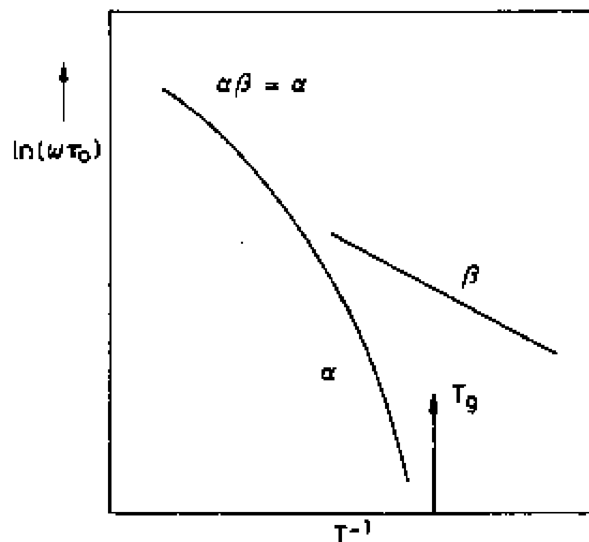

Fig. 3.13. Temperature dependence of the relaxation times [14].

By replacing τ with a temperature dependent τ in the Arrhenius equation, the Debye equation (Equation (3.27) and Equation (3.28)) can be written as

$$\varepsilon'(\omega) = \varepsilon_\infty + (\varepsilon_S^T - \varepsilon_\infty^T) \times \frac{1}{1 + \omega^2 \tau^2 \exp\left(\frac{H}{kT}\right)} \quad (3.40)$$

$$\varepsilon''(\omega) = \left(\varepsilon_S^T - \varepsilon_\infty^T\right) \times \frac{\omega\tau \exp\left(\frac{H}{kT}\right)}{1 + \omega^2 \tau^2 \exp\left(\frac{H}{kT}\right)} \quad (3.41)$$

where ε_S^T and ε_∞^T are the value of the ε_s and ε_∞ at temperature T. The relative permittivity ε′ and the loss peak ε″ decrease with increasing temperature, and the loss peak shifts toward higher temperatures, as shown below:

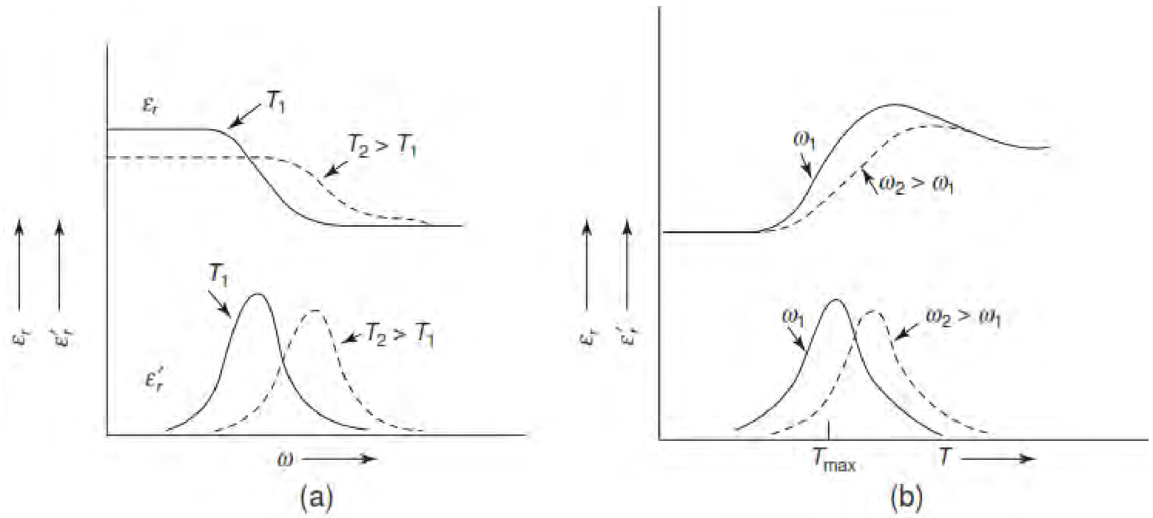

Fig. 3.14. a) ε′ and ε″ as a function of ω for fixed temperatures,
b) ε′ and ε″ as a function of temperature for fixed frequencies [11].

3.1.11 Time domain dielectric spectroscopy charging /discharging currents and Hamon approximation

Hamon approximation is applied to evaluation of the dielectric loss and the relaxation time from transient charging current data when a step voltage is applied to it. The discharge current of a dielectric can be expressed approximately by a power law function:

$$i(t) = K.t^{-s} \quad (3.42)$$

where s lies mostly within the interval (0, 1).

If we consider the relation between the discharge current i(t) and the decay function Ψ (discharge current normalized to a unit electrode area, a unit dielectric strength and a unit electric field)

$$i(t) = (\varepsilon_s - \varepsilon_\infty)\varepsilon_0 E_0 A.\Psi(t) \tag{3.43}$$

the decay function can be now written as

$$\Psi(t) = \frac{K.t^{-s}}{A\varepsilon_0 E(\varepsilon_s - \varepsilon_\infty)} = \frac{K}{C_0 U(\varepsilon_s - \varepsilon_\infty)} t^{-s} \tag{3.44}$$

where A is the surface of electrodes in the capacitor system, C_0 is the corresponding geometrical capacity, and U is the applied voltage.

The imaginary part of complex permittivity can be expressed as

$$\varepsilon'' = (\varepsilon_s - \varepsilon_\infty)\int_0^\infty \psi(x)\sin\omega x\,dx \tag{3.45}$$

Putting Ψ(t) into above equation will give

$$\varepsilon'' = \frac{K}{C_0 U}\int_0^\infty t^{-s}\sin\omega t\,dt \tag{3.46}$$

The Fourier transform of the power law function holds as following for s in interval (0, 2)

$$\int_0^\infty t^{-s}\sin\omega t dt = \Gamma(1-s)\sin[\frac{(1-s)\pi}{2}]\omega^{(s-1)} \tag{3.47}$$

Γ (1-s) is the value of the Euler's Gamma function for the argument 1 – s. Putting equation (46) into (47) will give:

$$\varepsilon''(\omega) = \frac{K}{CU}\Gamma(1-s)\sin[\left[\frac{(1-s)\pi}{2}\right]\frac{\omega^s}{\omega} \tag{3.48}$$

By substituting K by the expression for the discharge current (42) we get:

$$\varepsilon''(\omega) = (\omega.t)^s.\Gamma(1-s).\cos(s\pi/2).\frac{1}{C_0 U}\frac{i(t)}{\omega} \tag{3.49}$$

The relation between ω and t are given by the mathematical formula

$$(\omega.t)^s.\Gamma(1-s).\cos(s\pi/2) = 1 \tag{3.50}$$

This necessitates that the product ω.t be constant

$$\omega.t = \frac{1}{\left[\Gamma(1-s).\cos(s\pi/2)\right]^{\frac{1}{s}}} = m = konst. \tag{3.51}$$

Hamon proved that for s ∈ (0.3; 1.2) the constant m in the above equation is equal to:

$$m = 0.61 \pm 0.02 \;\; for\, n \in (0.3, 1.2)$$

which means that

$$t = \frac{0.61}{\omega} = \frac{0.61}{2\pi f} = \frac{0.1}{f} \tag{3.52}$$

If the conditions in (3.50) are met, then the ε″ in the equation (3.49) will acquire the following form:

$$\varepsilon''(f) = \frac{i\left(\frac{0.1}{f}\right)}{2\pi C_0 U f} \tag{3.53}$$

3.2 Conduction mechanisms

In order to better understand tantalum capacitors as MIS systems, these conduction mechanisms must first be fully understood. In this review we will discuss a number of ways in which an electric current flows through an insulating thin oxide film. It has gradually become clear that electric properties of thin oxide film insulators are determined not so much by intrinsic properties of the insulator but rather by other properties, such as the nature of the electrode insulator contact, due to various structure defects like impurities, vacancies, and interstitials acting as donors or acceptors. Electrical behavior of thin oxide films may also be significantly affected by a small biasing voltage causing high fields of the order 10^6 V/cm in the film at the cathode–insulator interface with subsequent field emission injection of large current from the cathode into the conduction band of the insulator. Typically, two possible mechanisms appear at the metal-insulator interface: Schottky–Richardson emission and Poole–Frenkel emission. The conduction mechanism in thin insulator films is dominated by the Schottky emission in a lower electric field, and by the Poole–Frenkel effect in a higher electric field; at high electric fields, the tunneling effect becomes obvious [15]. This tunneling enhances the Poole–Frenkel emission.

The following sections will focus on the more dominating and frequently mentioned mechanisms: specifically the Poole–Frenkel Effect, Space-Charge-Limited Current, the Schottky Effect and Fowler–Nordheim Tunneling.

3.2.1 Bulk-limited conduction

Bulk-limited conduction if it depends on trap properties of the insulator bulk.

Poole–Frenkel effect (PF)

The Poole–Frenkel effect (PF), known also as Frenkel–Poole emission, is a bulk-limited conduction mechanism that is often used to explain conduction in thin dielectric films. The electrons in thin dielectric film are generally trapped in localized states, they are not free to move around the crystal, but by thermal emission of charge carriers from Coulombic traps in the bulk of a dielectric or semiconductor, enhanced by the application of an external electric field, the Poole–Frenkel mechanism is caused. It involves the lowering of a potential energy barrier by applied field on one side of the trap which in turn increases the probability that an electron will escape from the trap to the conductive band. This process is shown in Fig. 3.15 where a Columbic potential at a donor center can be seen in the presence of an applied electric.

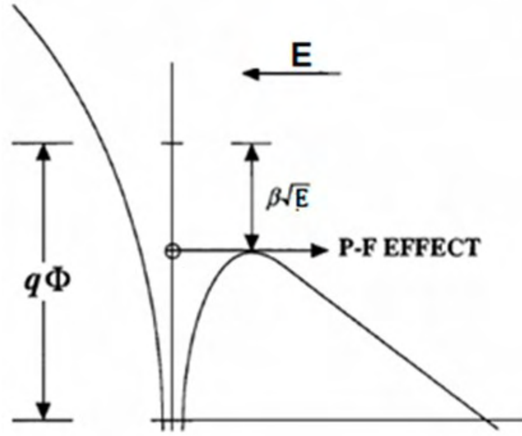

Fig. 3.15. Poole–Frenkel effect at a donor center [1].

qΦ in Fig. 3.15 is the ionization potential of the trap, the barrier is decreased by an amount $q\Phi_{eff}$, which is proportional to square root of the applied electric field β√E.

The decreasing of the trap side is now at an effective ionization potential $q\Phi_{eff}$ which can be written as:

$$q\phi_{eff} = q\phi - \beta_{PF}\sqrt{E} \tag{3.54}$$

The constant, β_{PF}, is the Poole–Frenkel coefficient and given by:

$$\beta_{PF} = \sqrt{\frac{e^3}{4\pi\varepsilon_0\varepsilon_r}} \tag{3.55}$$

where ε_0 is the permittivity of free space, and ε_r is the relative permittivity of the material.

When electrons escape over the effective barrier height, they enter the quasi-conduction band of the material. The quasi-conduction band and the ground state of the trap can be analogously compared to the conduction and valence bands of a crystalline solid. The conductivity due to thermal ionization of the Coulombic traps was approximated by Frenkel to be proportional to the free carrier concentration of the quasi-conduction band. He also used the Boltzmann approximation and assumed that the Fermi level was located at the middle of the band gap. From these assumptions the conductivity as a function of the electric field [1] can be written as

$$\sigma = \sigma_0 \exp\left(\frac{\beta_{PF}\sqrt{E}}{2kT}\right) \tag{3.56}$$

Where

$$\sigma_0 = C\exp[-\frac{q\phi}{2kT}] \tag{3.57}$$

where C is a proportionality constant. By multiplying equation (3.57) by the electric field, the current density J due to the Poole–Frenkel effect can be given as:

$$J = CE \exp[-\frac{q\phi - \beta_{PF}\sqrt{E}}{2kT}] \tag{3.58}$$

where J is the current density, k is the Boltzmann's constant and T is the temperature.

Space-Charge-Limited Current process

Space-Charge-Limited current (SCLC) conduction occurs when a contact electrode is capable of injecting either electrons into the conduction band or holes into the valence band of a semiconductor or insulator. The electrodes inject electrons but the electrons move so slowly in the solid that they create a negative space charge built up in the bulk; their number will exceed the intrinsic number of carriers (rate of charge-carrier injection is higher than the rate of recombination) and there will be a net negative space charge in the bulk of the insulator. This will cause a non-uniform electric field. The current is limited by the rate at which electrons cross the sample through the space charge. SCLC is a bulk limited process [1].

Child's law gives the space-charge limited current (SCLC) in a plane-parallel vacuum diode. As a function of the distance and potential difference between anode and cathode given as

$$I_a = JS = \frac{4\varepsilon_0}{9}\sqrt{2e/m_e}\,\frac{SV_a^{3/2}}{d^2} \tag{3.59}$$

where I_a is the anode current, J the current density, S the anode surface inner area, and d separation between the cathode and the anode.

The Mott–Gurney law predicts the current density due to SCLC in an insulator in the absence of any trapping effects; it can be written as

$$J = \frac{9}{8}\mu\varepsilon_0\varepsilon_r\frac{V^2}{L^2} \tag{3.60}$$

where μ is the free carrier mobility of the material, εr is the relative permittivity of the material, ε_0 is the permittivity of free space, V is the applied bias, and L is the thickness of the insulator.

3.2.2 Electrode limited process

When the observed current is limited by the rate of electron injection at one of the electrodes and not by the rate at which the carriers in the bulk are transported through the material, then the conduction is injection limited.

Schottky Effect

The Schottky Effect generated by thermionic effect is caused by electron transport across the potential barrier via field assisted lowering at the metal–insulator interface. The Schottky Effect is very similar to the previously mentioned Poole–Frenkel (PF) effect. Instead of a fixed positive charge as in the PF effect, the Schottky Effect depends on a mobile positive image charge created by the escaping electron. While the PF effect is controlled by trap barriers in the bulk, the Schottky Effect is associated with interfacial barriers between a metal and a semiconductor.

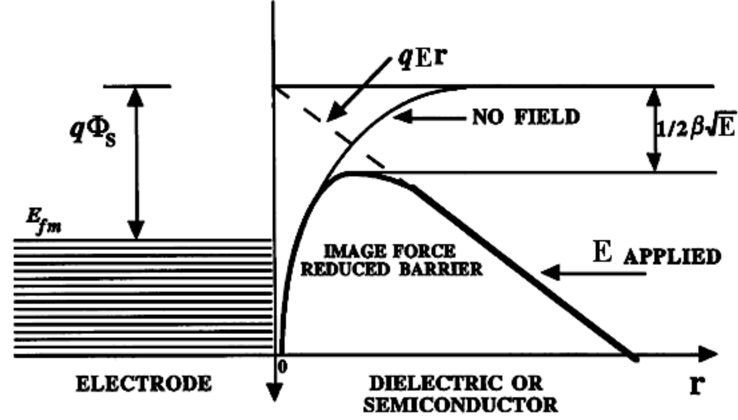

Fig. 3.16. Energy band diagram between a metal surface and a vacuum incorporating Schottky Effect with and without electrical field [1].

Therefore, the Schottky Effect is an electrode limited process. The Schottky current density is given by the following equation:

$$J_S = A^* T^2 \exp\left(\frac{\beta_S E^{1/2} - \phi_{FP}}{k_B T}\right) \tag{3.61}$$

Φ_{FP} is the contact potential barrier, T is absolute temperature, k_B is the Boltzmann constant, E is the applied field, and A* is the Richardson constant, and is given:

$$A^* = \frac{4\pi e m^* k^2}{h^3} \tag{3.62}$$

It is found that the logarithm of the Schottky current is linearly related to the square root of the applied electric field; the linear variation of the current corresponds either to the Poole–Frenkel effect or to Schottky emission conduction mechanism. For a trap state with Coulombic potentials, the expression is virtually identical to that of the Schottky emission. The barrier height, however, is the depth of the trap potential well; the Schottky coefficient is half of the Poole–Frenkel coefficient. Distinguishing between these two processes can be done by comparing the theoretical value of β with the value obtained experimentally through the calculation of the slope in the log J *vs.* E1/2 curves.

The slope of the Schottky plot, M_S, is proportional to β_s and is given by,

$$M_S = \frac{\beta_S}{2kT} \quad (3.63)$$

Fowler–Nordheim (FN) tunneling

Fowler–Nordheim (FN) tunneling is electric-field induced tunneling through a roughly triangular barrier. Representation of this process is shown below.

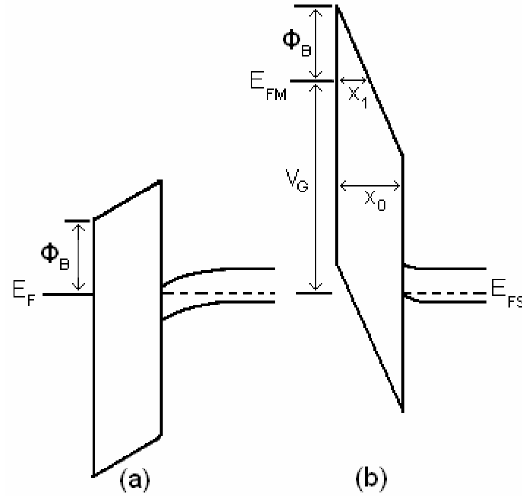

Fig. 3.17. Energy band diagrams (a) no field (b) high field [1].

The Fowler–Nordheim (FN) current density in the simplest form is given by the following equation:

$$J = AE^2 \exp\left(-\frac{B}{E}\right) \quad (3.64)$$

where

$$A = \frac{m}{m*} \frac{q^3}{8\pi h\phi_B} \quad (3.65)$$

$$B = \frac{8\pi}{3}\left(2\frac{m^*}{h^2}\right)^{1/2} \frac{\phi_B{}^{3/2}}{q} \quad (3.66)$$

where E is electric field, m the electron mass, m* the effective mass of the electron in dielectric, q the electron charge, h Planck constant, and Φ_B the barrier height at the injecting electrode.

3.3 Electrolytic capacitor

3.3.1 Parallel Plate Capacitor

The simplest model of capacitor consists of two conductive plates separated by a dielectric. The plates are connected to a constant voltage supply. Charge is stored on their facing surface with equal and opposite charge, the positively charged plate known as anode, and the negatively charged plate is the cathode. The density of charges can be easily measured by $\pm\rho = \pm Q/A$. As the electric field across the dielectric increases, this gives rise to a potential difference that increases proportionally to the charge. The ratio of the magnitude of the charge to the magnitude of the potential difference between the plates is defined as the capacitance of a capacitor.

$$C = \frac{Q}{V} \tag{3.67}$$

The capacitance of the device can be expressed as

$$C = \varepsilon_r \varepsilon_0 \frac{A}{d} \tag{3.68}$$

The capacitance depends mainly on plate geometry and the properties of the dielectric. It is directly proportional to the relative permittivity of the material separating the plates. The capacitance is greatest in devices made from materials with a high permittivity, large plate area, and small distance between plates.

Any dielectric material has a maximum electric field that can be applied, while still maintaining insulating properties. This is known as dielectric field strength of the insulating material. After this point the dielectric begins to breakdown and conduct current. The device can work within a range known as the working voltage. The working voltage can be defined by the manufacturer to be the maximum voltage at which the capacitor can operate.

3.3.2 Basic features of electrolytic capacitors

Electrolytic capacitors are often used when a large amount of charge is needed at relatively low voltage. Electrolytic capacitors are classified as such due to the fact that either one or both of the conductive plates is an electrolyte. An electrolyte is typically a solution that conducts electricity via the ions contained within the solution. The dielectric in an electrolytic capacitor is formed from the anode material itself by electrochemical process of anodization. The next step in the formation process, the anode, is typically a metal placed in an electrolyte bath and current flows through the anode to the cathode bath [1]. This current flow causes an oxidation of the anode surface, creating a thin oxide film that perfectly matches contours of the anode surface. The oxide will grow to a thickness determined by the applied voltage. As for the cathode electrode, it would be placed in contact with the dielectric to complete the

capacitor structure. However, since the chemically formed dielectric of the electrolyte capacitor is a very rough, thin, and fragile surface, the contact from the dielectric to the cathode plate must be made through a medium that can conform to the dielectric system [1]. For this we use a liquid electrolyte as a cathode in conjunction with its casing. The structure of electrolytic capacitor is shown below

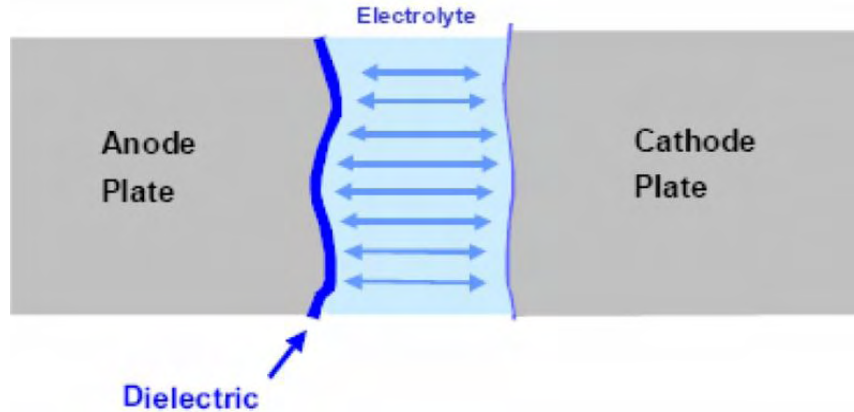

Fig. 3.18. Electrolytic capacitor [1].

Electrolytes have a lower conductivity than metal and therefore are used in situations when direct contact to the metal is not possible. The ionic current through the electrolyte helps to maintain the integrity by healing any dc leakage sites through reformation of dielectric in a fashion similar to how it was originally formed [1]. An electrolytic capacitor distinguishes itself from other capacitors in having high capacitance per volume and weight, which makes it particularly suitable for passing or bypassing low-frequency signals and storing large amounts of energy.

3.3.3 Construction of tantalum oxide capacitor

The construction of tantalum capacitor begins with a fine tantalum powder from pure elemental tantalum metal. This powder traditionally has a spherical grain with typical particle size is between 2 and 10 µm. Tantalum powder has been shrinking in diameter with improved manufacturing processes. This is according to the industry trends of increasing volumetric efficiency by having higher capacitances in the same or a smaller package. To accomplish this, the surface area within a given volume must be increased by using a finer tantalum particles size. The powder is mixed with a binder which allows smooth pressing and homogenous flow and powder loading into the press tool [3]. The anode of the capacitor is formed from tantalum powder by pressing it into a pellet around a tantalum wire. This pellet is a compact collection of the tantalum particles. Within the pellet there is a large amount of open volume. As the particles are pressed together their spherical geometry creates point contacts, electrically contacting them while leaving large gaps and channels between particles. The tantalum wire creates a common electrical contact for all tantalum particles within the pellet [1]. The pellet now has a tantalum wire surrounded by tantalum powder. At this point there are finite contacts between all the particles and wire, and these contacts are weak [1]. The pellet is than sintered in a vacuum at extremely high temperature 1400–1800 °C to

expand the bond areas of each contact point. This process decreases the volume of the pellet slightly by ensuring electrical connection between all the grains as illustrated in Fig. 3.19.

The sintering process helps to drive out any contaminants that were introduced during the pressing process. After sintering, the pellet is essentially pure tantalum. All particles are now electrically connected.

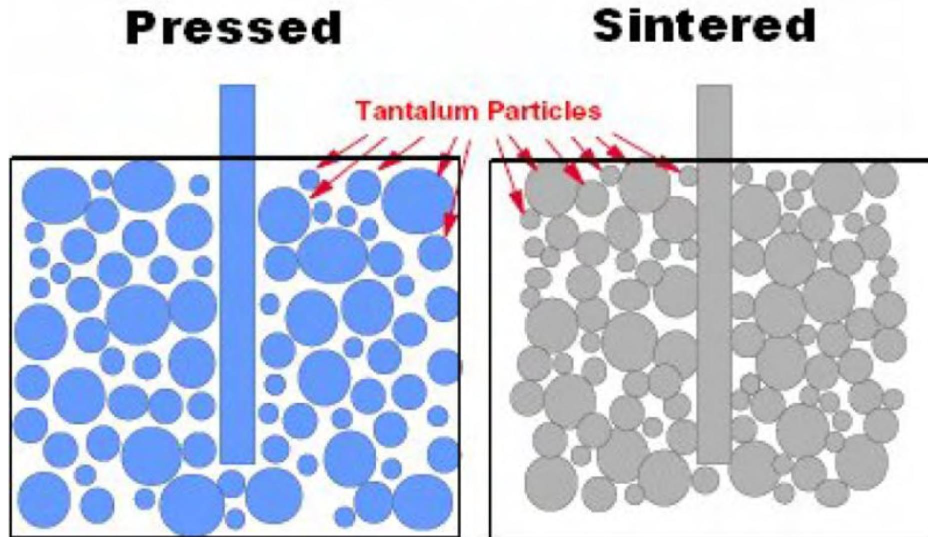

Fig. 3.19. Tantalum pellet after pressing and sintered [1].

Now that the anode is completed the next step in the process is to cover all exposed surfaces of tantalum metal with a dielectric layer. This is accomplished by submersion into an electrolyte bath and passing current through the system [1]. The liquid electrolyte fills all the voids and channels and makes a contact with tantalum particles and wire. Oxygen from the electrolyte then combines with tantalum to form an oxide. The type of oxide is determined by electrolyte solution and the outcome is tantalum pent-oxide (Ta_2O_5) [1]. The thickness and consistency of the oxide layer is controlled by the time, current, and formation voltage. The overall thickness is approximately 1.8 nm per volt of formation voltage [1].

$$2\ Ta \rightarrow 2\ Ta^{+5} + + 10\ e^{-}$$

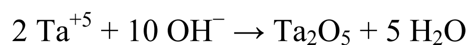

$$2\ Ta^{+5} + 10\ OH^{-} \rightarrow Ta_2O_5 + 5\ H_2O$$

The second electrode is cathode material that must be applied in liquid form to penetrate all voids and channels that have been formed. The pellet is dipped into an aqueous solution of $Mn(NO_3)_2$ which comes into contact with all dielectric layer within and around the pellet. The pellet is heated till 250 °C to dry the solution and convert it to MnO_2, according to the reaction

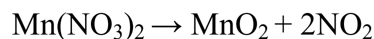

$$Mn(NO_3)_2 \rightarrow MnO_2 + 2NO_2$$

This dip and dry step is repeated till there is a thick and continuous coating of MnO_2 in contact with dielectric [1]. The silver paint is applied to the top of the MnO_2 to allow a low resistance external connection to the capacitor. Before the application of silver, a

coating of graphite solution is applied to eliminate interfacial resistances due to the contact and silver oxide formation at interfacial region [1]. The pellet is cured at 150–200 °C to dry the graphite and silver. The construction of the capacitor till this point is illustrated to Fig. 3.20.

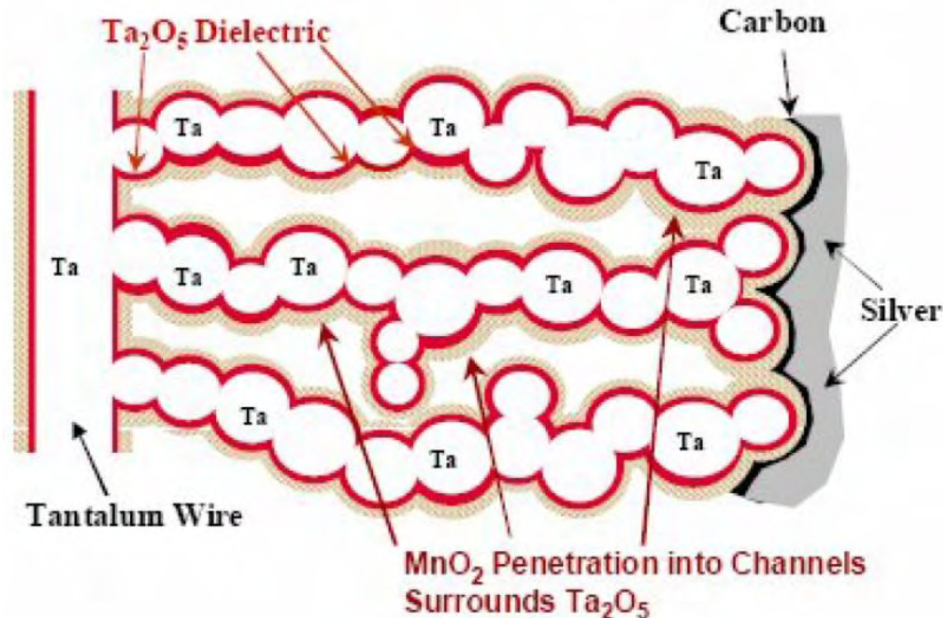

Fig. 3.20. Anode and cathode plate structures in tantalum pellet [1].

Lead-frame is connected to the silver paint with conductive epoxy to make anode connection. Wire is welded to cathode terminal of the lead-frame [1]. The last step is to enclose the capacitor in modeled plastic while allowing the lead frame to extend out of the model to create the contact as shown below:

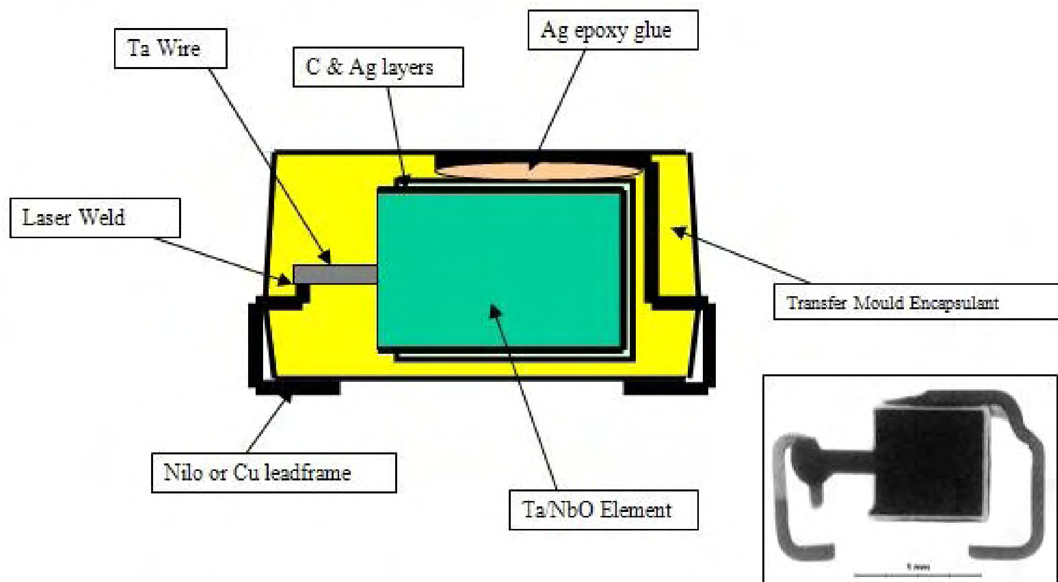

Fig. 3.21. Final assembly of tantalum and niobium oxide capacitor [3].

3.3.4 Stability of tantalum oxide capacitor

The self-healing process is based on thermally induced oxidization of the conductive MnO_2 counter electrode and converts conductive manganese dioxide into a lower oxidation level Mn_2O_3; this conversion dramatically increases the resistivity [16]. The complete reaction is

$$MnO_2 + \xrightarrow{heat} Mn_2O_3 + O^*$$

If the dielectric surface on the tantalum anode has thinner dielectric than surrounding area, a higher current will flow through that site as shown in Fig. 3.22 and will locally heat up the surrounding area. Thus the conductive site is effectively “plugged” or “capped” [16] as shown in Fig. 3.23.

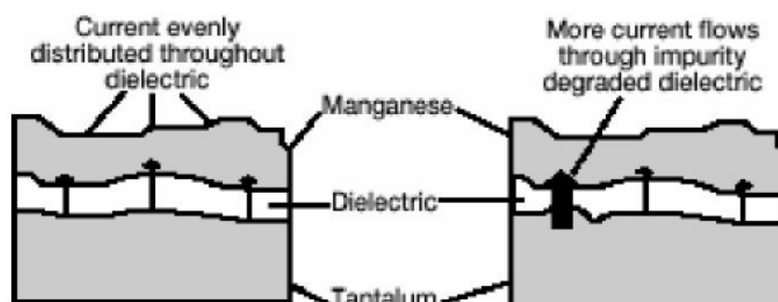

Fig. 3.22. Cross section showing self-healing system [16].

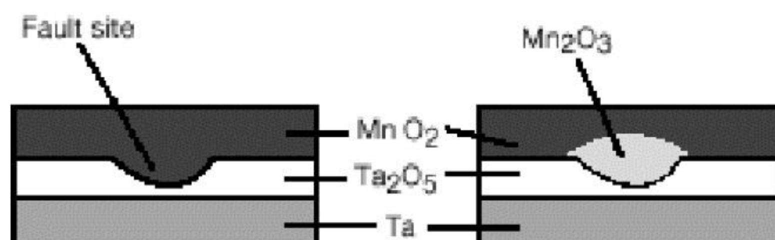

Fig. 3.23. The fault site in dielectric after self-healing process [16].

At a temperature higher than that required for self–healing, the dielectric will convert from an amorphous to a crystalline structure. This crystalline conversion begins at the fault site and spreads out across the dielectric, eliminating any previously healed sites [1]. Released oxygen is absorbed by tantalum, reaching exothermic reactive site in the presence of an abundant supply of oxygen. The heated MnO_2 rapidly supplies excess oxygen and converts to its lower oxidation level Mn_2O_3. This causes destructive burning of the component. This reaction is commonly referred to as ignition [1], as shown below.

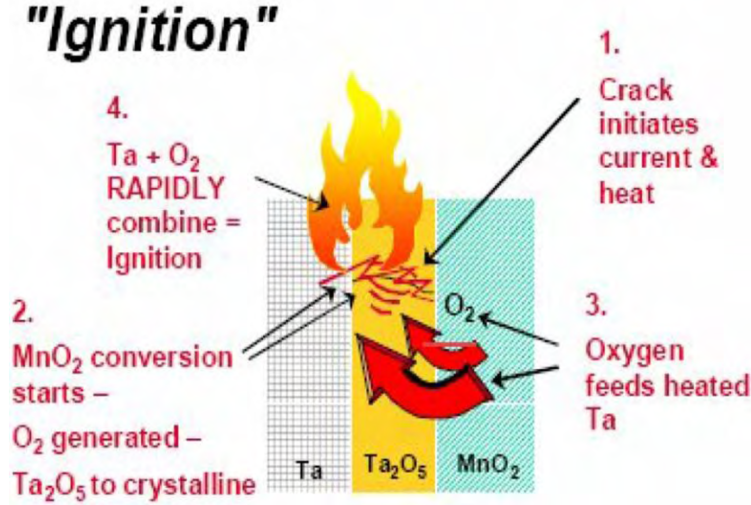

Fig. 3.24. Theoretical ignition of failure [1].

3.3.5 Electrical performance

Real capacitor is modeled by equivalent circuit as shown in Fig. 3. 26a. Here R_w represents wire connection resistance (typically in order of mΩ). The resistance R_w is a function of the temperature and the frequency. Equivalent series inductor L_{esi} is created when current is restricted to follow a defined physical path (typically in order of nH). R_{leak} accounts for leakage currents through the insulator dielectric and it depends on the applied voltage and temperature. The capacitance C is a function of the relative permittivity which mainly depends on temperature, and applied voltage. We can simplify the circuit by employing frequency–domain reduction technology and, assuming $\omega^2.R_{leak}^2.C^2 >> 1$, to that depicted on Fig. 3.26b. The quantity R is the equivalent circuit resistance and it is equal to:

$$R_{esr} = R_w + \frac{1}{\omega^2 R_{leak}^2 C^2} \tag{3.69}$$

It is frequency dependent. The equivalent series resistance represents the power loss and thus the heat dissipation in the capacitor. The real power is calculated as the following

$$P_{cap} = I_{C,rms}^2 R_{esr} \tag{3.70}$$

The capacitor will have a limit to how much RMS current (ripple current) it can accommodate. The model shown in Fig. 3. 26b also conveys another interesting fact: at high enough frequencies, the capacitor will actually start looking like an inductor! [17] The impedance of model capacitor is equal to:

$$Z_{cap} = R_{esr} + j\left(\omega L_{esl} - \frac{1}{\omega C}\right) \tag{3.71}$$

The ESR resistance represents the real part of the impedance while the imaginary part is comparable to reactance 1/(ωC) at low frequency and L_{esl} at high frequency.

The complex admittance Y is made up by R_{leak} in parallel with C as shown in Fig. 3.26a.

$$Y = \frac{1}{Z} = \frac{1}{R_{leak}} + jC\omega = j\omega C_0\left(\frac{C_p}{C_0} - j\frac{1}{R_p\omega C_0}\right) = j\omega C_0\varepsilon^* \tag{3.72}$$

where

$$\varepsilon' = \frac{C}{C_0} \tag{3.73}$$

$$\varepsilon'' = \frac{1}{\omega C_o R_{leak}} \tag{3.74}$$

The loss or dissipation factor of the dielectric is defined by expressing the loss angle tangent of the dielectric, which is an amount expressing the ratio of the current in R_{leak} with the current in C as shown

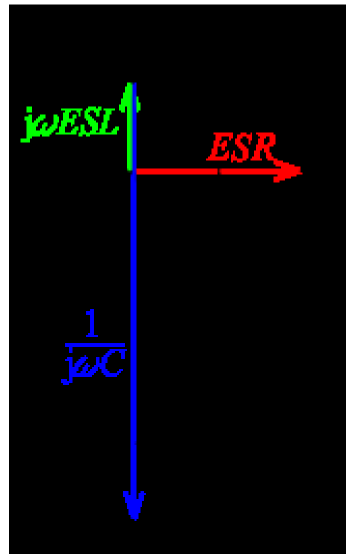

Fig. 3.25. The loss tangent is defined by the angle between
the capacitor's impedance vector and the negative reactive axis.

is written:

$$\tan\delta = \frac{1}{\omega C_0 R_{leak}} \tag{3.75}$$

Dissipation factor of the capacitor tan δ includes both losses from leakage current and dissipation factor. Dissipation factor refers to the power loss resulting from the phase difference between the applied ac. voltage and current.

By neglecting L_{esl} the complex impedance of the circuit can be written as follows:

$$Y = \frac{1}{Z} = \frac{1}{R_{esr} + \frac{1}{j\omega C}} \tag{3.76}$$

and the loss or dissipation factor of the capacitor is given as

$$\tan\delta = \omega C R_{esr} \tag{3.77}$$

$$\varepsilon' = \frac{C}{C_0(1 + tg^2\delta)} \tag{3.78}$$

$$\varepsilon'' = \frac{\omega C R_{esr}}{C_0(1 + tg^2\delta)} \tag{3.79}$$

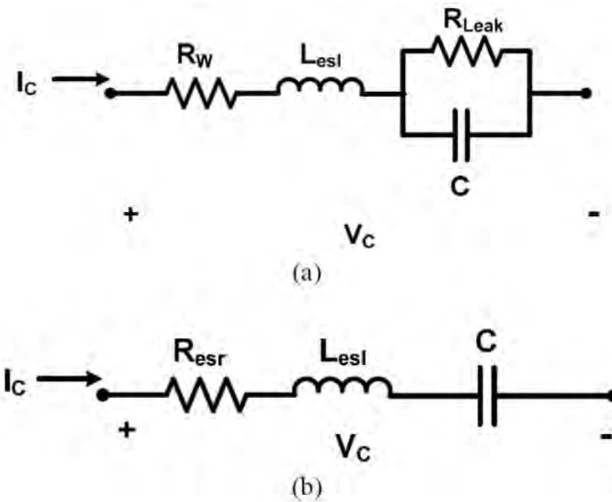

Fig. 3.26. a) Equivalent circuit representations of an electrolytic capacitor
b) normalized equivalent diagram of capacitor [17].

Self-resonant frequency is found at the frequency at which the capacitor passes through the transition from capacitive to inductive behavior, and it is equal

$$f_r = \frac{1}{2\pi\sqrt{L_{esl}C}} \tag{3.80}$$

It is common to add small capacitors in parallel with the main bulk capacitor to intentionally improve the very-high frequency performance of the circuit [17].

The modulus variation of the impedance Z with the frequency for real capacitor is drawn in Fig. 3.27. The normalized equivalent diagram represents its behavior precisely

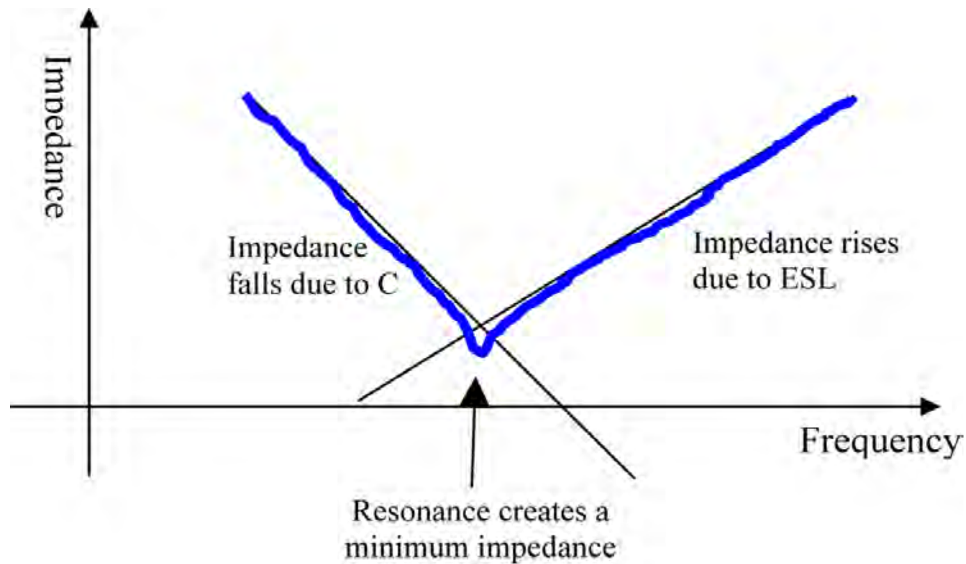

Fig. 3.27. Modulus of the impedance Z as a function of the frequency [18].

During the construction of solid tantalum capacitors, tantalum powder is pressed and sintered in a vacuum to form a pellet. This structure creates a distributed capacitive network near the pellet surface. The connection of these capacitor elements has to be made through the tantalum and the MnO_2 deposition. This arrangement brings about an increase in resistance to the elements located closer to the center of the pellet structure [1]. The tantalum capacitor with MnO_2 as the cathode plate material is both physically and electrically presented to the circuit as an RC-ladder network. As such, there are RC timing considerations for all the distributed capacitive elements of the package. At low frequency applications, all elements are able to respond. At high frequency, the response period required for the capacitive elements deeper in the pellet are higher than those for the capacitive elements in close proximity to the silver coating on the outside surface of the pellet. This effect is known as capacitance roll-off and is one of the most prevalent ways to observe the negative effects of ESR in these devices [1].

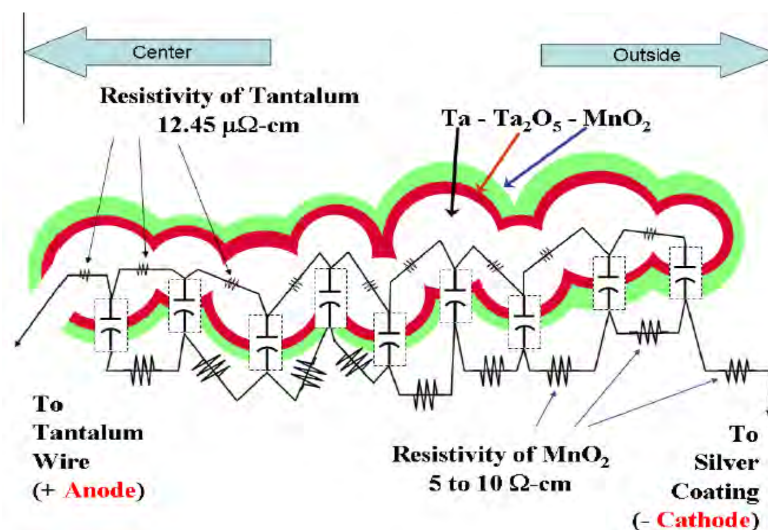

Fig. 3.28. Distributed capacitive elements within the tantalum pellet structure [19].

There are devises to circumvent this effect, by changing from MnO_2 to the conductive polymer the resistance in the path is reduced, allowing the capacitance roll-off to be moved to higher frequency range [20].

3.3.6 Niobium oxide electrolytic capacitor

Niobium oxide capacitors are in principle similar to the tantalum ones, because niobium has similar features. There were two key barriers to niobium usage in a broader industrial, which have only been overcome recently. Firstly, the diffusion rate of oxygen from the dielectric Nb_2O_5 to niobium metal is higher than tantalum, resulting in direct leakage current instability. The second barrier was a lack of high purity niobium powders, able to meet the demanding electrical and mechanical specifications necessary for capacitor manufacture. Tantalum pent-oxide has a dielectric constant $\varepsilon_r = 27$. Relative permittivity of niobium pent-oxide is $\varepsilon_r = 42$, which is almost 1.5 times higher. It causes, that the dielectric growth rate for tantalum dielectric is 1.7 nm/V, and for niobium it is 2.5 nm/V. For the same anodizing voltage niobium pent-oxide forms roughly 1.5 times thicker layer than the tantalum pent-oxide. Typical dielectric thickness of the niobium pent-oxide is 15 – 50 nm. It means that it behaves as a nano-layer and quantum effects must be considered [3]. High-capacitance surface mounted device (SMD) solid electrolyte capacitors are widely used as buffer, smoothing or filter elements in small electronic devices.

- **Niobium oxide electrolytic capacitor fabrication process**

High purity niobium metal powder with high specific surface area is pressed and sintered into a porous niobium anode. A tantalum wire is embedded into the powder to make an electrical contact. Then amorphous nanoscale dielectric oxide layer (thickness of the order of 100 nm expected to consist of Nb_2O_5) is formed on the sintered niobium compact by two anodic oxidation steps occurring in an aqueous electrolyte solution and separated by a thermal annealing in air [7]. Manganese dioxide (MnO_2) was chosen as a cathode due to its remarkable self-healing ability. It is applied by impregnation with an aqueous manganese nitrate $Mn(NO_3)_2$ solution and subsequent pyrolysis at elevated temperatures [7]. Then the cathode coating consisting of graphite and silver paints is applied and in the last step the whole capacitor is encapsulated into epoxy resin.

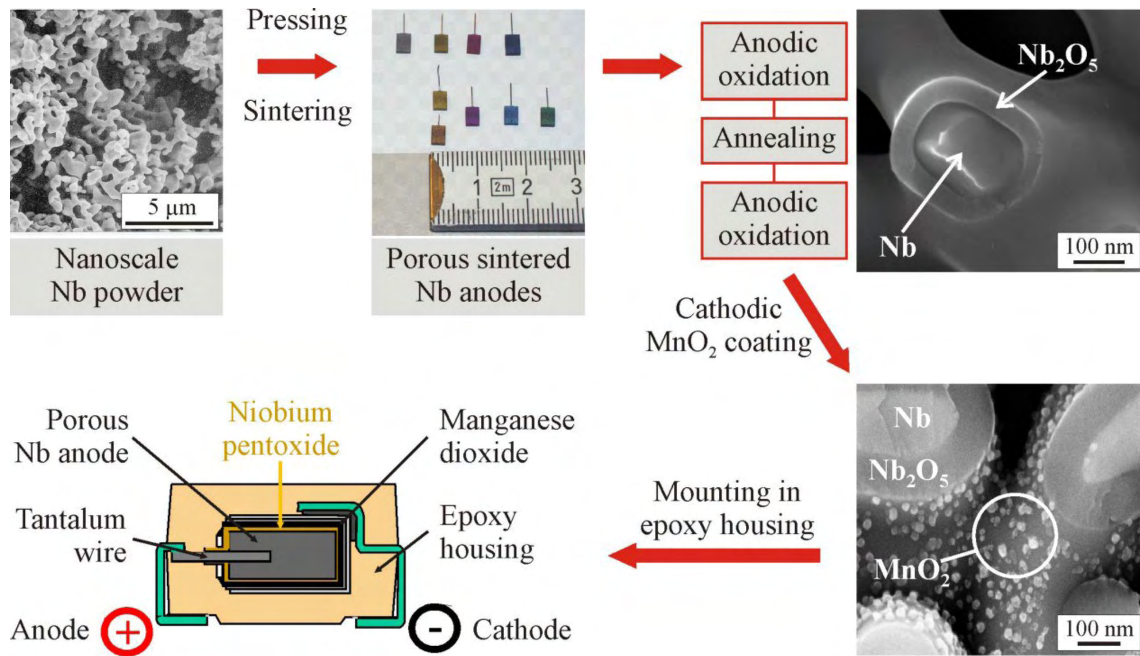

Fig. 3.29. Main steps of the fabrication process of niobium solid electrolyte capacitors. Anode material: sintered niobium powder. Dielectric material: anodically grown niobium pent-oxide. Cathode material: manganese dioxide [7].

3.3.7 Advantages of niobium oxide capacitor over tantalum capacitor.

1. Niobium has approximately half the density of Tantalum, which offers both economic and weight advantages.
2. The main advantage of niobium oxide is its much higher abundance in the nature compared to Ta (estimates range from 30 to 100 times more abundant) yielding significantly lower raw-material price [5].
3. The main problem when considering niobium as an alternate solution is that it requires a higher dielectric thickness to match the current level of reliability maintained with tantalum capacitors, thus negating the benefits associated with the higher dielectric constant [1].
4. An additional problem is that niobium must be heavily refined before it is useful.
5. Nb_2O_5 is characterized by a higher dielectric constant of ε_r =42 which is almost 1.5 times higher than tantalum pent-oxide which has a dielectric constant ε_r =27 since the capacitance increases with the dielectric constant.
6. The pent-oxide dielectric grows during the anodic oxidation out of the surface of the anode material by about one third of the thickness and into the powder by two thirds. Oxidation causes that volume of the whole system to increase. Density ratio between the anode and dielectric material is 2.03 for Tantalum capacitors. For niobium oxide capacitors it is only 1.62, which means, that ratio is 20% lower. It is assumed, that the mechanical stress caused by change of

volume during anodic oxidation is 20% lower for niobium oxide capacitors than for tantalum ones [2].

7. The fact that the Nb_2O_5 dielectric grows thicker than Ta_2O_5 also has one advantage: The dielectric operates at lower field strength for a given voltage rating [5].

3.3.8 MIS theory in electrolytic capacitors

The model of the MIS structure was proposed to give a physical interpretation of the Nb and Ta capacitors. The MIS structure consists from the metallic Nb or Ta, insulating layer made from Nb_2O_5 or Ta_2O_5 and semiconductor – MnO_2. For Ta capacitor, metal electrode consists from tantalum with work function 4.1 eV. Insulating layer Ta_2O_5 has band gap 4.5 eV and semiconductor MnO_2 has energy band gap 0.26 eV. The simplified band diagram of the ideal MIS structure before thermodynamic equilibrium is shown below, where χ is insulating layer affinity, W_M, W_S are work function of metal and semiconductor, respectively, E_C and E_V are energies of valence and conductive band of insulator and semiconductor, E_F is Fermi energy and E_G is forbidden energy gap of semiconductor and insulator. We start with ideal MIS structure, which serves as a foundation to understand tantalum and niobium oxide capacitor characteristics. This has at zero applied voltage no difference between metal work function of tantalum and the semiconductor MnO_2 work function including semiconductor electron affinity. The differences in the metal and semiconductor work functions cause a transfer of electron charge from metal to semiconductor when these components are brought into intimate contact. Without an external bias, this charge transfer will occur until the Fermi level E_F is constant through all the materials and the system is in equilibrium.

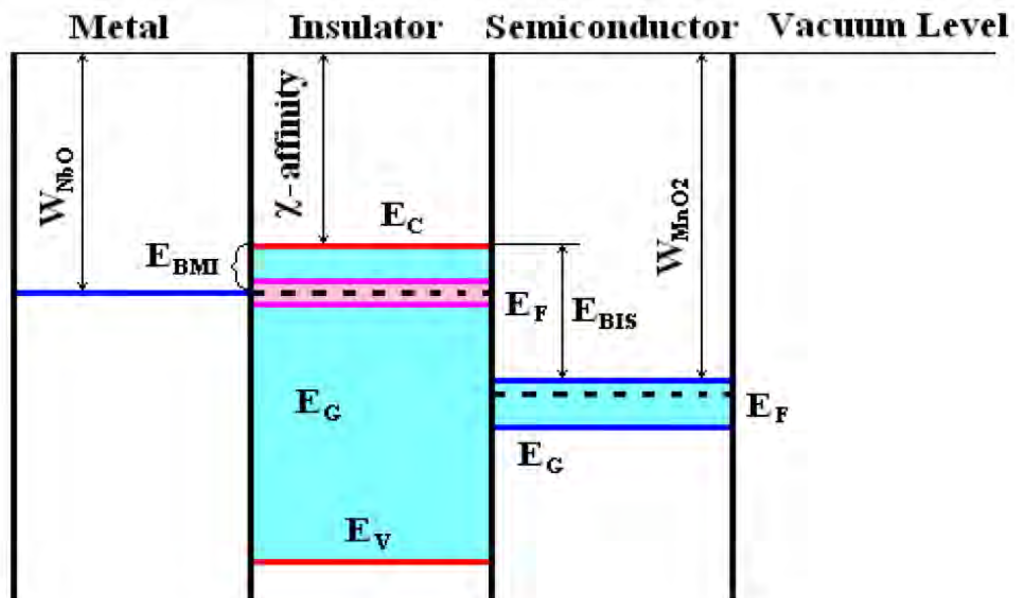

Fig. 3.30. MIS structure model for niobium and tantalum capacitors before thermodynamic equilibrium [3].

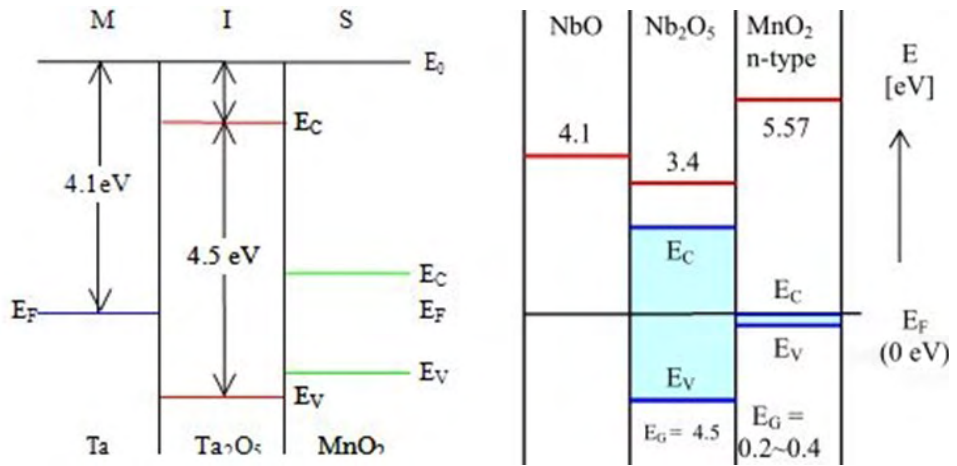

Fig. 3.31. Ideal MIS structure before thermodynamic equilibrium,
a) for tantalum capacitor [21], b) for niobium oxide capacitor [22].

MIS structure models of niobium, in equilibrium state and after application of voltage are shown below.

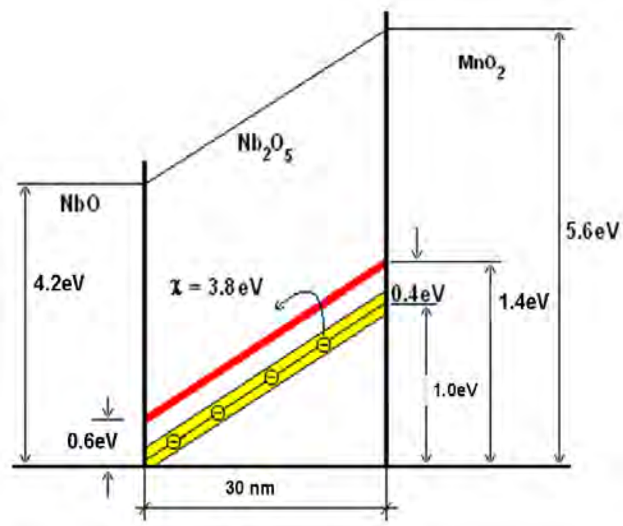

Fig. 3.32. MIS structure models of niobium oxide capacitor, in equilibrium state [2].

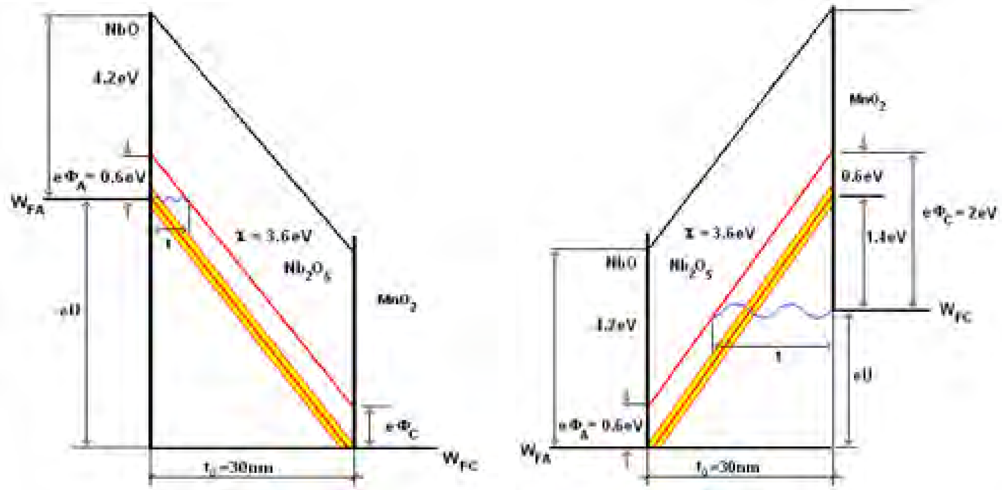

Fig. 3.33. MIS structure model for niobium oxide capacitors after application of negative
(a) and positive voltage (b) thermodynamic equilibrium [3].

Leakage current in forward mode is determined by the potential barrier between NbO and Nb_2O_5. In the reverse mode, it is given by the potential barrier between Nb_2O_5 and MnO_2 [3].

4 Experimental methods

The experimental study of dielectric forms the starting point of this research because the relation between a molecular quantity (dipole moment or polarizability) and a macroscopic observable (polarization or permittivity) is relatively well understood. So, we briefly discuss first the experimental approaches to the determination of the permittivity, which is not a constant but depends on temperature as well as on the frequency of the electric field.

In this research the electrical characteristics of tantalum and niobium oxide capacitors manufactured by AVX Company are presented. Within these classifications there were also several levels of working voltage, or oxide thickness.

4.1 Overview of the methods of measurements in the DRS

The main goals in characterizing these devices were to observe the dielectric properties, primarily relative permittivity and loss number frequency dependence. In addition some of these measurements were done as a function of temperature. Differences between the tantalum and niobium oxide capacitor were established.

There are two basic approaches to the measurement of the dielectric spectra – measurement in the time domain and measurement in the frequency domain. Time domain measurement records the time dependency of a suitable quantity, most frequently charging or discharging current, whereas in the frequency domain measurement, lumped circuit characteristics mostly impedance or admittances are measured as a function of the frequency of the applied electric field.

The scan time domain measurement method of measurement for determining the permittivity is to suddenly apply a voltage to the cell and measure the total charge accommodation on the electrodes, the response (charge) time curve of the materials response to the electric field in the time domain will be recorded.

The dielectric cell can be placed in any number of devices for making dielectric measurements, one of which is called auto-balancing bridge method. In practice, the configuration of the auto-balancing bridge differs for each type of instrument. Generally, an LCR meter, in a low frequency range, typically below 100 kHz, employs a simple operational amplifier for its I-V converter. This type of instrument has a disadvantage– inaccuracy at high frequencies because of performance limits of the amplifier. Wideband LCR meters and impedance analyzers employ the I-V converter consisting of sophisticated null detector, phase detector, integrator (loop filter), and vector modulator to ensure a high accuracy for a broad frequency range over 1 MHz. This type of instrument can attain a maximum frequency of 110 MHz.

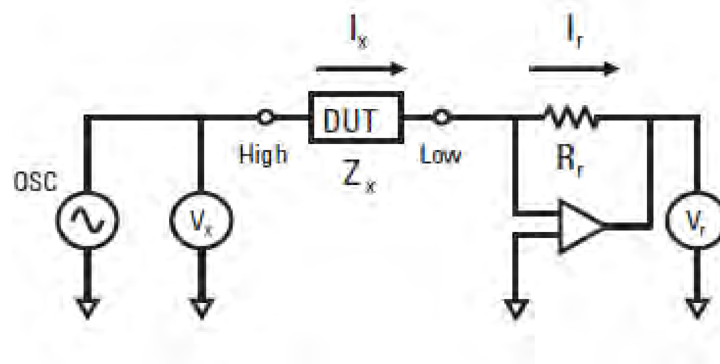

Fig. 4.1. Auto-balancing bridge method [23].

4.1.1 Frequency domain measurement

The measurement of the permittivity requires a cell, in which the sample is inserted. Once the dielectric to be measured is inserted into the cell (sometimes referred to as sample holder or dielectric fixture), the cell becomes a capacitor and, as such, can be included into a suitable electric circuit, where its properties (complex admittance or impedance) may be measured. Permittivity of the sample ε_r will then be calculated from the experimentally measured capacitance C as follows

$$\varepsilon_r = \frac{Cd}{\varepsilon_0 A} \tag{4.1}$$

For service mounted devices (SMD) there are several types of text fixture, in this work the 16034E (Agilent) was used. This 16034E text fixture allows an easy installation of the capacitor, simply pressing the loading lever to left, inserting the sample SMD (tantalum and niobium) components in the V-mount center section (between fixture jaws) and releasing lever.

The principle of the measurement is to apply an ac voltage with a certain frequency to the sample, then measure the current through the sample. The applied and the measured signals are compared, to obtain the complex impedance of the sample. From complex impedance at several frequencies, the complex permittivity and conductivity spectra are extracted.

4.1.2 Measurement systems

Various measurement systems, based on different physical principles, have to be employed in order to cover a broad frequency range of the dielectric spectrum:

- Frequency response analyzer (subhertz to 30 MHz)
- ac bridges and LCR meters (subhertz to 1 GHz)
- Time-domain spectroscopy (100 kHz to 10 GHz)
- Coaxial vector network analyzer (10 MHz to 100 GHz) [14].

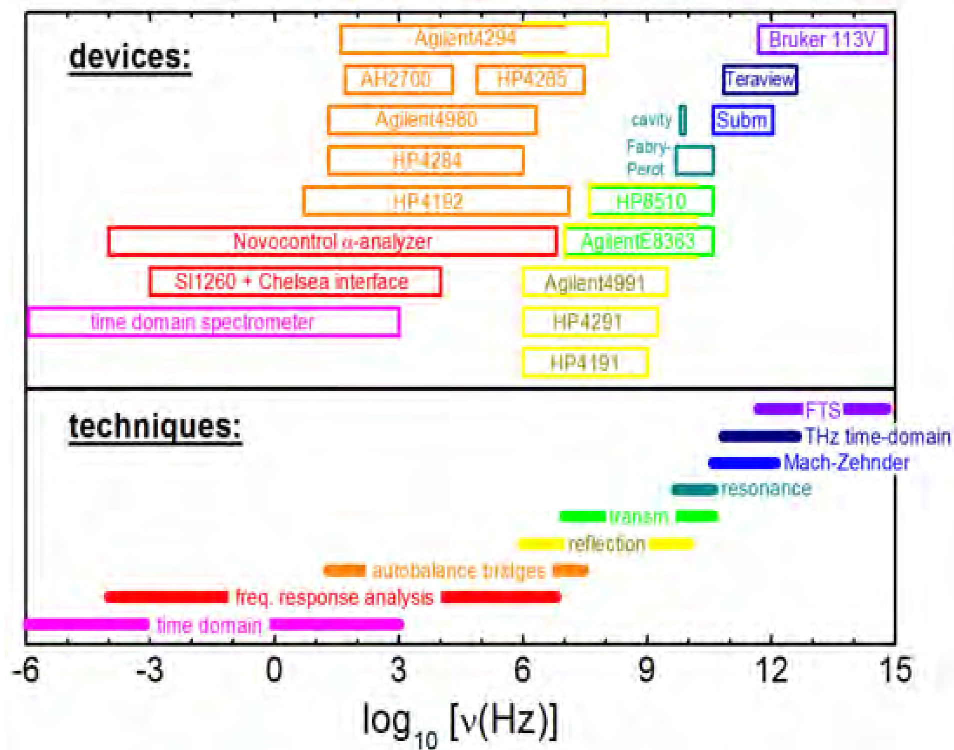

Fig. 4.2. Measurements system for dielectric relaxation spectroscopy [14].

Classification of instruments according to the frequency:

- low frequencies < 10 MHz,
- high frequencies 1 MHz – 40 GHz,
- microwave frequencies 35 GHz – 1100 GHz.

Classification of instruments according to the measurement system:

- time domain measurements.
- frequency domain measurements,
- autobalance bridges measurements,
- reflection,
- resonance and
- Fourier transforms spectroscopy (FTS) measurements.

4.1.3 Equipment for the measurement in the frequency domain

When using an impedance-measuring instrument to measure permittivity, the parallel plate method is usually employed. An overview of the parallel plate method is shown below

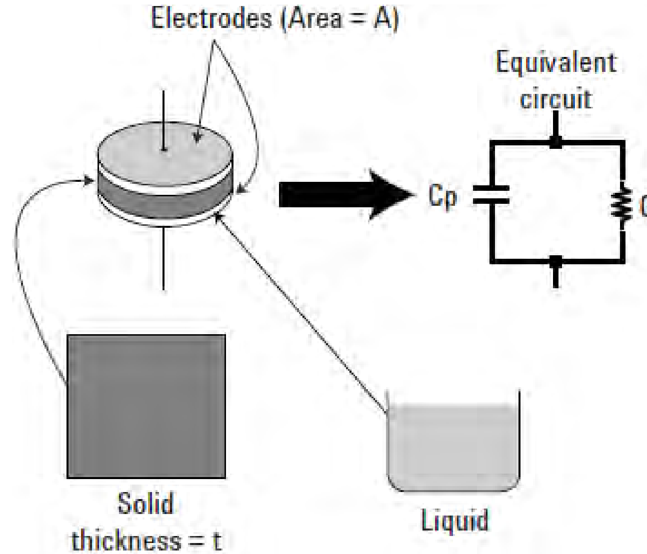

Fig. 4.3. Parallel plate method [24].

The parallel plate method, also called the three terminal methods in ASTM D150, involves sandwiching a thin sheet of material or liquid between two electrodes to form a capacitor. The measured capacitance is then used to calculate permittivity. In an actual test setup, two electrodes are configured with a test fixtures and a thin sheet of material is sandwiched between them. A bridge is designed to calculate the vector components of capacitance (C) and dissipation (D) between the electrode when the field is applied, the signal is processed and a software program would calculate permittivity and loss tangent.

$$Y = G + j\omega C_p \tag{4.2}$$

where C_p is parallel capacitor

$$Y = j\omega C_0\left(\frac{C_p}{C_0} - j\frac{G}{\omega C_0}\right) \tag{4.3}$$

$$\varepsilon_r^* = \left(\frac{C_p}{C_0} - j\frac{G}{\omega C_0}\right) \tag{4.4}$$

$$\varepsilon_r' = \frac{d \times C_p}{A \times \varepsilon_0} \tag{4.5}$$

$$\varepsilon_r'' = \frac{G \times d}{\omega \times A \times \varepsilon_0} \tag{4.6}$$

when simply measuring the dielectric material between two electrodes, stray capacitance or edge capacitance will be formed on the edges of the electrodes. This will causes that the measured capacitance is larger than the capacitance of the dielectric material [24]. The edge capacitance causes a measurement error, since the current flows through the dielectric material and edge capacitor. Guard electrode is the solution to the measurement error caused by edge capacitance. Guard electrode will absorb the electric field at the edge and the capacitance that is measured between the electrodes is only composed of the current that flows through the dielectric material Therefore, accurate measurements are possible [24]. The main electrode is called the guarded electrode, when it used the main electrode with a guard electrode.

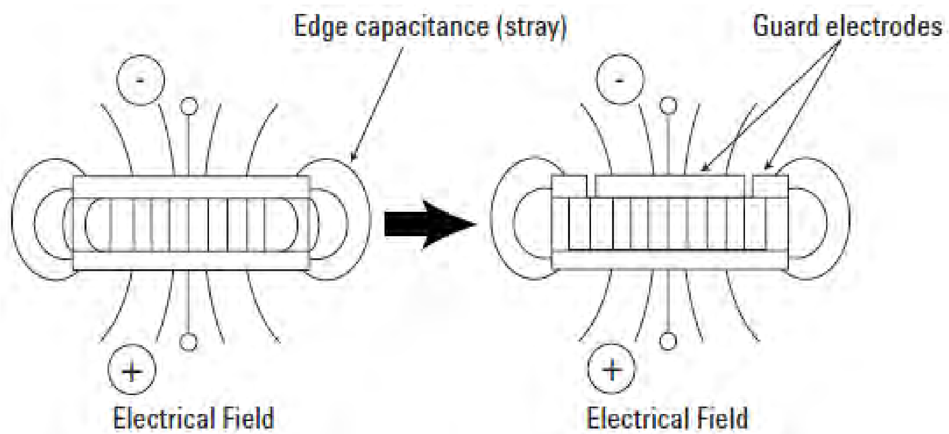

Fig. 4.4. Effect of guard electrode [24].

When the guard electrode surrounds the guarded electrode it is possible to measure the capacitance of the test material accurately, because the guard electrode can avoid the stray capacitance at the edge of the electrode as shown in Fig. 4.5 below.

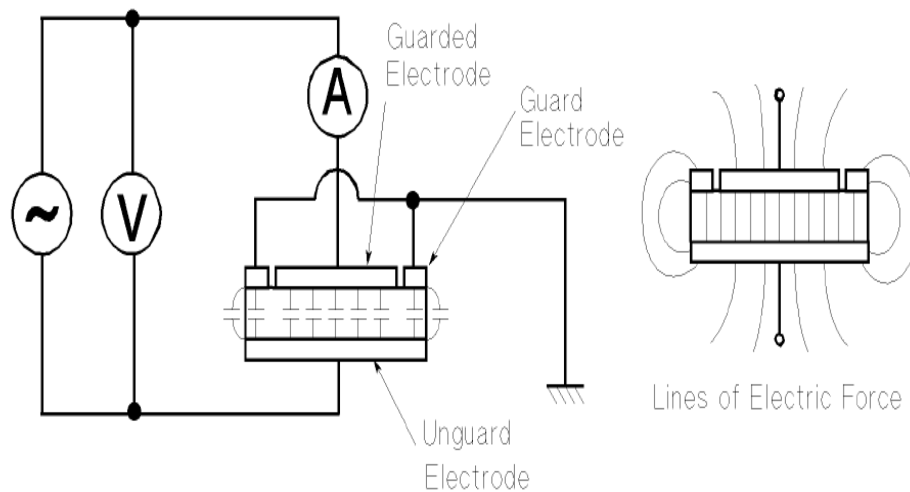

Fig. 4.5. Measurement of capacitance by using guarded electrode system [25].

4.2 Sample preparation

Samples of tantalum and niobium oxide capacitors were supplied by AVX Company as surface mounted devises (SMD). SMD tantalum or niobium oxide capacitors contain:

- tantalum/niobium oxide,
- manganese dioxide,
- carbon/graphite,
- silver,
- tin/tin-lead alloy plating,
- nickel-iron alloy or copper alloy depending on design and
- epoxide resin encapsulation.

These capacitors are physically small or rectangular with solderable terminal pads.

Oxide capacitors are polarized devices and operate satisfactorily in the correct dc mode. They will withstand a limited application of reverse voltage as stated in the datasheets. However, a reverse application of the rated voltage will result in early short circuit failure and may result in fire or explosion [26].

The following table shows sample specifications:

Name of the capacitor	Nominal capacitance [μF]	Rated voltage [V]	Formation voltage [V]	Dielectric grow rate [m/V]	Dielectric thickness [nm]	Plate area [cm^2]
NOJA	4.7	10	35	2.4×10^{-9}	84	10.8
TAJB	1	25	175	1.7×10^{-9}	297.5	12.47
TAJB	4.7	35	122.5	1.7×10^{-9}	208.2	40.9
TAJB	33	16	56	1.7×10^{-9}	95.2	131.4
TAJB	100	6.3	22	1.7×10^{-9}	37.4	156.8

Table 4.2.1 – Sample specifications

The normal working temperature range for our tested niobium oxide capacitor is 218 K to 378 K, the normal working temperature range for our tested tantalum capacitors 218 K to 398 K.

4.3 Sample holder

The sample holder or (test fixture) 16034E (Agilent) was used; It was chosen because of considering the physical layout of the contacts and also the usable frequency range. The 16034E (Agilent) with four terminal configurations was used to interconnect a DUT to the UNKNOWN terminals of an auto balancing bridge instrument bridge instrument, which generally is equipped with four BNC UNKNOWN terminals (H_c, H_p, L_p and L_c).

Compensations are recommended before measurement, to preform open compensation high and low electrodes should be separated from each other. This separation should be equivalent to the size of the device under test (dimension). Short compensation is performed by contacting the high and low electrodes together. After achieving the compensations, the device under test (DUT) is inserted into the text fixture.

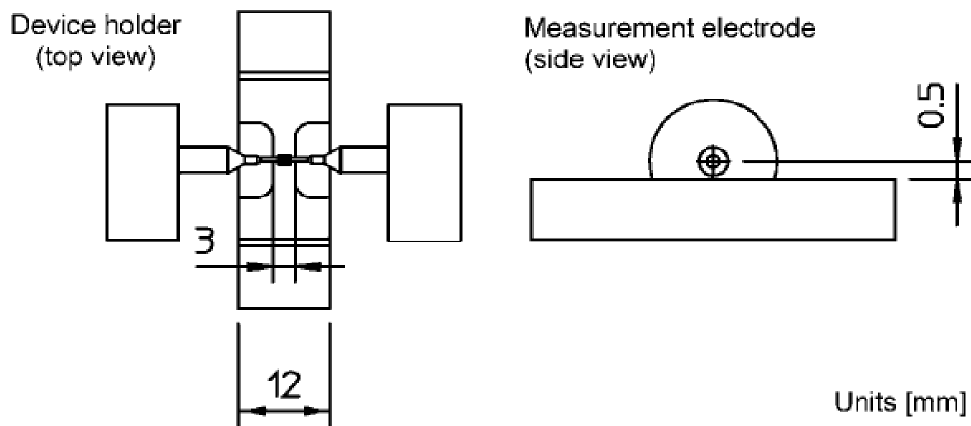

Fig. 4.6. Electrode dimension [27].

5 Objectives of the present work

Niobium oxide capacitors have been widely accepted in the market; they are lead and halogen free and provide high level of safety and security. A tantalum oxide and niobium oxide capacitor has been designed for new applications. Their compact construction and large capacitance makes them volumetrically efficient in choice in cellular phones, digital cameras, notebooks and LCD displays. This makes them subjects of intensive studies.

To improve the electric properties of amorphous Ta_2O_5 at commercial tantalum capacitor it is necessary to understand the formation and reduction of oxygen vacancies in dielectric and the processes occurring at interfaces in the capacitor.

Mechanical defects in the dielectric can be as the following:

- The simplest type is caused by damage occurring to the oxide after it has been completely grown on the metal surface. This can happen by striking the oxidized pellet on a hard surface, thereby physically breaking the oxide. Obviously this would occur on the external pellet surface [28].

- Damage to the oxide can also occur during deposition of the MnO_2 coating. In particular, when a capacitor having a tantalum pent-oxide dielectric is heat treated, typically 300 °C to 400 °C in subsequent steps several times, to convert the manganese salt solution to the MnO_2 oxygen atoms included in the dielectric film may be activated by the heat energy which is applied to the capacitor. The activated oxygen atoms tend to migrate into the electrode materials of the capacitor. Leakage currents are thereby produced. In other words, when the oxygen atoms become activated in the tantalum pent-oxide thin film, oxygen vacancies occur which generates a leakage current [29].

- Defects associated with impurities can arise from segregated impurities present in the tantalum at the surface of the metal. Higher purity of the tantalum powder (improvement of the leakage current characteristics).

- Defects associated with impurities present in the electrolyte, or the water.

- Improper electrolyte material, improper concentrations of electrolyte or inadequate temperature control, which cause the presence of crystallized oxide included in the oxide layer.

The first subject of this dissertation is the studying of the dielectric relaxation of thin film material Ta_2O_5 and Nb_2O_5 at electrolytic capacitor $Ta/Ta_2O_5/MnO_2$, $NbO/Nb_2O_5/MnO_2$, respectively, with a low frequency dielectric spectroscopy over a large temperature (187 K, 385 K), (218 K, 373 K), and frequency range 1 Hz – 10^7 MHz, 20 Hz – 1 MHz.

The second object was to ascertain the impact of the thickness of the oxide layer on dielectric relaxation and conductivity.

6 Measurements

Equipment for the measurement in frequency domain with autobalance bridges technology (four terminal pair) which was used in this work at Brno University of Technology, Department of Physics are Agilent HP 4284A [20 Hz – 1 MHz], and Agilent HP E4980A [20 Hz – 2 MHz]. Dielectric text fixture 16034E (Agilent) was used. Measuring with the precision LCR meter is based on bridge techniques with auto-calibration and our measured results are available over the frequency range 20 Hz – 2 MHz. It turned out to be necessary to carry out the correction before each measurement to avoid errors during the measurement. Both apparatuses provide the widest measurement range with high basic accuracy is 0.05% [30].

The autobalance bridge technique is the best technique for measurements below 40 MHz because it provides accurate measurements, and has the widest impedance measurement range. A wide range of ac and dc stimulus can be applied to the component. In addition it is the simplest measurement technique to use.

The impedance – measuring instrument HP 4284A, and HP E4980A measures vector components of impedance or admittance, capacitance (C) and dissipation (D), The whole measurement was controlled from a PC by using GBIP bus, and software program (Matlab) would calculate permittivity and loss number.

To maximize the accuracy of my results, Alpha-A analyzer system allowing high performance dielectric measurements available over the frequency range [3 µHz – 20 MHz], at Augsburg University (Germany), Department of Physics, was used in this work. Alpha-A analyzer provides high performance dielectric, conductivity, electrochemical, impedance and gain phase measurements in the frequency domain. The system combined with test interfaces optimized for special functionality [31].

For temperature dependence measurements it was necessary to use several devices that allow measurements in different temperature ranges; the first of them was a cryostat system which was supplied by Janis with regulated temperature from 500 K to 10 K at Brno University of Technology (Czech Republic), Department of Physics, and the other one was Quatro Cryosystem with regulated temperature 113 K – 673 K at Augsburg University (Germany), Department of Physics.

6.1 HP4284A precision LCR meter

The basic instrument was the HP 4284A precision LCR meter; it exhibits a wide range of test frequency from 20 MHz to 1 MHz with basic accuracy 0.05%. Corrections OPEN, SHORT, LOAD, and cable length selection were used for correction of stray admittances and residual impedance, and other error corrections can be performed with to the test fixture and the test lead. The whole measurement was controlled from a PC. Use was made of the existing control software which was developed in the Department of Physics a few years ago (based on software Matlab, VEE Pro, DK 92).

6.2 HP E4980A precision LCR meter

The basic instrument was the E4980A precision LCR meter, its exhibit a wide range of test frequency from 20 MHz to 2MHz with basic accuracy is 0.05%. This apparatus is much faster than HP 4284A with speeds of measurements being 5.6 ms (SHORT), 88 ms (MED), and 220 ms (LONG). Correction OPEN, SHORT, LOAD, and cable length selection, were used for correction of stray admittances and residual impedance in the same way as on the preceding HP 4284A precision LCR meter, and the other errors can be performed due to the test fixture and the test lead. For the measurement of surface mounted devises (SMD), dielectric test fixture HP 16034E (Agilent) was used. The whole measurement was controlled from a PC. Use was made of the existing control software which was developed in the department of Physics a few years ago (software Matlab, VEE Pro, DK 36).

6.2.1 Measurement error for HP (4284A E4980A) precision LCR meter

Compensation is also known as Correction it used to reduce the error sources existing between the DUT and the instrument's calibration plane. Compensation data is obtained by measuring the test fixture residuals [23]. There are three commonly compensation technology that used

- offset compensation,
- open/short compensation and
- open/short/load compensation.

In this work open/short compensation was used

Open/short compensation

The most popular compensation technique that used in the recent LCR measurement instruments is Open and short compensations. This method assumes that the residuals of the test fixture can be represented by the simple L/R/C/G circuit as shown in Fig. 6.1.

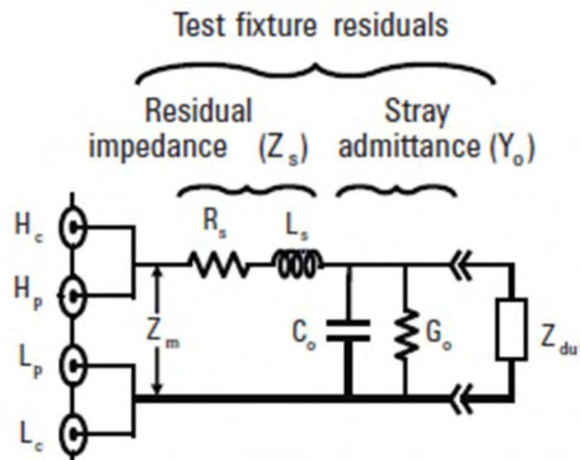

Fig. 6.1. Test fixture residuals [23].

H_C (high-current), H_P (high-potential), L_P (low-potential), L_C (low-current) in Fig. 6.1 above are UNKNOWN BNC terminals of LCR measurement instruments.

- **Open connection**

When the DUT contact terminals of the test fixture are open, as shown in Fig. 6.2, stray admittance Go + $j\omega C_o$ is measured as Y_o because residual impedance Z_s is negligible, thus $1/Y_o >> Z_s$.

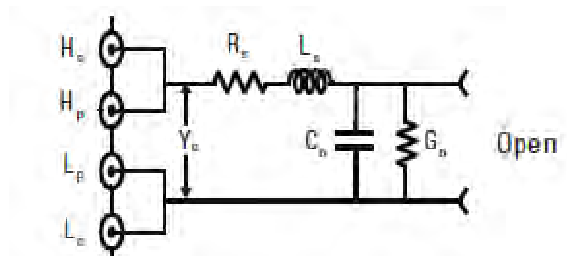

Fig. 6.2. Test fixture is in open connection [23].

$$Y_0 = G_0 + j\omega C_0 \tag{6.1}$$

$$R_s + j\omega L_s << \frac{1}{G_0 + j\omega C_0} \tag{6.2}$$

- **Short connection**

When the DUT contact terminals of the test fixture are shorted, as shown in Fig. 6.3, the measured impedance represents residual impedance $Z_s = R_s + j\omega L_s$ because Y_o is bypassed. Therefore, each residual parameter is known and, the DUT's impedance Z_{dut} can be extracted from the equation (90).

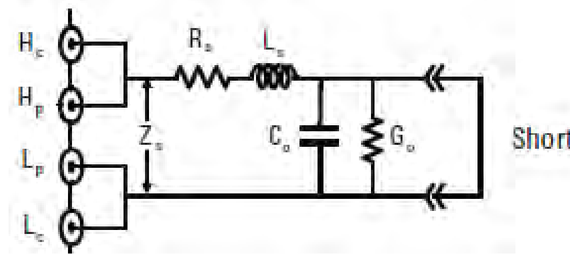

Fig. 6.3. Test fixture is in short connection [23].

$$Z_s = R_s + j\omega L_s \tag{6.3}$$

$$Z_{dut} = \frac{Z_{xm} - Z_s}{1 - (Z_{xm} - Z_0)Y_0} \tag{6.4}$$

where Z_{dut} is corrected DUT impedance, Z_{xm} measured DUT impedance, Y_0 stray impedance, and Z_s residual impedance.

6.3 Novocontrol Alpha-A analyzer

Alpha-A mainframe is the master unit of the Alpha-A modular measurement system. The system contains frequency analyzer with a sine wave and dc-bias generator and two ac voltage input channels. The system combined also with sample cells (test interfaces) are offered in standard parallel plate transmission and reflection geometry four wire contact arrangement and as interdigit comb electrodes. In this work BDS 1200 sample cells was used. This allows characterization of ferroelectrics, metal electrolyte interfaces, ion conductors, conductive liquids, ion and electron transport in electrolytes, and characterization of electrolyte metal interfaces and membranes. It can be combined with each temperature control system and most of the sample cell [31]. Data evaluation is performed by WinDETA and WinFit software packages. All system functions of the mainframe and connected test interfaces are controlled by the mainframe IEEE488 GPIB interface port by high level GPIB commands via an external host computer as shown below [32].

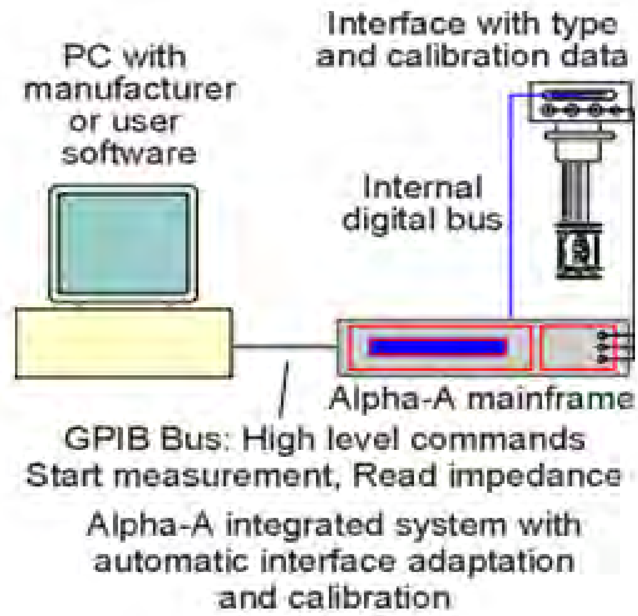

Fig. 6.4. Alpha-A mainframe system - setup [32].

The simplified circuit of Alpha-A mainframe is as shown below.

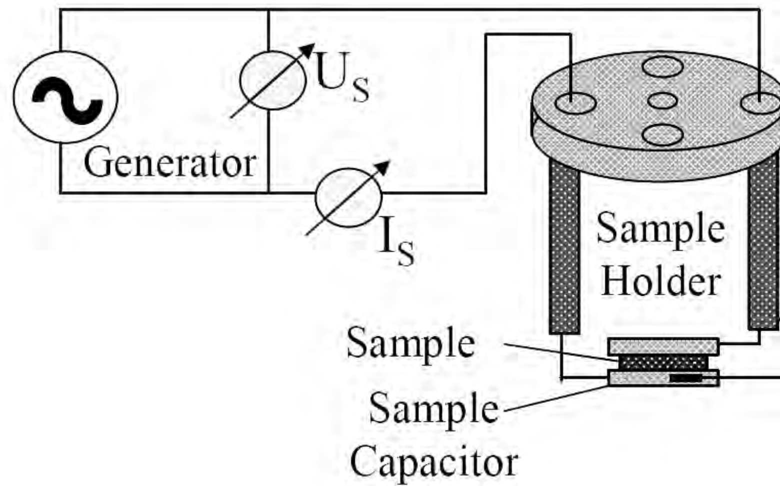

Fig. 6.5. Simplified measuring circuit illustrating the operation of Alpha-A system [33].

6.4 Temperature dependence instruments

Due to the circumstances, the experiment requires measurements at different temperatures from the ambient temperatures, and it was been necessary to use several devices that allow measurements in different temperature ranges. In this work I have used two different instrumentation technologies for frequency domain and temperature dependence, the first was at University of Augsburg by using Quatro Cryosystem and Alpha-A analyzer which allowed us to measure the temperature from 113 K up to a temperature of about 673 K, the second was at Brno University of technology by using He cryostats Janis with HP E4980A precision LCR meter which allowed us to measure the temperature from 500 K down to a temperature of about 10 K.

6.4.1 Instrumentation for frequency domain and temperature dependence at Augsburg University

- Quatro Cryosystem [113 K – 673K].

The Quatro Cryosystem is a high quality temperature control system for materials research. The system is modular and it can be used for dielectric and impedance spectroscopy, with all Novocontrol sample cells or Novocontrol impedance spectrometer.

The Quatro Cryosystem was designed for easy, safe and fully automatic operation enabling computer controlled experiments over several days without supervision as required for low frequency measurements [34].

The system was developed to set the temperature of the sample under test with high accuracy, all temperature experiments are supported by the software package WinDETA providing both isothermal control and temperature ramping.

The main parts of the system are the cryostat BDS 1100, gas heating module BDS 1310, pressurizer module BDS 1320, vacuum system with BDS 1350, liquid nitrogen dewar, Quatro controller BDS 1330 and power supply BDS 1340, as shown below respectively.

The Quatro controller consists of four circuits controlling the sample temperature, the gas temperature, the temperature of the liquid nitrogen in the dewar and the pressure in the dewar.

Fig. 6.6. The main parts of the Quatro Cryosystem [35].

Using the Quatro Cryosystem for dielectric measurements

After setting the temperature of the sample under test to the desired temperature (set point) by using Quatro Cryosystem and Quatro microprocessor controller, the liquid nitrogen evaporator will heat up the nitrogen gas in the dewar until specified pressure to create a highly constant nitrogen gas flow. The pressure and temperature in the dewar are measured by two channels (channel 1, channel 2) of the Quatro controller as shown in Figure 6.7.

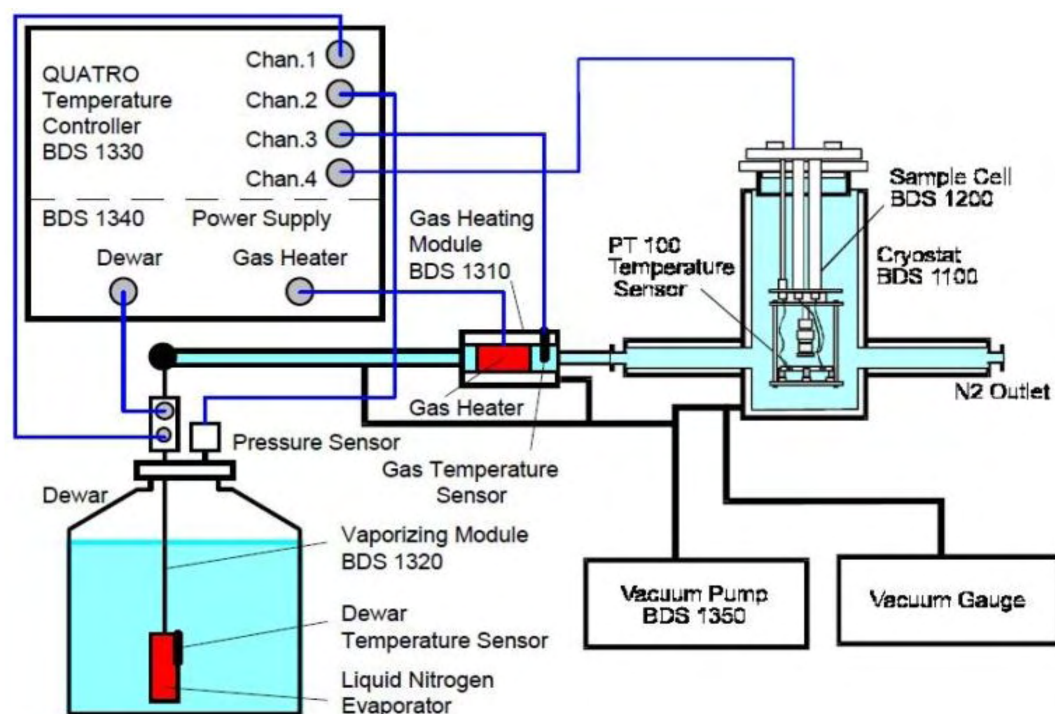

Fig. 6.7. Principle structure of the Novocontrol Cryo system and the QUATRO controller [36].

The nitrogen gas flows directly through the sample cell located in the cryostat. Due to the pressure, the cold gas in the dewar will flow in the vacuum isolated line to the gas heater module. The gas heater and sample temperature are measured by the two remaining channels (channel 3, channel 4) as shown above. After gas passes through the gas heater, it flows directly through the vacuum insolated sample by a 2 stage rotary vane vacuum pump, providing thermal isolation by low vacuum (< 10 μbar) cell mounted in a cryostat.

Due to the double control arrangement of the gas heating and high stability of the gas pressure, the temperature stability is better than 1 °C.

Temperature set point and sample temperature for Quatro Cryosystem 4.0

As can be seen from Fig. 6.8, the dashed line is the temperature setpoint which is stepped in several intervals of a typical experiment from 113 K to 673 K, whereas the solid line shows the sample temperature. The stabilization time is 8 minutes per temperature step. This means, that two dimensional dielectric measurements with 12 frequency sweeps at 12 different temperatures will be performed in less than two hours [36]. Figure 6.8 also shows that the sample temperature follows the setpoint without overshooting and oscillations.

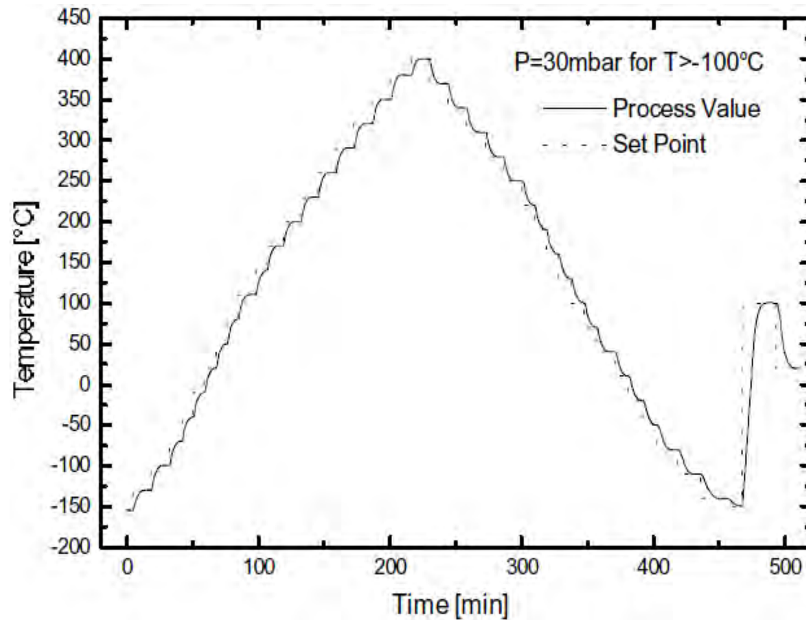

Fig. 6.8. The setpoint temperature and the sample temperature in dependence of time for NOVOCONTROL Quatro Cryosystem 4.0 [36].

In this work dielectric measurements were performed with the application of Quatro Cryosystem 4.0 and Alpha-A NOVOCONTROL analyzer with WinDETA software by the same company. Measurements were taken under cooling with 2 K/min speed. Measuring electric field frequency was from the range 1 Hz – 10 MHz.

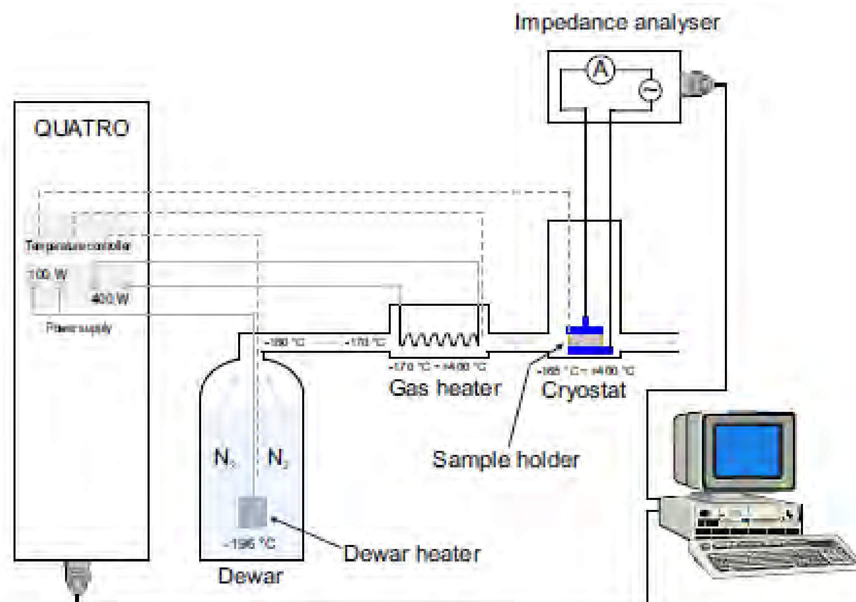

Fig. 6.9. The experimental setup [37].

6.4.2 Instrumentation for frequency domain and temperature dependence at Brno University of Technology

The cryostat CCS – 400/204, supplied by Janis Company, with cryogenic SHI-APD Model 204SL two stage cold head, uses as cooling medium helium. The cryostat is already quite advanced and allows temperature regulation from 500 K to 10 K. The entire system with a description of each part is shown in Fig. 6.10 below.

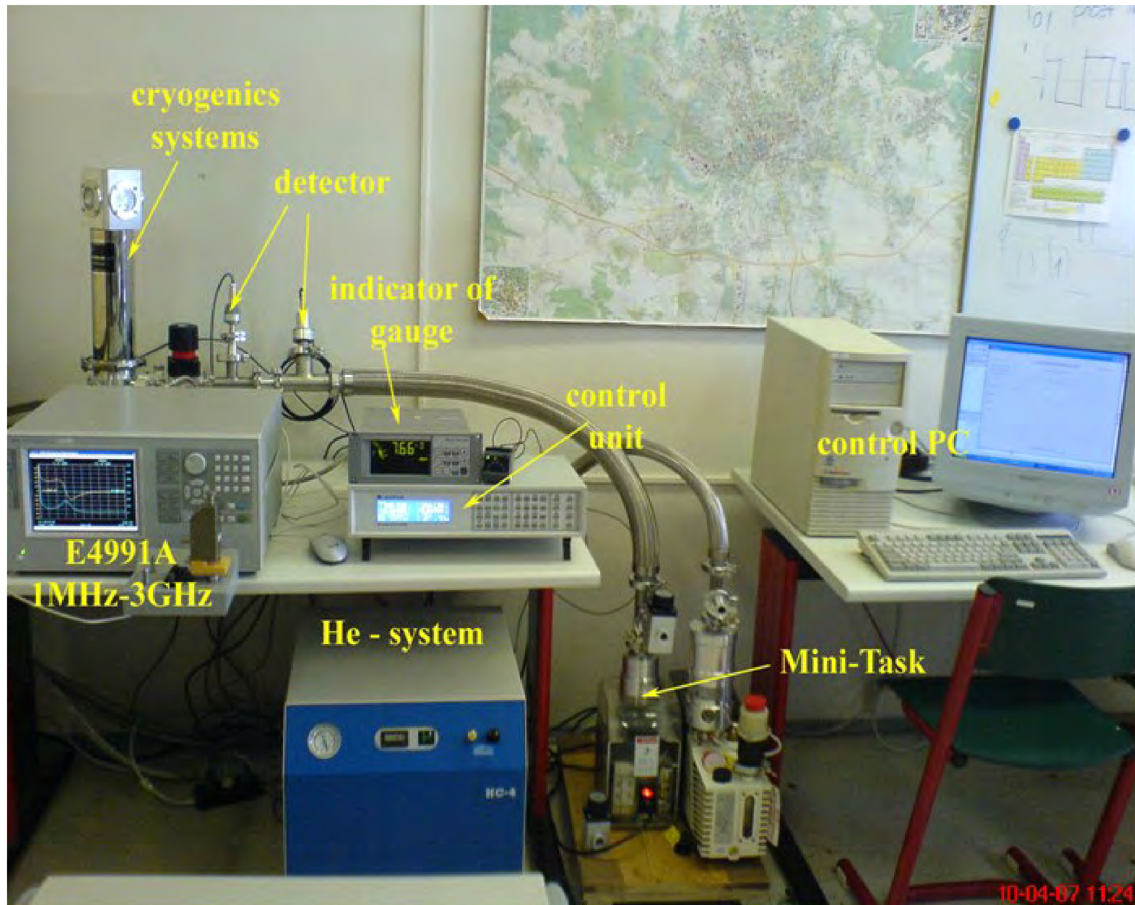

Fig. 6.10. Description of individual cryostat sections from the Janis Company [10].

The cryostat must be first pumped to minimize pressure in cryo-chamber. This procedure is necessary because of the thermal vacuum. After pumping there will be no increase in the temperature of the outer jacket of cryo-chamber; it will not become wet and there is no frost on it. The next step is to turn on the external compressor, which is a part of the system. The compressor pushes into the cryogenic system high purity helium; it results in a large thermal energy that is tempered through a built-in fan or water cooling. The minimum amount of water needed for cooling is 2.8 l/min. Loading and unloading of helium in cryo-system is secured by double skin hoses. These hoses introduce helium into the cryosystem and finally to the cold head. Temperature regulation in the cryosystem is ensured by resistance wires, which increase the temperature in the closed system. Thermal conduction between the cold head and the electrode system is ensured by a special electrically non-conductive thermal trap. The perimeter of the trap allows the transfer of heat even in vacuum. Communication of the measuring

device with the measured sample, which is located in the cryosystem, is ensured by 4 BNC connectors, all of which were used.

The control of temperature (LakeShore 340) and pressure in the cryosystem is ensured by pressure and temperature sensors. Temperature sensors are two (silicon diode (DT-670B)) and are placed as close to the cold head as possible. Pressure sensors are located between cabins and pump.

7 Result and Analysis

Dielectric and electric properties of thin oxide film at tantalum or niobium electrolytic capacitors were measured using the HP E4980A precision LCR meter with He cryosystem and Alpha-A Analyzer with Quatro system as described in previous section. All the measurements which were done in this work were in the standards operating temperature range of the tantalum and niobium oxide capacitor 218 K to 378 K and 218 K to 378 K, respectively, as written in the data sheet from the manufacturing AVX Company, Beside the measurement was also done at temperature of 187 K. Because changes in temperature around the capacitor affect the value of the capacitance because of changes in the dielectric properties.

The software supplied with the analyzer allowed the presentation of the measurement results in various form. In this work we only used C_p – G components of the parallel equivalent circuit, that were then recalculated to values of material parameters ε' and ε''. The purpose of this approach was the development, presentation and interpretation of the dielectric spectra.

As previously stated, the main goal of this thesis is to measure dielectric properties of thin oxide film at tantalum or niobium electrolytic capacitors. Since these capacitors are complex discrete devices, we need to be sure that we measure them properly in order to obtain useful data. As discussed above, AVX Company provided us with several types of these capacitors; the thickest oxide capacitors have a dielectric thickness of the order of 298 nanometers, while the thinnest ones are of the order of 37 nanometers. It was one of the objectives of the research to study eventual difference in the dielectric properties of thin oxide film between tantalum and niobium electrolytic capacitor. The second object was to ascertain the impact of the thickness of the oxide layer on dielectric relaxation and conductivity.

7.1 Dielectric relaxation spectrum for 1 µF / 50 V_{dc} tantalum electrolytic capacitor

Plots of dielectric relative permittivity *vs.* frequency at different temperature range for 1µF/50 V_{dc} tantalum electrolytic capacitor with oxide film thickness 298 nm are shown in the figures to follow. The relative permittivity shows a very large increase at low frequency and high temperature. It increases with increasing temperature, from ~ 39 at 418 K, at 1 Hz and to 27 at 187 K at 1 Hz. The strong increase of relative permittivity at low frequencies is due to the electrode polarization [38]. At higher frequency about 1 MHz and temperature 187 K, the relative permittivity drops to unphysical (wrong) values; at this frequency the parasites start to be dominate [39].

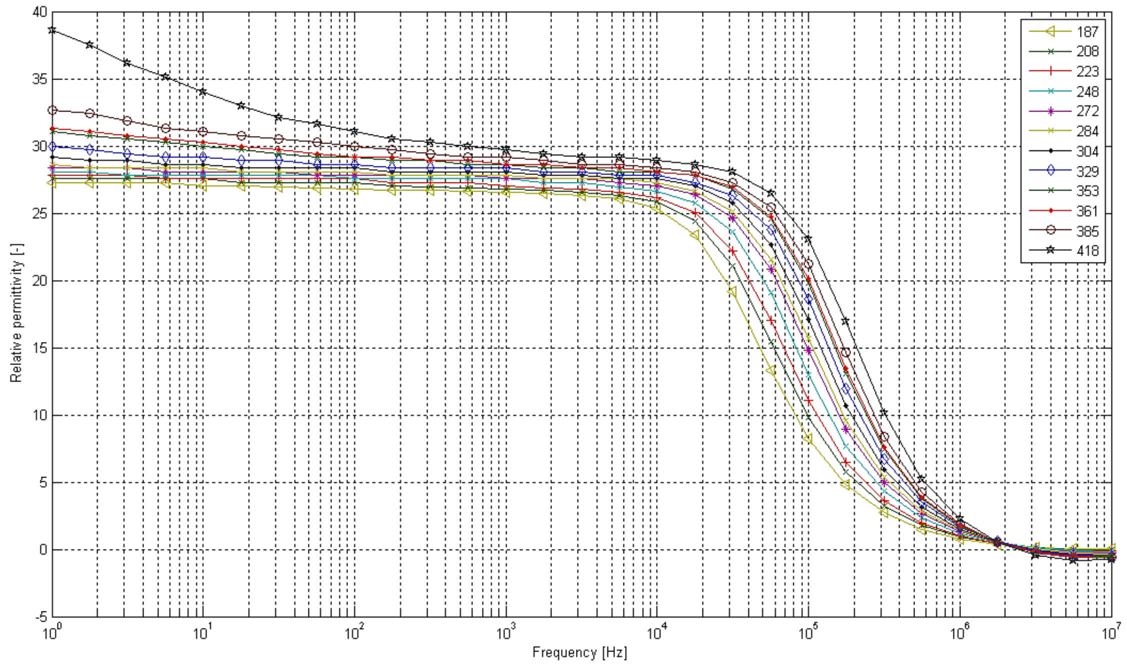

Fig. 7.1. Relative permittivity versus frequency of 1 μF / 50 V_{dc} tantalum capacitor at different temperatures: from 187 K to 418 K.

The relaxation peak starts to appear at frequency about 10 KHz as shown below. The relaxation peak moves towards the higher frequency with the increasing temperature. The relaxation peak shows almost no amplitude increase with temperature. This behavior has already been reported for Ta_2O_5 [40]. The frequency of the loss peak at 385 K is related to a characteristic relaxation rate or relaxation time $\tau_{peak} = 1 / \omega_{peak} = 1/ 2 \pi f_{max} = 9.05 \times 10^{-6}$ s of the fluctuating dipole. At low frequencies, electrode polarization related to the accumulation of charges at electrode effect starts to appear to influence the dielectric properties at low frequencies. Both relative permittivity and loss number are temperature dependent.

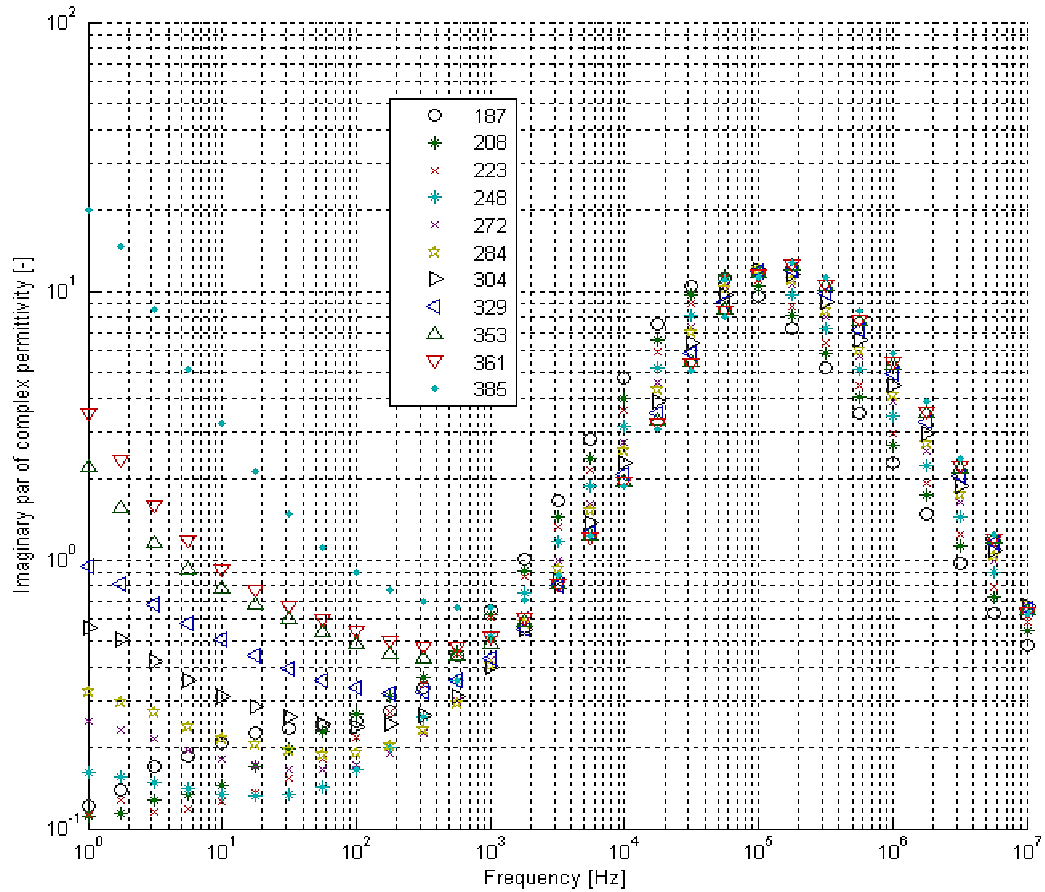

Fig. 7.2. Relaxation peak versus frequency of 1 μF / 50 V_{dc} tantalum capacitor at different temperatures: from 187 K to 418 K.

The loss peak frequency follows the Arrhenius law as shown in figure below with the activation energy of 0.048 eV.

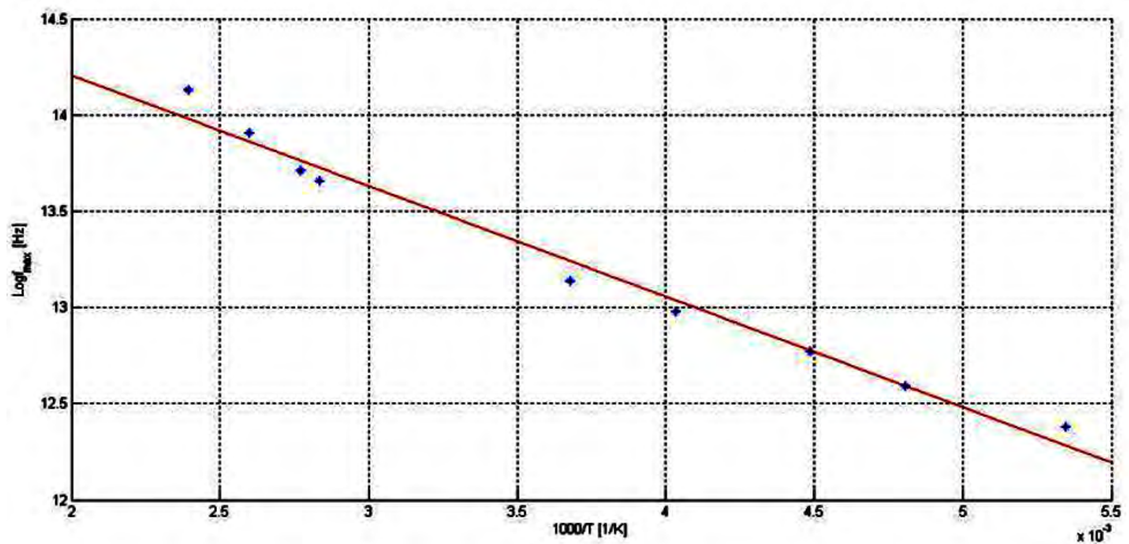

Fig. 7.3. Arrhenius plot of the frequency value of relaxation peak.

In order to evaluate the change in the dielectric loss (dissipation factor) curve we obtained values $\Delta\varepsilon$, α_{HN}, β_{HN} and τ_{HN} as a function of frequency by fitting the observed values to HN equation (3.29). Figure 7.4 shows examples of the Non-Linear Least Square (NLLS) fit of dielectric curve to a single relaxation HN function. We found that HN equation can very well fit the observed dielectric loss as a function of frequency except for a slight deviation of the observed value from the fitting curve at low frequencies. This slight deviation may be due to dc conductivity.

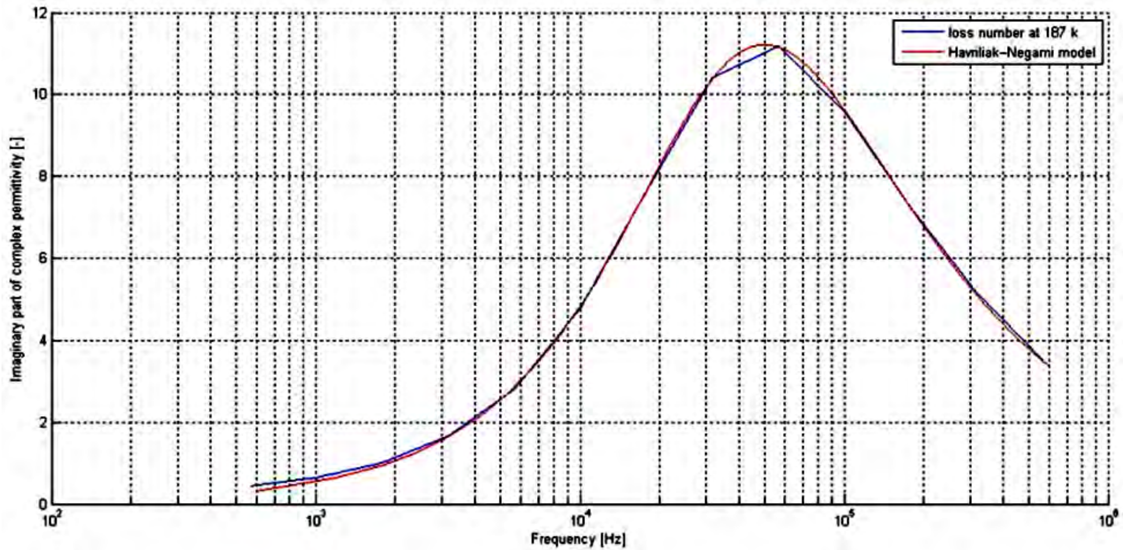

Fig. 7.4. Non-linear least square fit of relaxation peak of complex permittivity versus frequency, a single HN equation at 187 K.

Figure 56 shows the values of α_{HN}, which indicate that the width of the loss peak increases with decreasing temperature

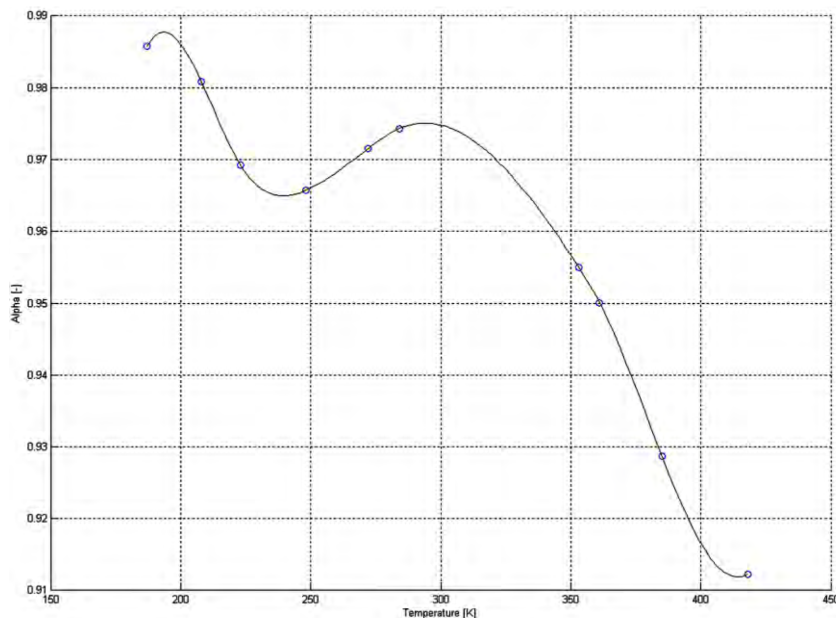

Fig. 7.5. Temperature dependence of the shape parameter α_{HN} of 1 μF / 50 V_{dc} at different temperatures: from 187 K to 418 K.

The asymmetry parameter, β_{HN}, increases with increasing temperature as shown below

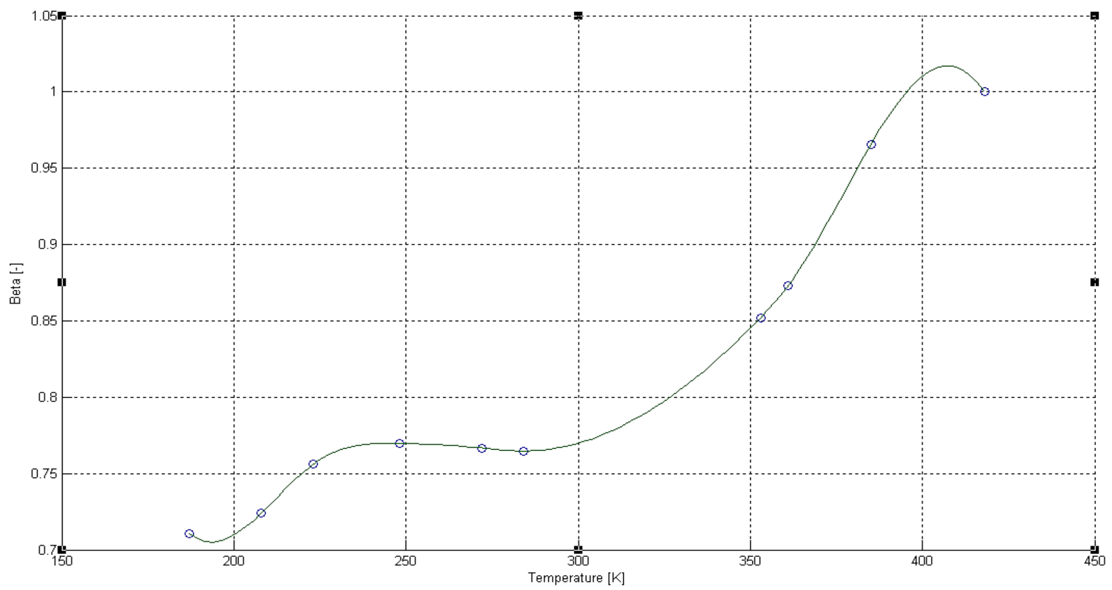

Fig. 7.6. Temperature dependence of shape parameter β_{HN} of 1 μF / 50 V_{dc} at different temperatures: from 187 K to 418 K.

Figure 58 shows the dependence of dielectric strength $\Delta\varepsilon$ on frequency; the dielectric strength $\Delta\varepsilon$ of the α-relaxation increases with the temperature

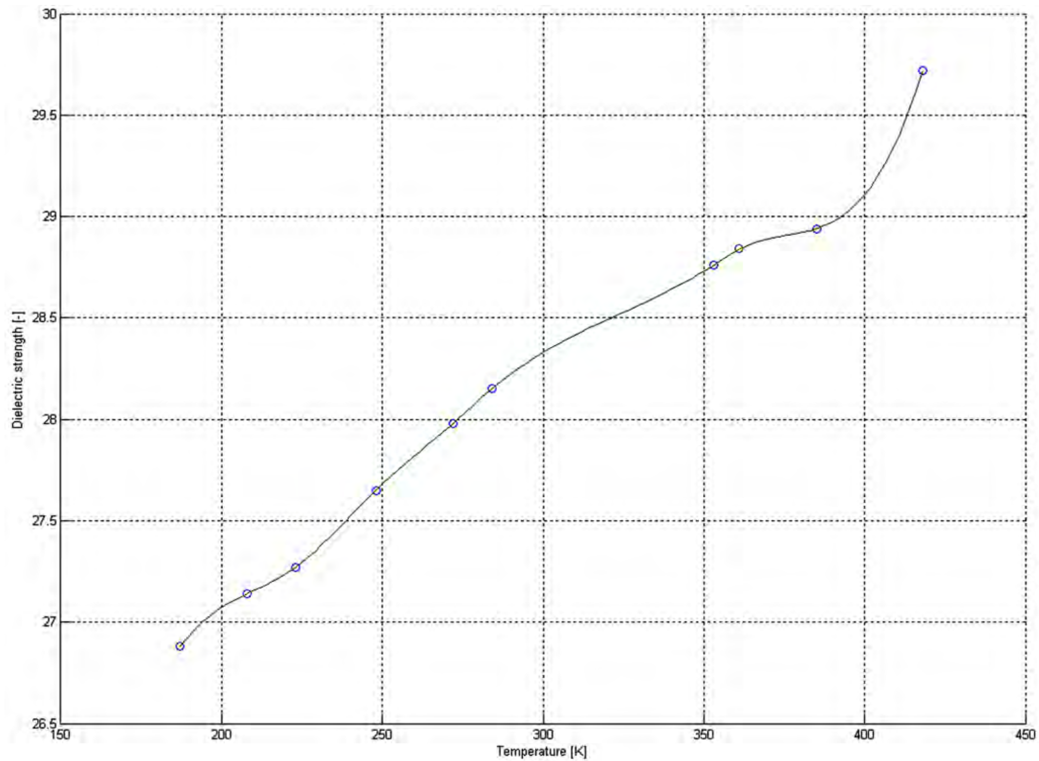

Fig. 7.7. Temperature dependence of dielectric strength of 1 μF / 50 V_{dc} at different temperatures: from 187 K to 418 K.

In Table 7.1.1, the parameters are determined at ten different temperatures. The width parameter α_{HN} increases with decreasing temperature whereas other parameters β_{HN}, $\Delta\varepsilon$ and τ decrease with decreasing temperature.

Table 7.1.1. Havriliak–Negami parameters of 1 μF / 50 V_{dc} at different temperatures: from 187 K to 418 K.

T [K]	α_{HN} [-]	β_{HN} [-]	$\Delta\varepsilon$ [-]	τ_0 [s]
187	0.985	0.710	26.88	4.198×10^{-6}
208	0.980	0.724	27.14	3.370×10^{-6}
223	0.969	0.756	27.27	2.817×10^{-6}
248	0.965	0.769	27.65	2.303×10^{-6}
272	0.971	0.766	27.98	1.965×10^{-6}
284	0.974	0.764	28.15	1.829×10^{-6}
353	0.955	0.852	28.76	1.164×10^{-6}
361	0.950	0.873	28.84	1.105×10^{-6}
385	0.928	0.965	28.94	9.057×10^{-6}
418	0.912	1	29.72	7.231×10^{-6}

7.2 Dielectric relaxation influence over several thicknesses

In order to understand the dielectric relaxation of amorphous Ta_2O_5 in more depth, several thicknesses have been studied. According to the dielectric relaxation results we identified that for all the thicknesses under study the relaxation peak approximately shifted the same toward higher temperatures with frequency (same activation energy), the peaks located at different frequencies with approximately the same magnitude as shown below.

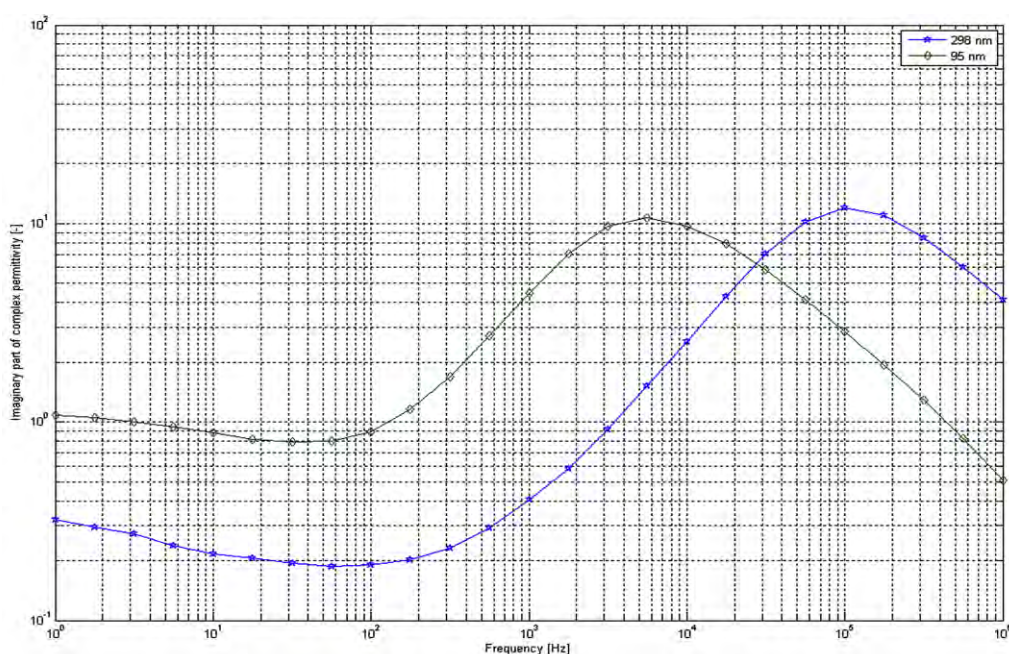

Fig. 7.8. Dielectric relaxation peak versus frequency results for two different thicknesses of Ta_2O_5 (298 nm, 95 nm) and different electrode area at 284 K.

Figure 7.9 shows the capacitance – temperature curves and dissipation factor for two different tantalum capacitors (1 μF / 50 V_{dc}, and 33 μF / 16 V_{dc}) with two different thicknesses of Ta_2O_5 (298 nm, 95 nm) and electrode area (12.47 cm^2, 131.4 cm^2) at 284 K. both curves show the capacitance decreases with increased frequency.

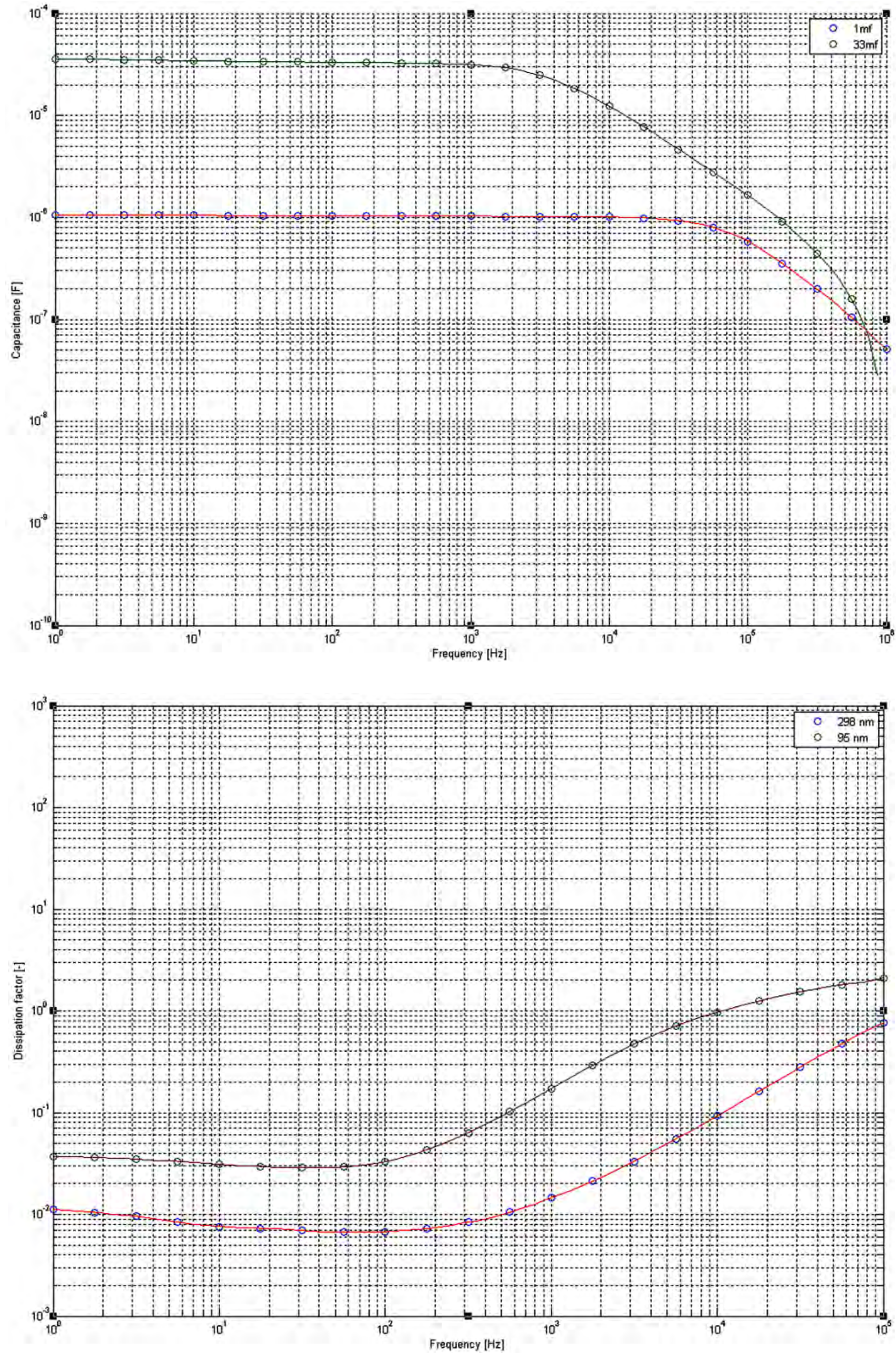

Fig. 7.9. Capacitance *vs.* temperature curves and dissipation factor for (1 μF / 50 V_{dc}, and 33 μF / 16 V_{dc}) tantalum capacitors

7.3 Relative permittivity and dissipation factor as function of temperature and frequency

The capacitance – temperature curves for Ta_2O_5 (1 μF / 50 V_{dc}) are shown in Fig. 7.10. Clearly the capacitance decreases at low temperature, the decrease of the capacitance with increased frequency is in keeping with specification data of solid tantalum capacitor [41]. This is the main reason for limiting these types of capacitors to low frequency applications. The dielectric constant and loss was studied as a function of temperature and frequency for Ta_2O_5 (1 μF / 50 V_{dc}). Figure 7.11 shows the influence of the temperature on the relative permittivity and dielectric loss, the relative permittivity increased with temperature at all frequencies, the relative permittivity and dissipation factor were 28 and 8 % at temperature 300 K and frequency 100 Hz, respectively, as seen in Fig. 7.11. Dissipation factor at higher frequency and low temperature increased considerably. The Ta_2O_5 dielectric relaxation was observed approximately at the same frequencies at different temperature range. This would indicate that the phenomenon is intrinsic to this dielectric and its interface. Indeed a wide range of relaxation phenomena are associated with process at metal–dielectric, semiconductor–dielectric, and electrolyte–dielectric interface [41].

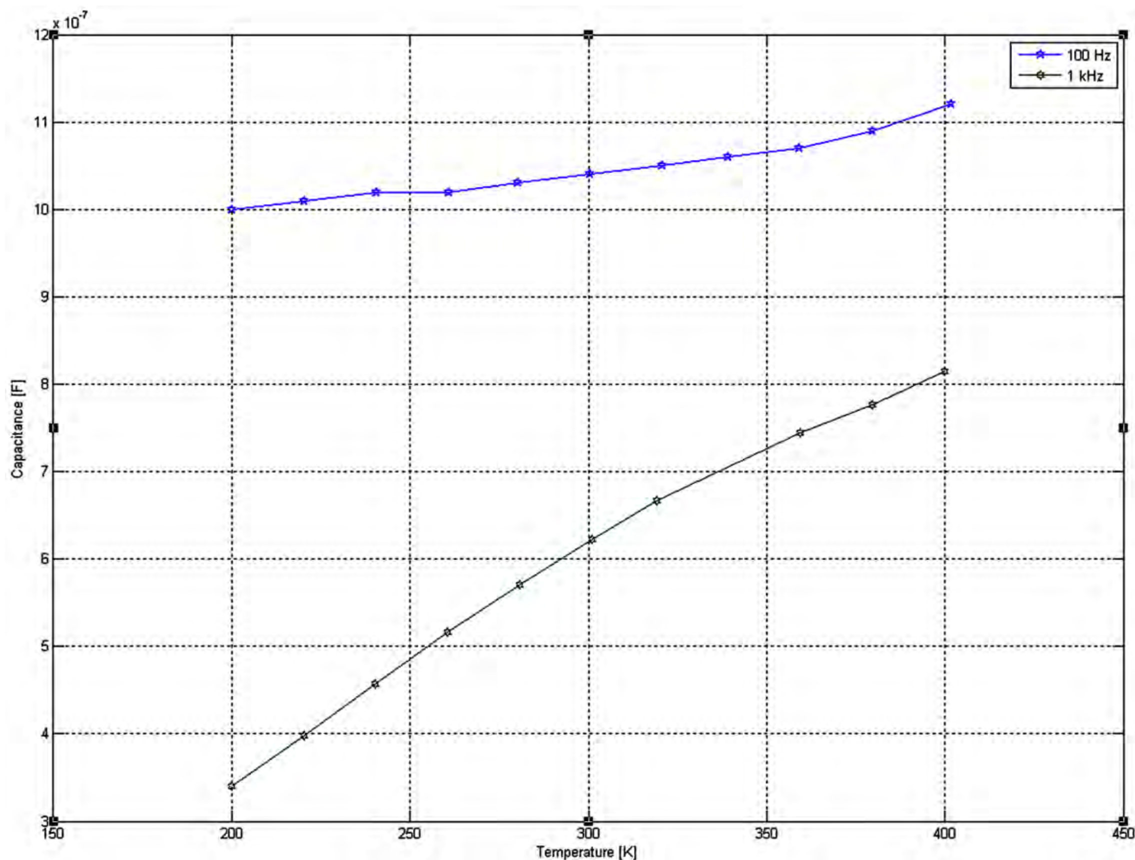

Fig. 7.10. The capacitance – temperature curves for (1 μF / 50 V_{dc}) tantalum capacitor.

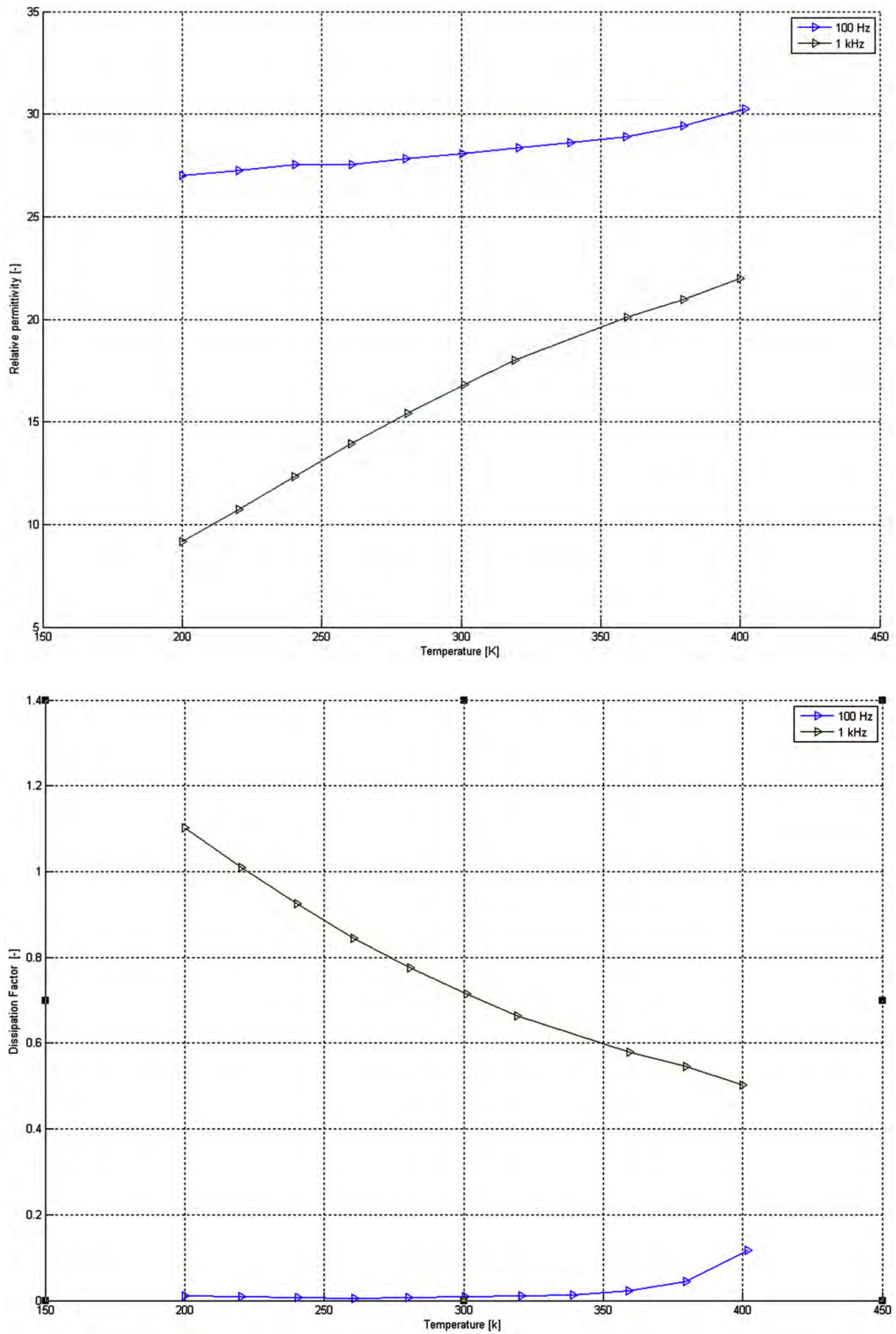

Fig. 7.11. Effect of temperature for Ta_2O_5 1 μF / 50 V_{dc} on (a) relative permittivity, (b) dissipation factor.

In order to further explain the transport mechanism in the present thin oxide film, electrical conductivity at different temperatures was studied.

Figure 7.12 shows the frequency dependence of electrical conductivity at various temperatures for 1 μF / 50 V_{dc} tantalum capacitor. The electrical conductivity depends on frequency according to the "universal dynamic response" [42] and can be related as

$$\sigma(\omega) = \sigma_{dc} + A.\omega^n \tag{7.1}$$

where A is the temperature dependent parameter and the exponent n is a characteristic parameter representing the many body interactions of the electrons, other charges and impurities. It varies from 0 to 1 and for ideal Debye type behavior it is equal to 1 [40]. As shown in Fig. 7.12 for all temperatures, the conductivity exhibits a steady increase in low frequency regime. Above a characteristic frequency, the conductivity increases with increase in frequency with characteristics ω^n dependence.

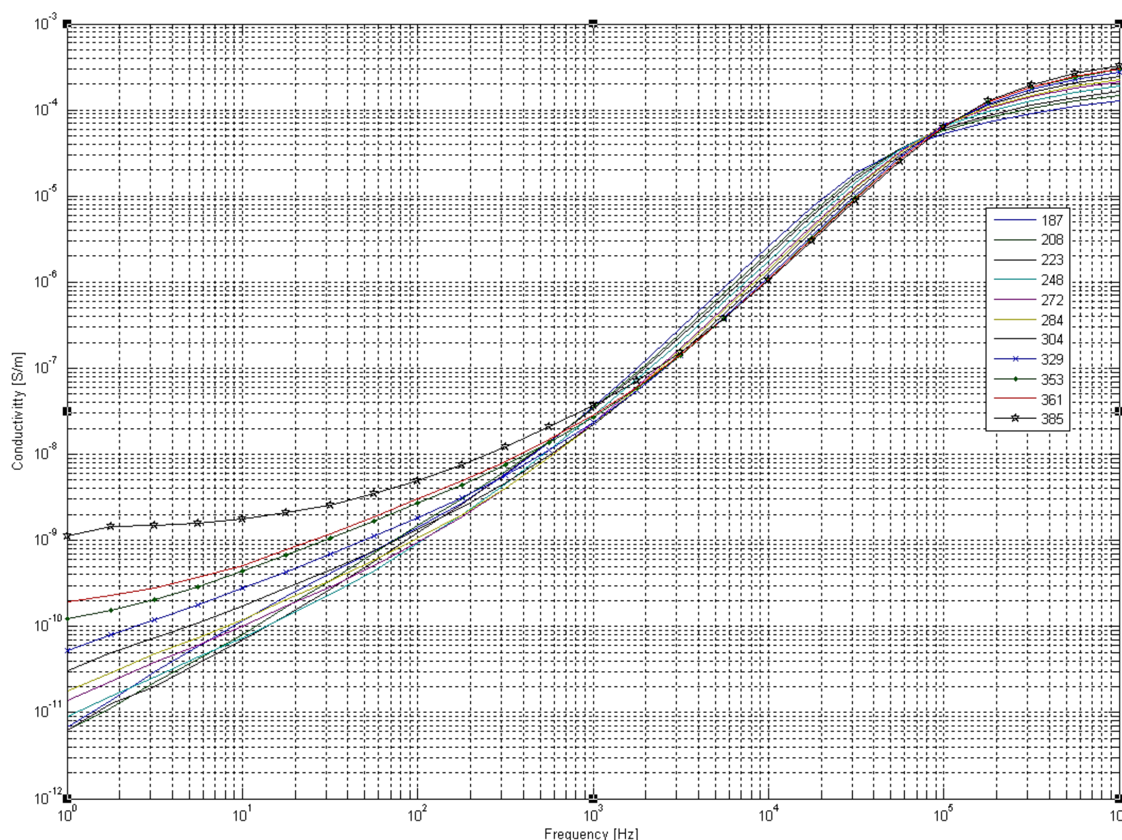

Fig. 7.12. The real part of the ac conductivity as a function of frequency at different temperatures for 1 μF / 50 V_{dc} tantalum capacitor.

7.4 Dielectric relaxation spectrum for 4.7 μF / 10 V_{dc} niobium electrolytic capacitor

The DRS method was used to obtain the dielectric properties of niobium thin oxide film 4.7 μF / 50 V_{dc} in a broad temperature range. The thickness of the oxide film as given by the producer was 84 nm and we obtained the electrode area A = 10.8 cm^2. Dielectric

measurements were performed using HP4284A impedance analyzer with Janis cryostat system at the Brno University of Technology. Temperature was varied in the 218 – 373 K range, working with liquid helium; temperature control and measurement was performed with LakeShore Cryotronics 340 temperature controller. The heating rate amounted to 1 K/min; data acquisition of C_p and G and the setting of temperature were automated with the use of a PC.

Figure 7.13 shows the real part of complex permittivity (relative permittivity) ε′ as a function of frequency in the temperature range 218 – 373 K; the relative permittivity was 48 at 373 K at the low frequency of 20 Hz. The relative permittivity increases with increasing temperature, corresponding to an increase in the dipole movement to follow the electric field.

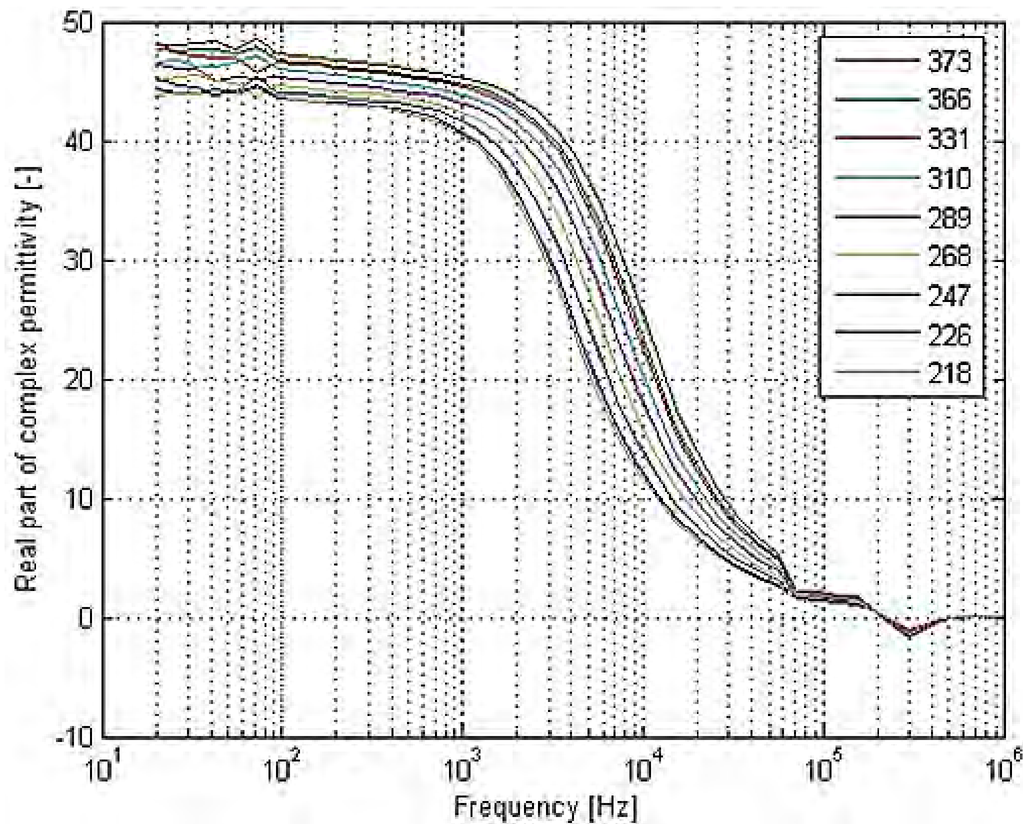

Fig. 7.13. Real part of complex permittivity as a function of frequency in the temperature range 218 – 373 K.

Figure 7.14 shows the imaginary part of complex permittivity ε″ as a function of frequency at the same temperature range. The peak of ε″ exists at about 10 kHz.

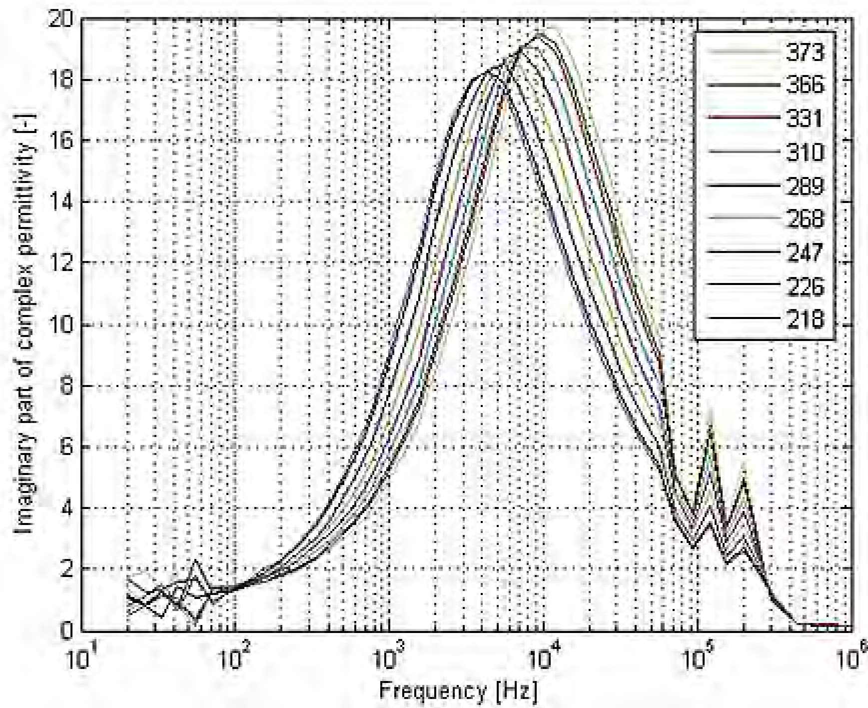

Fig. 7.14. Imaginary part of complex permittivity as a function of frequency at different temperature range.

In order to evaluate the change in the dielectric loss curve of the α–relaxation we obtained values $\Delta\varepsilon$, α_{HN}, β_{HN} and τ_{HN} as functions of temperature by fitting the observed values to HN equation (3.29). Fig. 7.15 shows examples of the Non-Linear Least Square (NLLS) fit of dielectric curve to a single relaxation HN function. We found that HN equation can very well fit the observed dielectric loss as a function of frequency except for a slight deviation of the observed value from the fitting curve at low frequencies. This slight deviation may be due to a dc conductivity.

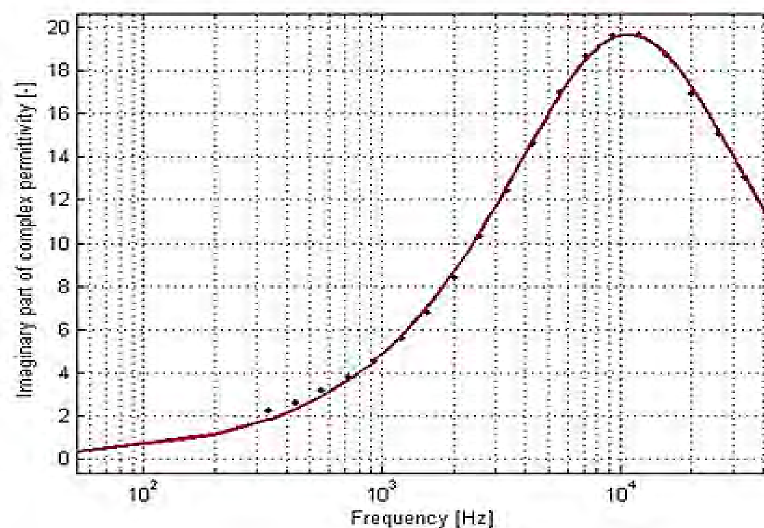

Fig. 7.15. Non-linear least square fit of imaginary part of complex permittivity versus frequency, a single HN equation at 373 K.

Figure 7.16 shows that the Arrhenius plot provides straight lines for $f_{max} = f(1/T)$. The relaxation time $\tau_{max} = 1/2\ \pi\ f_{max}$ for the maximum frequency in $\varepsilon''(\omega)$ is obtained by fitting the HN equation. The activation energy given by the linear fit is 0.055 eV.

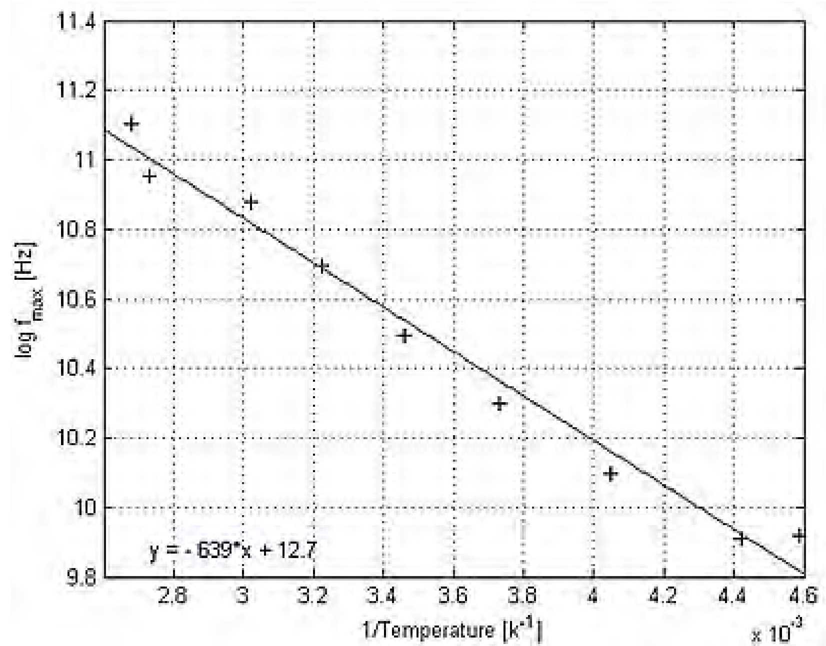

Fig. 7.16. The Arrhenius plot – log f_{max} *vs*. 1/T for niobium oxide.

Figure 7.17 shows the dependence of dielectric strength $\Delta\varepsilon$ on temperature; the dielectric strength $\Delta\varepsilon$ of the α-relaxation increases with the temperature

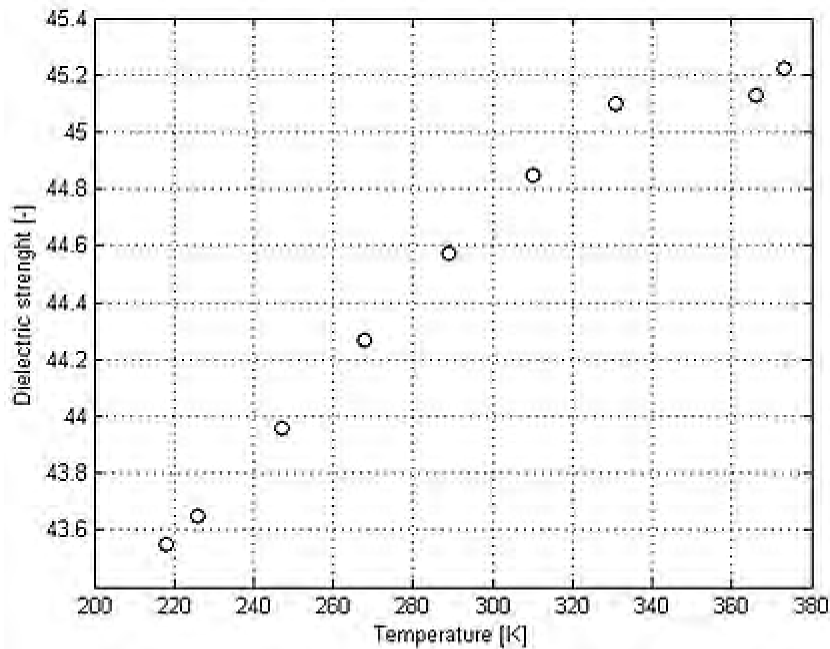

Fig. 7.17. Temperature dependence of dielectric strength for niobium thin oxide film.

The asymmetry parameter, β_{HN}, increases with increasing temperature as shown below.

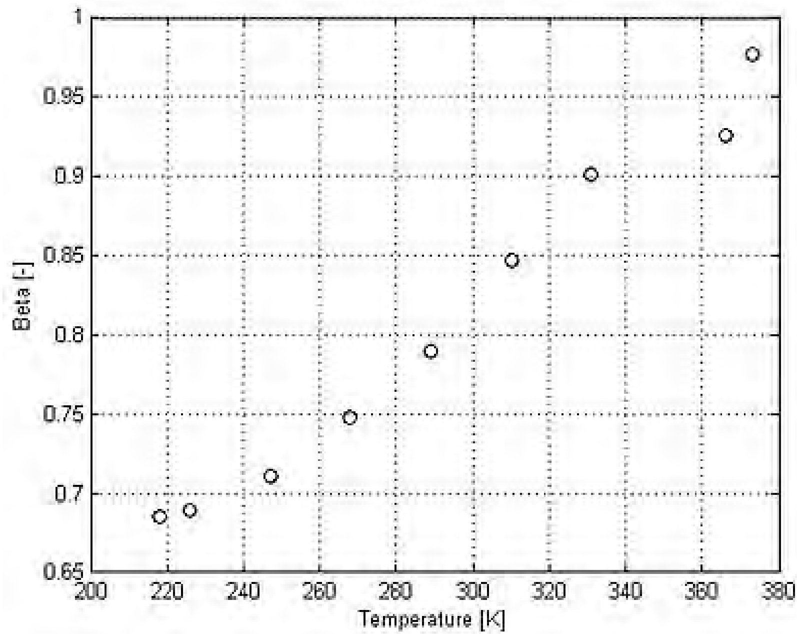

Fig. 7.18. Temperature dependence of shape parameter β_{HN} of niobium thin oxide film

Figure 7.19 shows the values of α_{HN}, which indicate that the width of the loss peak increases with decreasing temperature. At about 218 K its value ~ 1, in other words, the relaxation behavior can be described by the Cole-Davidson equation at this temperature.

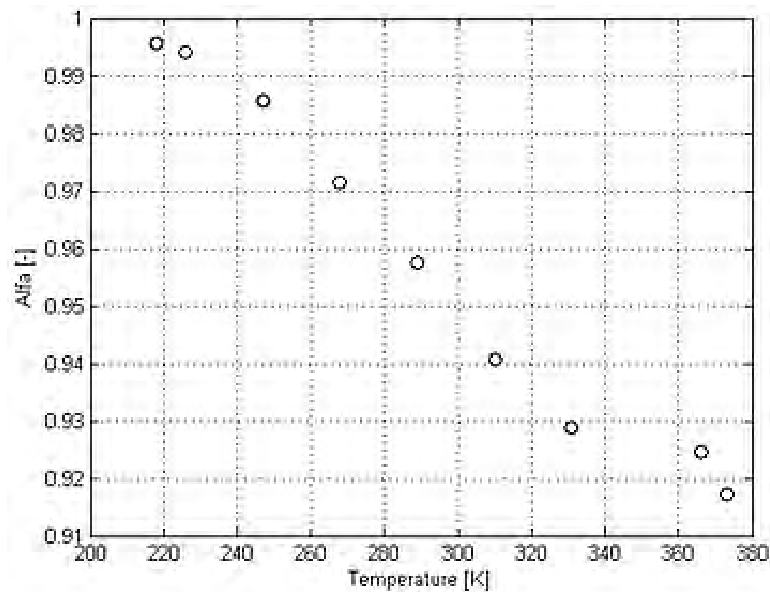

Fig. 7.19. Temperature dependence of the shape parameter α_{HN} of niobium thin oxide film.

In Table 7.3.1, the parameters are determined at nine different temperatures. The width parameter α_{HN} increases with decreasing temperature whereas other parameters β_{HN}, $\Delta\varepsilon$ and τ decrease with decreasing temperature.

Table 7.3.1. Havriliak – Negami parameters for niobium oxide capacitor 4.7 µF / 50 V_{dc} at different temperatures: from 218 K to 373 K.

T [K]	α [-]	β [-]	Δε [-]	τ [S]
373	0.917	0.917	45.22	1.8×10^{6}
366	0.924	0.926	45.13	1.7×10^{5}
331	0.928	0.900	45.10	1.8×10^{5}
310	0.940	0.847	44.85	2.2×10^{5}
289	0.957	0.790	44.57	2.7×10^{5}
268	0.971	0.748	44.27	3.3×10^{5}
247	0.985	0.711	43.96	4.1×10^{5}
226	0.994	0.689	43.65	4.9×10^{5}
218	0.995	0.685	43.55	4.9×10^{5}

7.5 Room temperature measurement on 4.7 µF / 10 V_{dc} niobium electrolytic capacitor and electrolytic tantalum oxide capacitor 1 µF/ 50 V_{dc}

The complex permittivity of the niobium oxide capacitor 4.7 µF/ 10 V_{dc} and tantalum oxide 1 µF/ 25 V_{dc} was measured at room temperature. This temperature falls within the normal operating range for these devices. Dielectric measurement has been carried out with Agilent E4980A impedance analyzer, and Agilent 16034E 2-terminal test fixture for surface mounted devices (SMD). The thickness of the oxide layer for the niobium oxide capacitors 4.7 µF/10 V_{dc}, as given by the producer, is 84 nm (as given in chapter 7.4) and we obtained the electrode area A = 10.88 cm^2. The thickness of the oxide layer for the tantalum oxide capacitors 1 µF/50 V_{dc}, again as given by the producer, is 297.5 nm and we obtain the electrode area A = 12.47 cm^2.

Figure 7.20 shows the real part of the complex permittivity as a function of frequency. If niobium and tantalum capacitors are compared with each other, the real part of the complex permittivity for niobium oxide capacitor is 46 at 3 kHz; at low frequencies it is increased to approximately 50 at 20 Hz, whereas for tantalum capacitor, the real part of the complex permittivity is 26 at 3 kHz and 27 at low frequency 20 Hz. The increase of permittivity at low frequencies suggests that the low frequency behavior could be attributed to an electrode polarization mechanism related to the accumulation of mobile charges at electrodes.

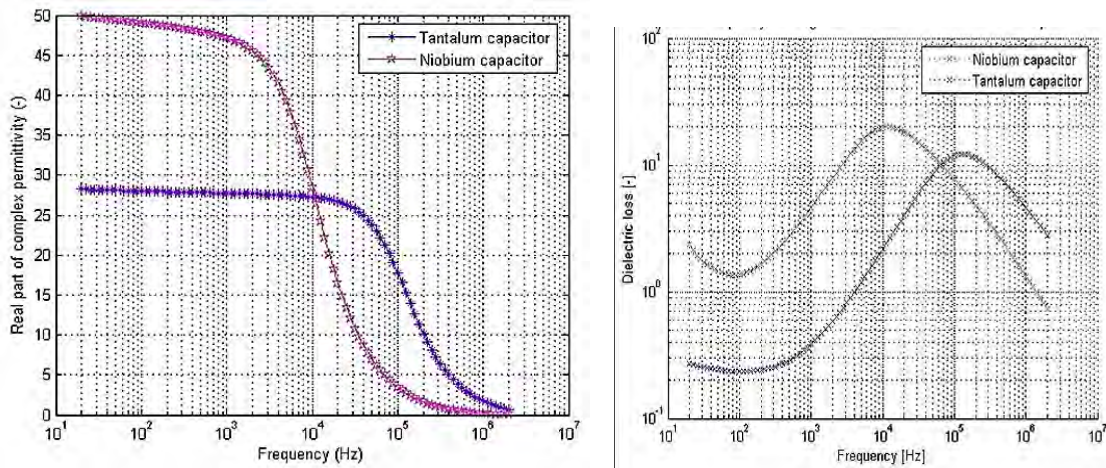

Fig. 7.20. a) Real part, and b) imaginary part of complex permittivity for niobium oxide capacitor4.7 µF/ 10 V_{dc} and tantalum capacitor 1 µF/ 25 V_{dc}.

Figure 7.21 shows the dissipation factor of the niobium and tantalum oxide capacitor; respectively, it is obvious that at low frequencies it takes its minimum value, and starts to increase at higher frequencies. These increased conductions have been observed in crystalline form of Ta_2O_5 [40].

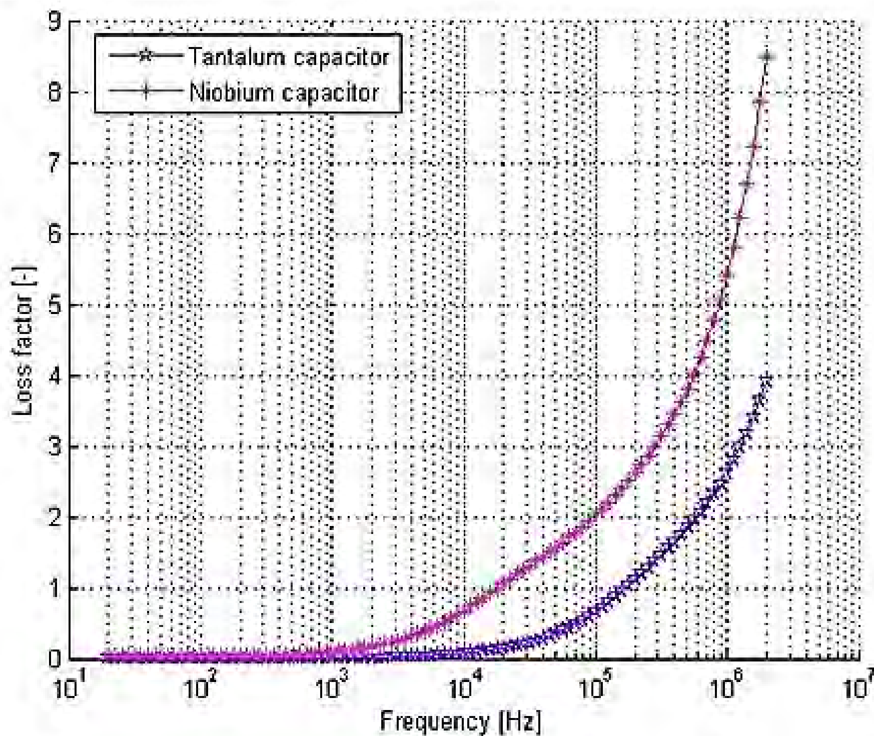

Fig. 7.21. Loss factor of the 4.7 µF/ 10 V_{dc} niobium and 1 µF/ 25 V_{dc} tantalum oxide capacitor.

The dielectric used inside the capacitor to separate the conductive plates in both niobium and tantalum oxide capacitor is not a perfect insulator resulting in a very small current flowing or "leaking" through the dielectric due to the influence of the powerful

electric fields built up by the charge on the plates when applied to a constant supply voltage.

The conduction shown in Fig. 7.22 for niobium and tantalum oxide capacitor at room temperature it starts at 17 μS/m and 0.1 μS/m at 20 Hz, respectively, and quickly increases to a final value of 1.3 S/m and 0.1 S/m at 2 MHz, respectively. It is clear that the conductivity of niobium oxide capacitor is higher than that of tantalum oxide capacitor. Conductivity is also affected by electrolyte concentration; greatest conductivity being due to greatest mobility of ions, and when there is too much electrolyte, ions are too crowded, hence they are less mobile, which in turn brings about less conductivity [43].

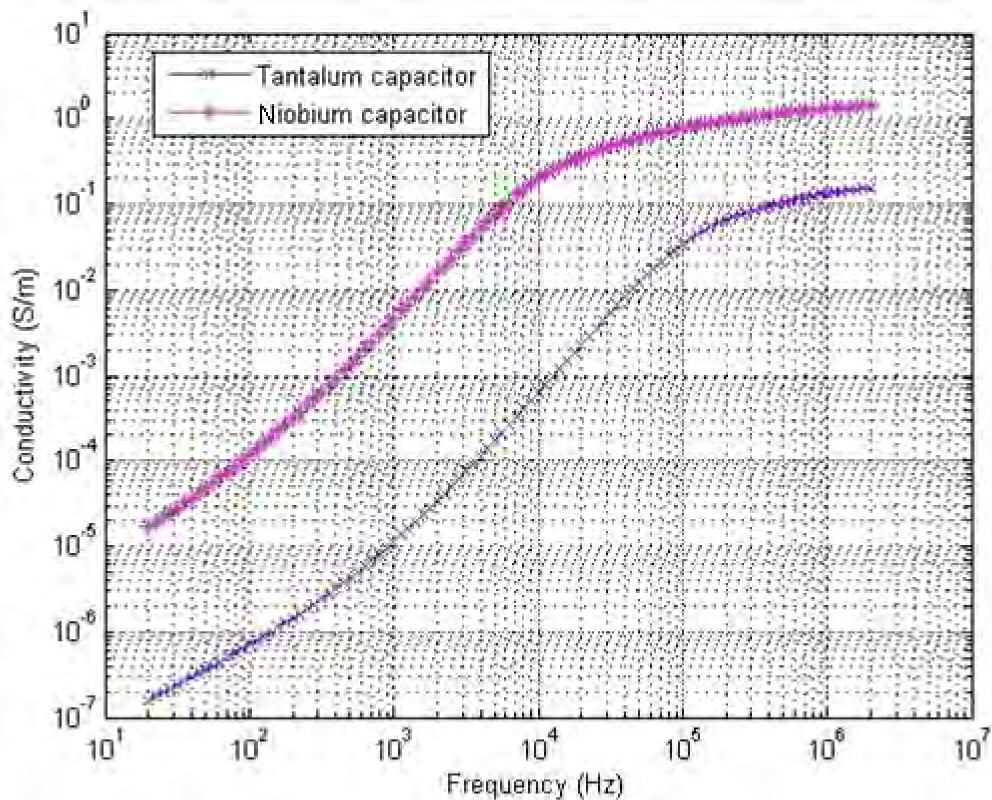

Fig. 7.22. Conductivity *vs*. frequency for niobium 4.7 μF/ 10 V_{dc} and 1 μF/ 25 V_{dc} tantalum capacitor.

The conductivity of tantalum pent-oxide was lower than that of niobium oxide capacitor and this is because of that the current in both capacitors is driven mainly by the concentration of oxygen vacancies [44].

8 Conclusions

Niobium electrolytic capacitor was described from the material point of view and compared to tantalum capacitor. The difference between them is that the anode is already oxidized and provides better resistance against burning. The second stable oxide (NbO_2) is responsible for the additional self-healing effect, which dramatically reduces the short circuits.

The niobium oxide capacitors differ from tantalum oxide ones only by the parameters of the structure, not by the principles. Lower potential barriers and higher number of defects in the dielectric, caused by additional stable oxide, result in higher leakage current.

The purpose of this work was to investigate dielectric and conductivity relaxation spectra, by using tantalum and niobium electrolytic capacitor. The objective was first to measure and then to analyze the observed frequency and temperature behavior of Ta_2O_5 and Nb_2O_5. Second Ta_2O_5 capacitor has been studied overall several thicknesses with a low frequency dielectric relaxation spectroscopy, as well as the conductivity of Ta_2O_5 and Nb_2O_5 over a wide frequency and temperature range.

The results acquired show:

Relaxation peak has been observed in the temperature and frequency range available for Ta_2O_5, 187 K – 385 K, 1 Hz – 10^6 MHz. The low frequency behavior of the relaxation peak could be attributed to an electrode polarization mechanism related to the accumulation of mobile charges at electrodes. The relaxation peak follows the Arrhenius law dependence with the activation energy of 0.048 eV. In conductivity spectra, Ta_2O_5 exhibits a steady increase in the low frequency regime. Above a characteristic frequency, the conductivity increases with increase in frequency with characteristics ω^n dependence. The onset of the increase of conductivity with frequency depends on temperature.

Dielectric thickness influence has been identified that for all the thicknesses under study the relaxation peak approximately shifted the same toward higher temperatures with frequency (same activation energy), the peaks located at different frequencies with approximately the same magnitude.

Capacitance low-temperature and dissipation factor low-temperature performance curves for tantalum (1 μF / 50 V_{dc}) capacitor and these clearly show the capabilities and limitations of tantalum capacitors at low temperature.

Relaxation peak has been observed in the temperature and frequency range available for Nb_2O_5, 218 K – 373 K, 1 Hz – 1 MHz. The low frequency behavior of the relaxation peak could be attributed to an electrode polarization mechanism related to the accumulation of mobile charges at electrodes. The relaxation peak follows the Arrhenius law as with the activation energy of 0.055 eV.

The dielectric used inside the capacitor to separate the conductive plates in both niobium and tantalum oxide capacitor is not a perfect insulator resulting in a very small current flowing or “leaking” through the dielectric due to the influence of the powerful electric fields built up by the charge on the plates when applied to a constant supply

voltage. The conductivity of niobium oxide capacitor is higher than that of the tantalum oxide capacitor, due to a higher number of defects in the dielectric, caused by additional stable oxide. The magnitude of the conductivity is heavily dependent upon the quality of the dielectric and the dielectric/interface electrode. Tantalum pent-oxide capacitors have been widely used, but their use has produced problems of unacceptably large leakage current in thin films thereof.

Appendix

The Arrhenius equation is as follows (for 1 μF / 50 V_{dc} tantalum capacitor)

$$\tau = \tau_{0a} \exp\left(-\frac{H}{kT}\right)$$

$$\ln \tau_1 = \ln \tau_{0a} - \frac{H}{k}.\frac{1}{T_1}$$

$$\ln \tau_2 = \ln \tau_{0a} - \frac{H}{k}.\frac{1}{T_2}$$

$$\frac{k}{H}\left(\ln \tau_1 - \ln \tau_2\right) \equiv \left(\frac{1}{T_1} - \frac{1}{T_2}\right)$$

$$\frac{H}{k} = -\left(\frac{\ln \tau_1 - \ln \tau_2}{\frac{1}{T_1} - \frac{1}{T_2}}\right)$$

$$\text{H}= -k.\left(\frac{14.1 - 12.4}{2.4\times 10^{-3} - 5.3\times 10^{-3}}\right)$$

$$\text{H} = 1.38\times 10^{-23}\times 586\times 1.602\times 10^{-19} = 0.050 \text{ eV}$$

9 Literature

[1] HOLMAN, B. *The electrical characterization of tantalum capacitor as MIS devices*. [Dissertation thesis]. Clemson University, August 2008.

[2] WILCOX, S, P. *Dielectric properties of thin insulating films*. [Master of applied science]. British Columbia University, 1968.

[3] SITA, Z. *Transport characteristics in niobium pent-oxide nanolayers*. [Dissertation thesis]. Brno University, April 2011.

[4] http://www.webelements.com/compounds/tantalum/tantalum_oxide.html

[5] http://en.wikipedia.org/wiki/Tantalum_pentoxide

[6] http://ref.rushkolnik.ru/v72264/?page=2

[7] DAVID, B. EELS investigation of stoichiometric niobium oxides and niobium-based capacitors. Dissertation Thesis, University of Karlsruhe (TH), France, 2009.

[8] http://www.chem.ufl.edu/~itl/4411/lectures/lec_16.html

[9] http://www.global.tdk.com/techmag/electronics_primer/vol1.htm.

[10] STRANIK, R. *Dielectric Relaxation Spectroscopy of Glycerol*. [Dissertation thesis]. Brno University, 2007.

[11] KWAN, C. K: *Dielectric Phenomena in solid*. Elsevier Academic press, USA, 2004.

[12] http://www.doitpoms.ac.uk/tlplib/dielectrics/variation.php.

[13] http://www.gamry.com/application-notes/basics-of-electrochemical-impedance-spectroscopy/

[14] LIEDERMANN, K. *Dielectric Relaxation Spectroscopy*. VUT v Brně, 2004.

[15] CHEN, S.C., LOU, J. C., CHIEN, C. H., LIU, P., and CHANG, T.C.: *An Inter-facial Investigation of High-K Dielectric Material Hafnium Oxide on Si Substrate*. Elsevier, 2005. p. 167 – 172

[16] ZEDNICEK, T., GILL, J. Voltage derating rules for solid tantalum and niobium capacitor. CARTS Europe, 2003.

[17] http://www.usna.edu/EE/ee320/Supplements/dcdc2_capacitors.pdf.

[18] http://www.planetanalog.com/document.asp?doc_id=527522

[19] PRYMAK, J, RANDALL, M, BLAIS, P, LONG, B. Why that 4.7μF Drop to 37μF, 30μF, or Low. KEMET Electronic Cooperation. USA, March, 2008.

[20] Technical update-Comparison of ceramic and Tantalum Capacitor. KEMET Electronic Cooperation, USA, November, 2008,

[21] SIKULA, J., PAVELKA, J., V. SEDLAKOVA, V., HLANKA, J., VASINA, P., ZEDNICEK,T . *Tantalum capacitor as a Metal-insulator-semiconductor structure*. http://www.kyocera.co.jp/prdct/electro/pdf/technical/cap_mis00.pdf.

[22] SIKULA, J., HLAVAKA, J., SEDLAKOVA, V., GRMELA, L., HOESCHL, P., ZEDNICEK, T., SITA, Z. *Conductivity Mechanisms and Breakdown of NbO Capacitors*. CARTS Europe, 2003.

[23] Agilent Technologies Impedance Measurement Handbook. Inc. 2006, Application Note 5950-3000 USA.

[24] Agilent Solutions for Measuring Permittivity and Permeability with LCR Meters and Impedance Analyzers, Agilent technologies Inc. 2006, Application Note 1391-1 USA, 5980-2862EN.

[25] Agilent 16451B Dielectric test fixture Operation Manual, 2008, USA.

[26] Product Safety Information Datasheet. AVX. 2014.

[27] Accessories Selection Guide for Impedance Measurements, Agilent technologies Inc, 2014, application note 5965-4792EN USA.

[28] Dc leakage failure mode. Vishay Technical Note, Inc., 2004, VSD-TN0003-0402. 2004

[29] Coating electrode with tantalum pent-oxide film, annealing film by exposure to ultraviolet radiation and ozone, repeating to form uniformly oxidized thick film providing high capacitance with low leakage current. USA Patent, Publication number US 5837593 A, 1998.

[30] LCR / Impedance Measurement Basics. Hewlett-Packard Company, 1997.

[31] http://www.indiamart.com/atech-systems/products.html.

[32] http://www.novocontrol.de/html/ana_alpha_main.htm.

[33] FELDMAN, Y. Dielectric spectroscopy of complex systems in Time and Frequency Domains: Problems and solutions. Hebrew University of Jerusalem, department of Applied Physics.

[34] http://www.novocontrol.de/html/temp_contr_quatro.htm.

[35] http://www.novocontrol.de/html/acc_sys_modules.htm.

[36] SCHUMBURG, G. Novocontrol cryo system for dielectric applications improved by the new QUATRO 4.0 controller. Dielectric newsletter.P.7-10. 1995.

[37] FRUBING, P. Dielectric spectroscopy. University of Potsdam, Institute of Physics, Advanced lap, 2011.

[38] MANCEAU. J_P., BRUYERE, S., JEANNOT, S., SYLVESTRE, A., GONON, P. *Dielectric relaxation study in Tantalum Pentoxide Capacitors*, Annual Report Conference on Electrical Insulation and Dielectric Phenomena. 2006. France

[39] ZEDNECIK, T., VRANA, B., MILLMANN, W, A., GILL, J., REYNOLDS, C. *Tantalum and niobium technology roadmap*, AVX a kyocera group company. Technology leadership across the board, P.1-7.

[40] SETHI, G., OLSZTA, M., LI, J., SLOPPY, J., HORN, M., DICKEY, E., LANAGAN, M. *Structure and dielectric properties of amorphous tantalum pentaoxide thin film capacitors.* Annual Report Conference on Electrical Insulation and Dielectric Phenomena.P.815-818. 2007.

[41] MATHEW, T.: Measurement of the low temperature electrical properties of solid tantalum capacitor. Cryogenics 41, P. 285-288. 2001.

[42] MACDONALD, J, R. *Comparison of the universal dynamic response power-law fitting model for conducting systems with superior alternative models*. Solid State Ionics, Vol. 133, Issues 1–2, P. 79–97. 2000.

[43] http://www.mcat-review.org/electronic-circuit-elements.php.

[44] SITA, Z., BILER, M., KARNIK, T., SIKULA, J., SEDLAKOVA, V. *Dielectric Improvement in NbO Capacitors*, CART EUROP, 2004, P.1-10.

Publications

[1] BIOLEK, D.; ABUETWIRAT, I. Analysis of digital filters via SPICE- family programs. Elektrorevue – Internet journal, 2006, P. 1. ISSN: 1213- 1539.

[2] ŠKARVADA, P.; GRMELA, L.; ABUETWIRAT, I.; TOMÁNEK, P. Nanooptics of locally induced photocurrent in Si solar cells. In Photonics Prague 2008. Prague: Zeithamlová Milena, Ing. Agentura Action M, 2008. P. 96-97. ISBN: 978-80-86742-25- 0.

[3] PALAI-DANY, T.; ABUETWIRAT, I. Vliv měřicího systému a zpracování dat na parametry dielektrické relaxační spektroskopie v časové oblasti. In 17. medzinárodná konferencia DISEE 2008. 1. Bratislava: FEI STU Bratislava, 2008. P. 203-206. ISBN: 978-80-227-2933- 8.

[4] ABUETWIRAT, I. Dielectric relaxation spectroscopy as a tool for investigation of dielectric thin films and fabrication method thereof for microcapacitor integration. In Proceedings of IEEE Workshop Králíky 2009. Brno: .P. 14-17. ISBN: 978-80-214-3938- 2.

[5] ABUETWIRAT, I.; HOLCMAN, V.; LIEDERMANN, K. Dielectric Relaxation Spectroscopy as a Tool for the Investigation of Thin Oxide Layers. In Physics of Materials 2009. 1. Košice, Slovakia Republic: FEI TU Košice, 2009. P. 123-126. ISBN: 978-80-8086-122- 3.

[6] ABUETWIRAT, I.; BRZOBOHATÝ, J. On the stability of current- mode operational amplifiers. In Proceedings of IEEE Workshop Králíky 2009. Brno. 2009. P. 421-424. ISBN: 978-80-214-3933- 7.

[7] ABUETWIRAT, I. Dielectric and electric properties of niobium oxide electrical capacitor. In Proceedings of 8th international conference KRÁLÍKY 2010. Brno: FEKT VUT Brno, 2010. P. 12-15. ISBN: 978-80-214-4139- 2.

[8] ABUETWIRAT, I. Impedance analyzer measurement of ceramic capacitor and high value resistor. In POSTER 2010. 1. Prague: Czech Technical University in Prague, 2010. P. 1-4. ISBN: 978-80-01-04544- 2.

[9] ABUETWIRAT, I. Conduction mechanism in thin insulator film metal-insulator-semiconductor capacitor. In Proceedings of 9th international conference VSacKÝ CÁB 2011. Brno: FEKT VUT Brno, 2011. P. 12-15. ISBN: 978-80-214-4319- 8.

[10] ABUETWIRAT, I.; PALAI-DANY, T. Dielectric Properties of Niobium Oxide Film and Tantalum Oxide Film at Electrolytic Niobium And Tantalum Capacitors. In 9th ELEKTRO 2012 international conference. 1. Žilina, Slovakia Republic: FEKT VUT Brno, 2012. P. 484-488. ISBN: 978-1-4673-1178- 6.

[11] ABUETWIRAT, I.; PALAI-DANY, T. Dielectric Properties of Niobium Oxide Film at Electrolytic Niobium Capacitor. In proceedings of the 18TH conference EEICT 2012. Brno: Ing. Zdenek Novotný, CSc, 2012. P. 224-228. ISBN: 978-80-214-4462- 1.

[12] ABUETWIRAT, I. Description of dielectric spectrum obtained by dielectric relaxation spectroscopy using Havriliak – Negami function. In proceedings of the 18TH conference EEICT 2012. Brno: Ing. Zdenek Novotný CSc, 2012. P. 219-223. ISBN: 978-80-214-4462- 1.

[13] ABUETWIRAT, I.; LIEDERMANN, K. Measurement of the temperature dependence of complex permittivity at different frequencies for niobium oxide film at commercial electrolytic capacitors. In New Trends in Physics, NTF 2012. 1. Brno: Brno University of technology, 2012. P. 27-30. ISBN: 978-80-214-4594-9.

[14] ABUETWIRAT, I.; LIEDERMANN, K. Measurement of the temperature dependence of complex permittivity at different frequencies for niobium oxide film at commercial electrolytic capacitor. In Proceedings of the Scientific Conference Physics of Materials 2012. Košice: Faculty of Electrical Engineering and Informatics, Košice University of technology, 2012. P. 133-138. ISBN: 978-80-553-1175- 3.

[15] PALAI-DANY, T.; ABUETWIRAT, I. The Improved Simple Regulation of Small Heating Systems. In New Trends in Physics NTF2012. 1. Brno: FEKT VUT Brno, 2012. P. 179-182. ISBN: 978-80-214-4594- 9.

[16] ABUETWIRAT, I. Dielectric and electric properties of tantalum thin oxide film at commercial electrolytic capacitor. In 16th International Student Conference on Electrical Engineering. 1. Prague: CTU Prague, 2012. P. 1-4. ISBN: 978-80-01-05043- 9.

[17] DALLAEVA, D.; BILALOV, B.; ARKHIPOV, A.; ABUETWIRAT, I. Osobennosti mezhdisciplinarnogo podhoda k izucheniju estestvennyh nauk na sovremennom jetape. In Materials of III All Russian conference: Innovation, science. education: ways of integrations, problems, contradictions. First. Derbent: FGBOU VPO DGTU v g. Derbente, 2012. P. 70-72. ISBN: 5-230-12933- 6.

[18] ABUETWIRAT, I.; CHVÁTAL, M. Measurement of the temperature dependence of complex permittivity at different frequencies for niobium oxide film at commercial electrolytic. In Proceedings of the conference VSACKÝ CÁB 2012. 1. VSACKÝ CÁB: FEKT VUT Brno, 2012. P. 4-7. ISBN: 978-80-214-4579- 6.

CURRICULUM VITAE

Name: Inas Faisel Abuetwirat

Date and Place of Birth: 04-10-1980, Tripoli-Libya

Contact: abuetwiratinas@yahoo.com

Education:

Secondary School, 1999.

BSc. Degree in Physics, 1999–2003. The Higher Teacher Preparation Institute, Tripoli.

MSc. Degree in Microelectronic devices, Faculty of Electrical Engineering and Communication, Brno University of Technology, 2004–2006.

Languages:

Arabic: native language.

English.